Petrologic Study of the Danburg, Sandy Hill, and Delhi Intrusions: Constraints on Magmatism in the Southern Appalachians

A thesis presented to

the faculty of

the College of Arts and Sciences of Ohio University

In partial fulfillment

of the requirements for the degree

Master of Science

Cody M. Strack

August 2015

This thesis titled

Petrologic Study of the Danburg, Sandy Hill, and Delhi Intrusions: Constraints on Magmatism in the Southern Appalachians

by

CODY M. STRACK

has been approved for

the Department of Geological Sciences

and the College of Arts and Sciences by

Craig B. Grimes

Assistant Professor of Petrology

Robert Frank

Dean, College of Arts and Sciences

ABSTRACT

STRACK, CODY M., M.S., August 2015, Geological Sciences

Petrologic Study of the Danburg, Sandy Hill, and Delhi Intrusions: Constraints on Magmatism in the Southern Appalachians

Director of Thesis: Craig B. Grimes

Three undeformed, spatially related plutons were investigated to constrain their petrogenesis and to define their context in the magmatic history of the Southern Appalachians. New SHRIMP-RG ^{207}Pb-corrected ^{206}Pb/^{238}U zircon ages are presented for the Danburg granite, Sandy Hill granite, and Delhi syenite. The Danburg and Sandy Hill plutons yielded statistically equivalent ages of 307.0±4.7 Ma and 304.7±3.0 Ma, respectively, whereas the Delhi syenite zircons yielded an age of 468.9±4.8Ma. The age for the Delhi intrusion contrasts with previous estimates that it was part of the Alleghanian or Acadian orogenies, which were based solely on field relations. Whole rock geochemistry of the Alleghanian-age Danburg and Sandy Hill granites are indicative of post-collisional granites; the Delhi geochemistry is most similar to anorogenic granitoids. Mafic enclaves are dispersed throughout the Danburg granite and are proposed to represent the presence of a quenched mafic melt that was coeval with the Danburg based on textural features, linear geochemical trends, and a statistically similar SHRIMP-RG ^{207}Pb-corrected ^{206}Pb/^{238}U titanite age of 307.3±3.7Ma. Accessory mineral thermobarometry of 771±27°C and 6.5±1.7 kilobars for the Danburg granite and 765±50°C and 5.1±1.4 kilobars for the enclaves supports the interpretation of crystallization under similar conditions. A transpressional model of convergence

between the Suwannee terrane and Laurentia with minor mantle involvement is the preferred tectonic setting due to documented major shear zones, largely granitic plutonism, and the presence of mafic enclaves.

DEDICATION

This thesis is dedicated to my family for their endless support through a new and challenging experience. A special thanks goes to my mother for always being available to listen and reminding me life goes on.

ACKNOWLEDGMENTS

I would like to thank my adviser, Dr. Craig Grimes, for steering me through a master's thesis. I would like to thank my committee members Dr. Doug Green and Dr. Greg Nadon for their input and flexibility in getting the thesis defended. Lastly, I'd like to acknowledge my fellow Grimes advisees, Cody MacDonald and Jeb Brown, for support and encouragement.

TABLE OF CONTENTS

Page

LIST OF TABLES

Page

LIST OF FIGURES

Page

CHAPTER 1: INTRODUCTION

1.1 Statement of Purpose

Granitic plutonism marks the culmination of the assembly of the Pangean supercontinent, but identification of the intrusive rocks emplaced during this time is not always apparent from field observations alone. Numerous tectonic and magmatic events at the present-day, southeastern margin of Laurentia produced variable overprinting fabrics and the juxtaposition of rock units by faults that are not always visible in outcrop, but may be better understood through the acquisition of well-constrained, hih-precision age and whole rock geochemical data. The multi-phase Danburg/Sandy Hill and Delhi granitoids located in northeast Georgia were emplaced in the Charlotte belt, which is one of the peri-Gondwanan terranes that were accreted onto the Laurentian margin as part of the Appalachian orogen. These spatially related plutons have been previously interpreted as part of a suite of felsic intrusives emplaced during the Alleghanian orogeny, reflecting the final Laurentian mountain-building event in the amalgamation of Pangea (Dvoracek, 2003) (Figure 1-1).

The Delhi syenite has a controversial origin. Allard and Whitney (1994) proposed that the Delhi cuts the Danburg, indicating it is younger in age although no clear contact relations are visible in the field and no age had been determined for the Delhi intrusion prior to this study. McSween and Harvey (1997) suggested instead that the Delhi was part of the Concord plutonic suite, a ~400 Ma, post-Acadian intrusive suite in the Charlotte belt composed primarily of gabbros and syenites. Furthermore, the Delhi intrusion has been suggested as a potential source for the mafic enclaves within the Danburg granite

(Dvoracek, 2003). Previous whole rock Rb/Sr Alleghanian ages have been reported for the Danburg, enclaves and Sandy Hill bodies (Dvoracek, 2003). Application of new U-Pb geochronology allows confirmation of these ages; Pb/U in single, refractory crystals (i.e., zircon) often provides a more robust age than whole rock Rb/Sr, which is more susceptible to open system chemical exchange.

The connection between the Danburg and included mafic enclaves is an additional question that is addressed in this study. Age constraints and textural evidence allow interpretation of the relationship between the two lithologies, which in turn, has implications for the petrogenesis of the Danburg as well as other nearby Alleghanian plutons reported to contain mafic enclaves (e.g., Appling, Siloam, Sparta) (Dvoracek and Roden, 2005). Determining the characteristics of these plutons will add to the growing compendium of information regarding the formation of southern Appalachians and assist in constraining the geodynamic setting. This study characterizes these undeformed plutons using a combination of petrology, geochemistry, and geochronology to provide conclusive, robust interpretations of the nature of the relationship between these rocks and their petrogenesis.

1.2 Regional Geology/Geologic Background

The Appalachians mark multiple episodes of orogenesis through the evolution of the eastern margin of Laurentia from the rifting of Rodinia to the amalgamation of Pangea,. The major orogenies that define the Appalachians are the Taconic (Ordovician - Silurian), Acadian (Devonian), and Alleghanian (Carboniferous - Permian) occurred due

to collision of various crustal blocks the Laurentian margin, but the timing and extent of these blocks is controversial (Hatcher, 2005) (Figure 1-2). The Appalachians are often separated by geographic province into the northern, central, and southern portions, all with fairly distinct tectonic histories due to the diachroneity of the collisional events. The plutons in this study all originate from the Southern Appalachian Orogen (SAO).

The SAO represents a complex assmbalge of numerous terranes that have been deformed through multiple periods of compression and extension. Carolinia is a large terrane within the SAO that was accreted onto the Laurentian margin during one of the major Appalachian orogenies. Carolinia consists of the Charlotte belt, Carolina Slate belt, and other minor crustal blocks (Figure 1-1A) that are exotic to Laurentia and believed to be a Precambrian to Cambrian island arc terrane, composed primarily of volcanic, volcaniclastic, pyroclastic, and sedimentary rocks (Sinha et al., 2012, Pollock et al., 2012). Substantial plutonism occurred in the Carolinia, prior to)?) the intrusion of Alleghanian-aged granitoids. Although the timing of the metamorphism of older plutons is eqiuvocal, it is apparent the majority of the metamorphosed plutons were emplaced, accreted, and altered before the Alleghanian intrusive event that created the Danburg, Sandy Hill, and Delhi granitoids. (Dvoracek, 2003). Sinha et al. (2012) favored accretion of Carolinia during the Silurian – Devonian (420Ma – 360Ma) as part of the Acadian orogeny (Figure 1-3). This model contrasts with interpretation of Pollock et al. (2012), who suggested Carolinia collided with Laurentia during the Late Ordovician – Early Silurian (460Ma – 430Ma) during the Taconic Orogeny (Figure 1-4). These

interpretations reflect conflicting lines of evidence in the existing datasets, which are often complicated by the multiple overprinting magmatic and tectonic events.

Alleghanian magmatism is characterized by a suite of syn- to post-tectonic granitoids emplaced across Appalachian terranes at approximately ~330-290 Ma (Speer et al., 1994), representing the final magmatic expression of the assembly of Pangea in North America (Figure 1-1A). Over the past 4 decades, there has been debate over the tectonic setting of emplacement, lithospheric sources, and the duration over which these granitoids formed. Early studies suggested formation in a westward-verging supra-subduction setting during the closure of the Rheic Ocean as the cause of the intrusive event (Wenner, 1981). However, more recent analyses discredit this idea through multiple lines of evidence:

(1) Southern Appalachian Orogen (SAO) magmatism was heavily felsic with <5% of the plutons having mafic-intermediate compositions (Samson et al., 1995).

(2) No geographic trend in $^{87}Sr/^{86}Sr$, $^{143}Nd/^{144}Nd$, K_2O, or Sr compositions exist across the strike of the orogen (Samson et al., 1995).

(3) The relatively small volume of magmatic rocks in the SAO are in contrast with the often voluminous and overlapping plutons found above subduction zones (Speer et al., 1994).

Alternative models favoring crustal thickening resulting from transpression and associated anatexis have been considered more likely to generate a suite of this size and composition (Samson et al., 1995, Mueller et al., 2013). Additionally, heat may have been added to the crust following the collisional events and delamination of the mantle

lithosphere leading to subsequent upwelling of asthenospheric mantle (Samson et al., 1995, Sacks and Secor, 1990, Nelson, 1992). Speer et al. (1994) concluded that contemporaneous deformation accompanied the Alleghanian, suggesting that the melting mechanisms were dependent on deformation with some combination of decompression melting, emplacement of hot asthenosphere against the lower crust, and/or volatile influx. The varying and evolving tectonic models may also signify changing tectonic regimes over time. More precise geochronologic constraints are required to further evaluate temporal-spatial trends across the SAO and may help refine the actual geodynamic setting as well as gain insights into amalgamated lithospheric blocks.

Constraining the role of each terrane accreted onto Laurentia is integral to understanding the Alleghanian orogeny. A large terrane under recent scrutiny, the Suwannee Terrane (SWT), is exotic to North America and was docked onto the southeastern coast as the final event of the Alleghanian, and thus likely contributed to the final amalgamation of Pangea and associated magmatism (Mueller et al., 2013). The SWT is thought to be a composite terrane that consists of Amazonian lower crust and African upper crust (Mueller et al., 2013), differing from the Grenville-age gneisses comprising basement characteristic of Laurentia. Mueller et al. (2013) considered the most likely method of accretion to be dextral transpression due to the lack of documented subduction-related magmatism in the Southern Appalachians, resulting in crustal thickening and ultimately anatexis. The boundary of the suture zone between the SWT and Laurentia is not well-constrained; however, multiple interpretations agree that the suture cuts obliquely across the SAO from southern Mississippi to South Carolina. The

Goat Rock and Bartlett's Ferry shear zones within the SAO represent possible components of a broad suture zone (Mueller et al., 2013) (Figure 1-2). These fault zones are compatible with COCORPS geophysical data, which show a wide area of southeast-dipping reflectors (McBride and Nelson, 1988). Potentially, these reclectors(?) represent the suturing and obduction of SWT onto Laurentian lithosphere (Mueller et al., 2013). Additionally, Sacks and Secor (1990) have proposed that delamination occurred at the Suwannee suture.

The convergence of the Suwannee terrane and Laurentia is thought to have produced a distinctive intrusive event marked by the presence of numerous granitic plutons that outcrop in the SAO (Speer et. al, 1994). What remains to be fully constrained is the absolute timing of collision as well as the mantle and lithospheric sources from which these plutons were generated. Oxygen isotope data from whole rock and quartz (Wenner, 1981) and hafnium isotope data (Lin, 2013) indicate contributions from a juvenile (mantle) source in several plutons, especially those intruding Carolinia. Mafic enclaves are reported from several SAO plutons, and could conceivably represent juvenile mantle contributions added to the crust.

1.3 Local Geology and Previous Work on the Danburg, Sandy Hill, and Delhi Plutons

The plutons in this study intrude the Charlotte belt and are located in northeast Georgia within Wilkes and Lincoln counties (Figure 1-1A). To the south/southeast lies a linear succession of shear zones including the Modoc, Bartlet's Ferry, and Goat Rock with the northern boundary delineated by the Middleton-Lowndesville fault zone (Allard

and Whitney, 1994). The country rocks surrounding these intrusions comprise various metamorphosed volcaniclastic units (chlorite to amphibolite grade), igneous bodies, as well as biotite schists and gneisses (Figure 1-1B).

Previous work on the plutons sampled for this study includes descriptive petrography and geochemistry of the Danburg granite, mafic enclaves, and the Sandy Hill granite. The Danburg and Sandy Hill are spatially related plutons, although the contact between the two is buried and their exact field relationships are unknown. No metamorphic aureole can be confirmed at their contact zone (Dvoracek, 2003). The Sandy Hill granite exists on the southern periphery as a small band of exposures, mapped as in contact with the more areally extensive Danburg pluton (Figure 1-1B). Both are compositionally and texturally homogenous (Dvoracek, 2003). Mafic enclaves are abundant (~2%) in the Danburg pluton yet are absent in the Sandy Hill pluton. The Sandy Hill granite has a higher quartz, alkali feldspar, and muscovite content (Figure 1-5).

Whole rock $^{87}Rb/^{86}Sr$ ages of 307±7 Ma for the Danburg, 303.8±0.4 Ma for the enclaves, and 294±9 Ma for the Sandy Hill have been reported and support the interpretation of an Alleghanian age for the plutons (Dvoracek, 2003). However, alteration of feldspars in the Sandy Hill was observed by Dvoracek (2003) who noted the whole rock age should be considered suspect. Additionally, there is evidence for substantial chemical exchange between the mafic enclaves and the Danburg granite, which could influence whole rock ages. Strontium ratios suggest a chemically primitive(?) lower crustal source for the Danburg ($^{87}Sr/^{86}Sr = 0.7048±0.0002$) with the enclaves giving a similar, statistically indistinguishable ratio ($^{87}Sr/^{86}Sr =$

0.70471±0.00001). The Sandy Hill yielded a distinctively higher initial ratio ($^{87}Sr/^{86}Sr$ = 0.70716±0.00005), which probably reflects contributions from remelting of isotopically evolved crustal material. Despite the age and Sr-isotopic differences, Dvoracek (2003) suggested the Sandy Hill was contemporaneous with the Danburg intrusion, but likely generated from different sources.

Dvoracek (2003) also concluded the likely petrogenesis of the Danburg granite is a post-collisional environment where crustal processes were dominant, even though the Danburg has subduction/mantle-related geochemical affinities. On the basis of regional isotopic studies most workers no longer favor an interpretation of Alleghanian plutonism to be the result of a subduction-setting, and so alternatively Dvoracek (2003) proposed that any subduction-signatures were inherited from the source rocks melted to form the Danburg intrusion.

The textural and chemical analyses documented in this study indicate that the Danburg granite and included mafic enclaves are related through magma mixing and mingling, although it is often difficult to clearly identify the origin of mafic enclaves in this and similar occurrences due to extent of chemical exchange occurring with the host granite. Dvoracek and Roden (2005) suggested that the parental source was likely an evolved intermediate magma or gabbroic differentiate with alkaline affinities, as opposed to a basaltic parent, for the enclaves based on elevated Zr and Ba contents as well as evolved mineral chemistry, and instead. The nearby Delhi syenite was proposed by Dvoracek (2003) as a possible candidate for the parental magma from which the enclaves derived, but little work has been done on the Delhi intrusion apart from the recognition

that it is syenitic in composition (McSween and Harvey, 1997) (Figure 1-5). Compositional variation in the enclave population has previously been explained by preferential segregation of mineral phases rather than multiple injections of distinct magmas.

1.4 Summary

The geologic relationship between the Danburg pluton and nearby intrusions and mafic enclaves, as well as to the more regionally extensive suite of Alleghanian plutons, has not been established. The goal of this investigation was to analyze the three previously mentioned plutons and the mafic enclaves to constrain their geologic relationship and establish a tectonomagmatic framework for emplacement. Using petrography, whole rock major element geochemical methods, and SHRIMP-RG U-Pb geochronology the following hypotheses were tested: 1) The Danburg pluton, Sandy Hill, and Delhi syenite are coeval; 2) The Danburg granite and included mafic enclaves are coeval, and 3) are the result of mixing of two discrete liquids. Geochemical and geochronological constraints on these units, including the enclaves, provide a better understanding of their geologic relations to one another, as well as to the Alleghanian granites throughout the Southern Appalachian Orogen (SAO) in general.

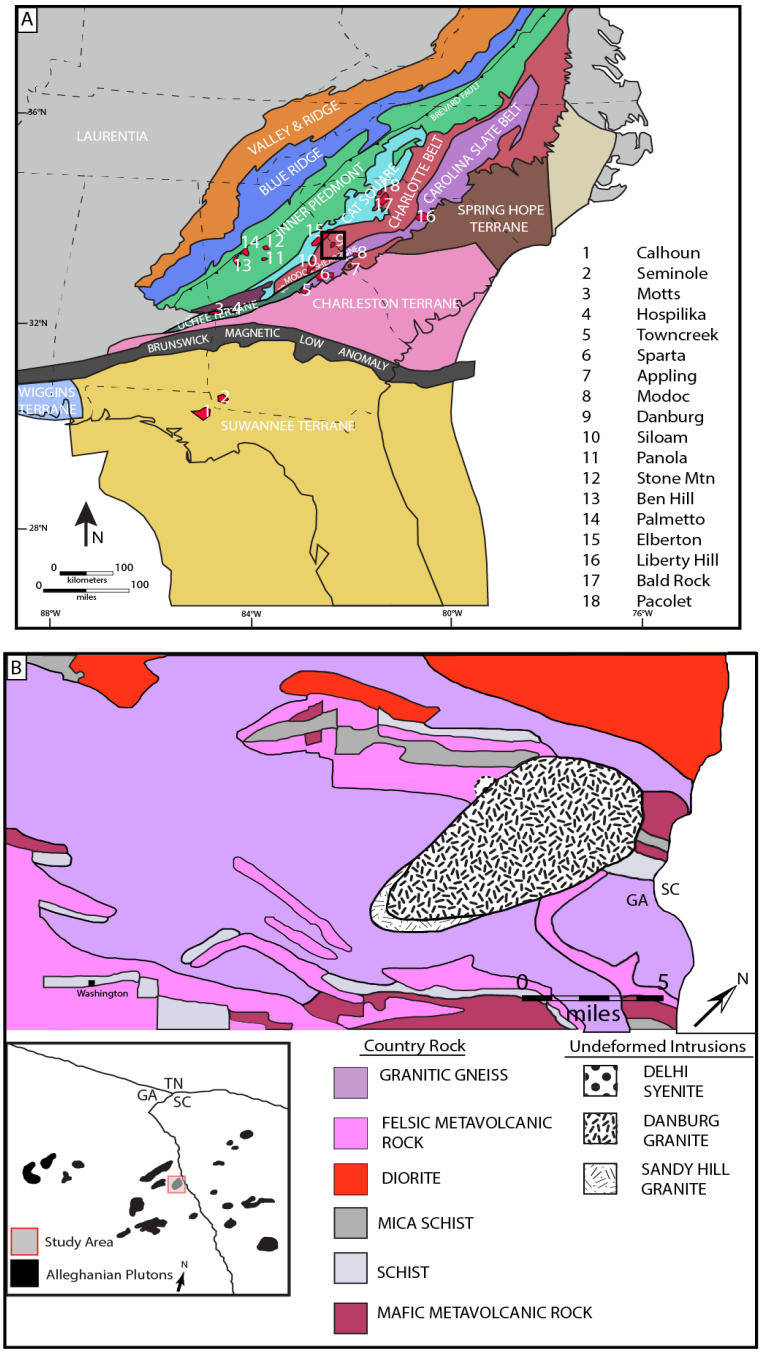

Figure 1-1: 1A) A simplified geologic map of the Southern Appalachians with the location of 16 plutons with inferred Alleghanian-ages. The black box surrounds the study area. 1B) A revised geologic map of the study area, after Allard and Whitney (1994). The Sandy Hill granite has only been identified along the southeastern margin of the Danburg pluton. The extent of the Delhi syenite is not well known. The revised map shows the Danburg pluton cutting the Delhi Syenite based on the results of this study.

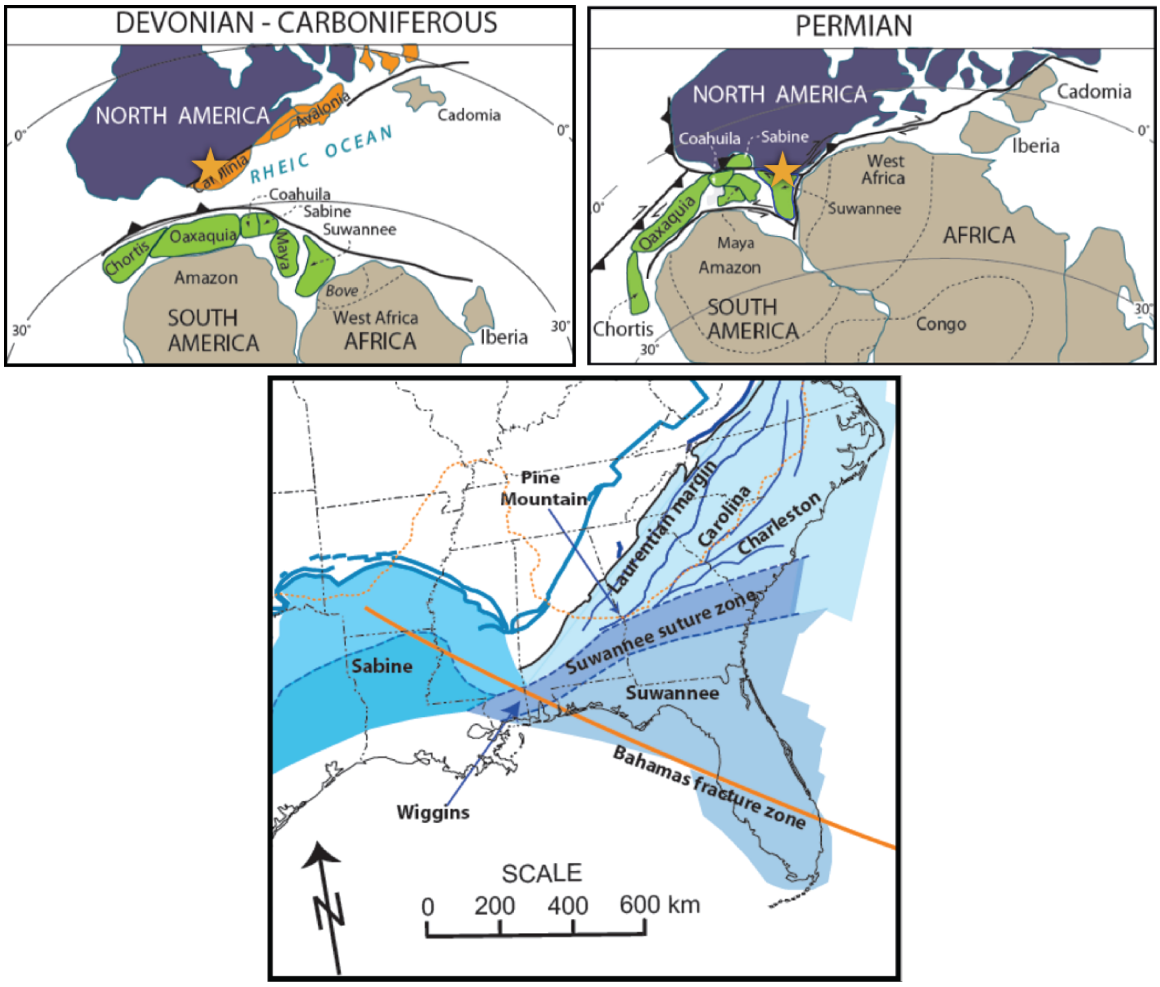

Figure 1-2: The top figures show one model of the paleogeographic positioning of the major continental bodies during the Devonian, Carboniferous, and Permian representing the amalgamation of Pangea. The gold star represents the study area in relation to the larger tectonic setting. The lower figure shows current positions of the constituent terranes that were involved in the Appalachian orogenies and proposed location of Suwannee suture zone (after Mueller et al., 2013).

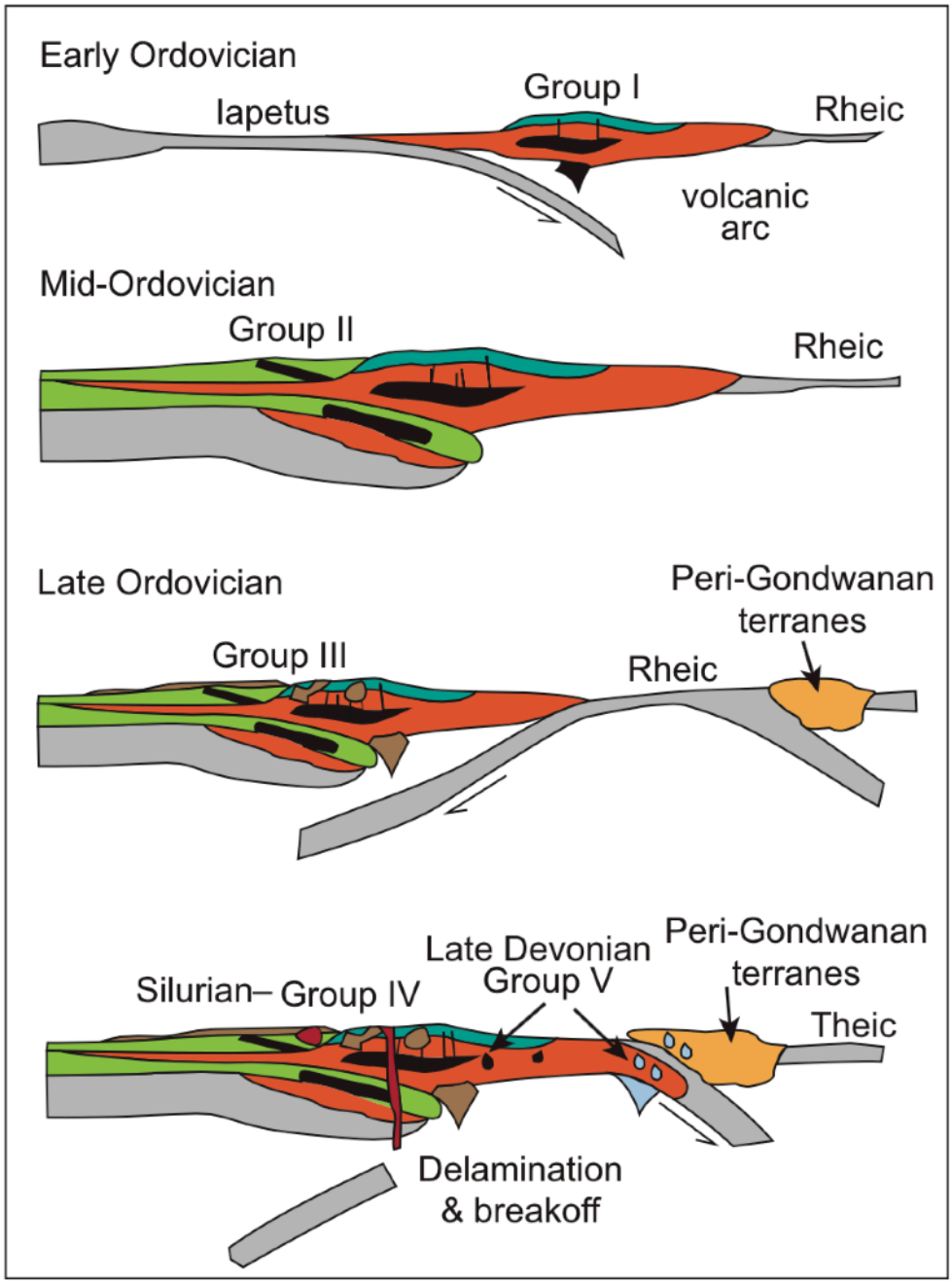

Figure 1-3: A geodynamic reconstruction of Central Appalachian tectonics. Carolinia is part of the "Peri-Gondwanan" terranes shown to collide with Laurentia after the Silurian (after Sinha et al., 2012).

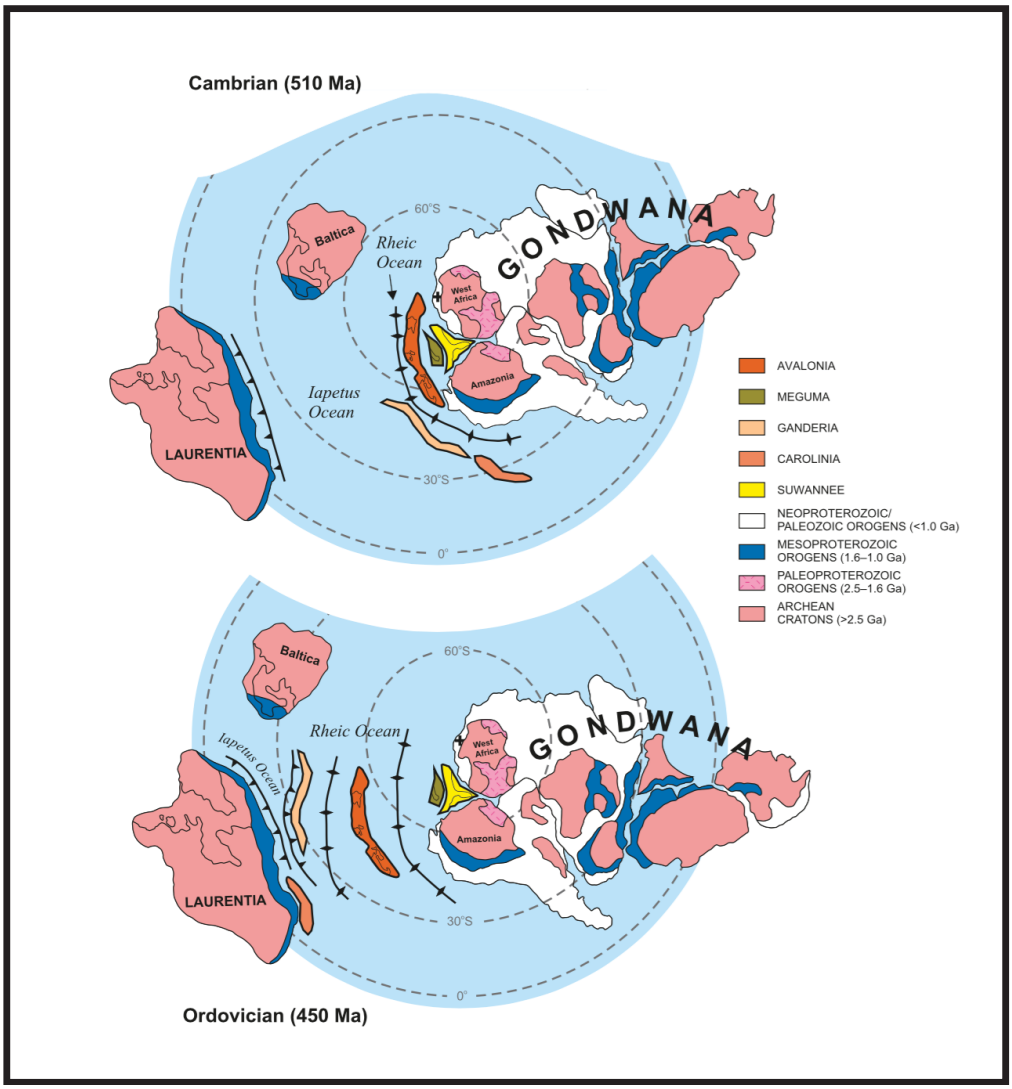

Figure 1-4: A paleogeographic reconstruction of the southern hemisphere outlining the accretion of peri-Gondwanan terranes onto Laurentia (after Pollock et al., 2012).

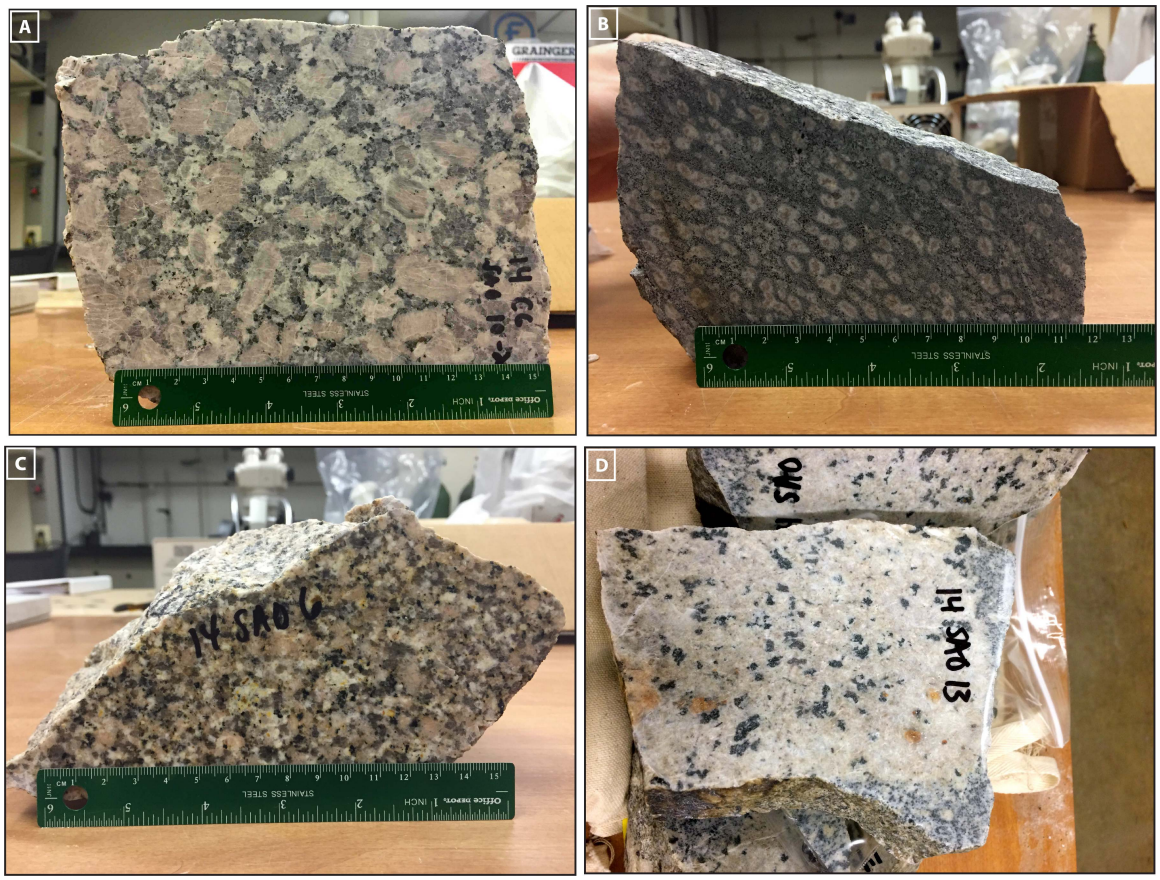

Figure 1-5: Representative hand samples from the plutons of this study: A) porphyritic Danburg granite, B) mafic enclaves within the Danburg granite C) equigranular Sandy Hill granite D) Delhi syenite.

CHAPTER 2: METHODS

2.1 Field Sampling

Twelve samples were identified for focused petrographic and geochemical characterization. These comprise three representative rocks from the Sandy Hill intrusion, one representative sample from the Danburg pluton, four enclaves representative of the textural diversity observed in the field, and two samples from the Delhi pluton that were prepared for whole rock geochemistry. Samples of the Danburg pluton were collected on site in northeast Georgia (Lincoln and Wilkes counties) from a currently inactive quarry (Figure 2-1). Representative samples of both the granite and mafic enclaves were selected from fresh blocks that had been mined from the quarry face. Samples of the Sandy Hill intrusion were collected from outcrops near the Danburg quarry. The Delhi samples were provided by Dr. Douglas Dvoracek of the University of Georgia, since the outcrop is currently on private land and access to the outcrop was restricted (Table 2-1) (Figure 1-5). Twelve billets were cut from the samples using rotary diamond saws, and thin sections were prepared by Spectrum Petrographics.

2.2 Whole Rock Geochemistry

In preparation for whole rock geochemistry, samples were progressively crushed to gravel sized chips and then pulverized for 3 minutes using a tungsten-carbide mill. The resulting powders were fused into glass discs (32 mm diameter) using a Li-borate flux (50% $Li_2B_4O_7$ 50% $LiBO_2$) with a flux:sample ratio of 3:1. A non-wetting agent, lithium iodide (LiI), was also added. Each bead was prepared using an 11 minute cycle on a

single burner XRF-Scientific Phoenix Fusion Machine. Glass beads were analyzed for for SiO_2, TiO_2, Al_2O_3, FeO, MnO, MgO, Ca_2O, Na_2O, K_2O, P_2O_5, and trace elements Ba, Rb, Sr, Y, Zr, Nb, and Ce. Analyses were conducted on the Rigaku Supermini200 at Ohio University and using the Fundamental Parameters (FP) method and calibrated against 12 USGS rock standards. GSP-2 (granodiorite) was used as the running standard throughout analysis. Based on the repeated analyses of the standard, relative uncertainty for element oxides is typically better than 1-2%, except for P_2O_5 and NaO (<5%). Relative uncertainty for Ba, Rb, Zr, and Nb was better than 10%. These are comparable to the long term (~1 year) uncertainties obtained using the Supermini200 at OU for major and trace elements. The elements Sr, Y, and Ce had relative uncertainties ~20-30%.

2.3 SHRIMP-RG Analysis

2.3.1 Zircon Pb/U Age and Trace Element Geochemistry

Zircon U-Pb analyses were conducted on the SHRIMP-RG (reverse geometry) ion microprobe co-operated by U.S. Geological Survey and Stanford University in the SUMAC facility at Stanford University between 5/15/2014-5/19/2014. Samples were progressively broken down to gravel size chips that were crushed to sand-size using a tungsten-carbide mill. The sand was sieved to separate particles >355 microns to assist in heavy liquid separation. The powders were washed with distilled water and dried under heat lamps. Zircon grains were concentrated by heavy mineral separation processes using methylene iodide (MI; density = 3.32 g/cm^3). Afterwards, the zircons were hand selected for purity, mounted on double-sided tape on glass slides in ~1 x ~6 mm rows, cast in a 25

mm diameter by 4 mm thick epoxy disc, ground, and polished to a 1 micron finish. All grains were imaged with transmitted light and reflected light on a petrographic microscope, with the addition of scanning electron microscopy — cathodoluminescence (SEM CL) on a JEOL 5600 SEM at Stanford University to identify internal structure, inclusions, possible identification of cores, and physical defects.

For mounts SAO-1, SAO-2, and SAO-4, secondary ions were sputtered from the target spot using an O_2^- primary ion beam, which was accelerated at 10 kV and had an intensity varying from 2.6 to 3.4 nA. The primary ion beam spot had a diameter between 20-24 microns and an anticipated depth of ~2-3 microns for the analyses performed in this study. Before every analysis, the sample surface is cleaned by rastering the primary beam for 60 seconds, and the primary and secondary beams were auto-tuned to maximize transmission. The duration of procedure typically required 2.5 minutes prior to data collection. The acquisition routine includes analysis of $^{30}Si^{16}O^+$, $^{48}Ti^+$, $^{56}Fe^+$, $^{89}Y^+$, $^{155}Gd^+$, $^{172}Yb^{16}O^+$, $^{90}Zr_2{}^{16}O^+$, $^{180}Hf^{16}O^+$, $^{204}Pb^+$, a background measured at 0.046 mass units above the $^{204}Pb^+$ peak, $^{206}Pb^+$, $^{207}Pb^+$, $^{208}Pb^+$, $^{238}U^+$, $^{232}Th^{16}O^+$, and $^{238}U^{16}O^+$. Trace element measurements (Ti-Hf) are measured briefly (typically 0.5-2 sec/mass) immediately before the geochronology peaks, and in mass order. All peaks are measured on a single EPT® discrete-dynode electron multiplier operated in pulse counting mode with 5 scans (peak-hopping cycles) through the mass sequence from 46 through 254. The counting times on each peak are varied according to the sample age and the U and Th concentrations to improve counting statistics and age precision, or to maximize sample throughput where high-precision necessary. Measurements were made at mass resolutions of M/DM =

9,200-9,600 (10% peak height), which fully separates interfering molecular species, particularly for the REE, from the isotope of interest. The high-abundance sensitivity and high mass resolution of the SHRIMP-RG, in addition to HCl washing of the mount and rastering the area before data is collected, assures that the background count-rates are low and any counts found at mass of $^{204}Pb^{+}$ are actually from Pb in the zircon and not surface contamination. In practice greater than 95% of the spots analyzed have no common Pb.

For mounts SAO-1, SAO-2, and SAO-4, zircon concentration data for Ti, Fe, Y, Gd, Yb, Hf, U, and Th and all of the measured trace elements were standardized against well-characterized, homogeneous in-house zircon standards MADDER, which is calibrated relative to MAD-green (4196 ppm U, Barth and Wooden, 2010). MADDER was co-mounted with unknowns on each mount and measured during each analytical session. Calculated model ages for zircon are standardized relative to Temora-2 (416.8 Ma; Black et al., 2004), which was analyzed every 4th analysis throughout the duration of the analytical. Data reduction for geochronology follows the methods described by Williams (1997), and Ireland & Williams (2003), using the Microsoft Excel add-in programs Squid2.51 and Isoplot3.764 of Ken Ludwig (2009; 2012). U-Pb calibration constant for zircon was calculated based on the variation of *ln*(UO/U) vs. *ln*(Pb/U) of the standard Temora-2 measured during the analytical session, with a fixed slope of 2. The measured $^{206}Pb/^{238}U$ was corrected for common Pb using ^{207}Pb, whereas $^{207}Pb/^{206}Pb$ was corrected using ^{204}Pb. The common-Pb correction was based on a model Pb composition from Stacey and Kramers (1975) and no additional error was propagated from the uncertainty in the model common-Pb composition. All reported $^{206}Pb/^{238}U$ model ages

and uncertainties for individual analyses include error summed in quadrature from the external reproducibility (1σ SD) of the standard Temora-2 during each individual analytical session (16-24 hours). The calculated weighted mean model ages and/or calculated intercept ages on Concordia plots are reported at 2σ (standard error) and include uncertainty propagated from the standard error of the mean for the calculated calibration constant (0.20%, 0.26%, 0.24%, and 0.21% (1σ) for SAO-1.1, SAO-1.2, SAO-2, and SAO-4, respectively), which is derived from the reproducibility of the standards (mount SAO-1 was analyzed during two analytical sessions).

Data reduction for the trace element concentrations are performed in MS Excel. Average count rates of each element of interest are ratioed to the appropriate high mass normalizing species (see above) to account for any primary current drift, and the derived ratios for the unknowns are compared to an average of those for the standards to determine concentrations. Spot to spot precisions (as measured on the standards) vary according to elemental ionization efficiency and concentration. For the MADDER zircon, precisions generally range from ±6%, 4%, 11%, 7%, 3%, 7%, 2%, and 11% for Ti, Fe, Y, Gd, Yb, Hf, U, and Th, respectively (all values at 1σ standard deviation).

2.3.2. Titanite Pb/U Age and Trace Element Geochemistry

Titanite U-Th-Pb analyses were conducted on the SHRIMP-RG (reverse geometry) ion microprobe co-operated by U.S. Geological Survey and Stanford University in the SUMAC facility at Stanford University between 05/14/2014 and 05/15/2014. Titanite grains were concentrated using the same procedures outlined for

zircon in the previous section. Imaging and preparation for SHRIMP-RG analyses also followed the same procedures as outlined above.

For titanite analyses, secondary ions are sputtered from the target spot using an O^- primary ion beam, which was accelerated at 10 kV and had an intensity varying from 6.4 to 6.6nA for mount number CG-SAO3. The primary ion beam spot had a diameter between 23-26 microns and a depth of ~1-3 microns. Before every analysis, the sample surface is cleaned by rastering the primary beam for 60 seconds, and the primary and secondary beams were auto-tuned to maximize transmission. The duration of procedure typically required 2.5 minutes prior to data collection. The acquisition routine includes analysis of $^{89}Y^+$, $^{90}Zr^+$, $^{91}Zr^+$, $^{93}Nb^+$, $^{139}La^+$, $^{140}Ce^+$, $^{146}Nd^+$, $^{147}Sm^+$, $^{153}Eu^+$, $^{157}Gd^{16}O^+$, $^{178}Hf^+$, $^{163}Dy^{16}O^+$, $^{172}Yb^{16}O^+$, a high mass normalizing species ($^{40}Ca^{48}Ca^{48}Ti^{16}O_2^+$), followed by $^{204}Pb^+$, a background measured at 0.045 mass units above the $^{204}Pb^+$ peak, $^{206}Pb^+$, $^{207}Pb^+$, $^{208}Pb^+$, $^{232}Th^+$, $^{238}U^+$, $^{232}Th^{16}O^+$, $^{238}U^{16}O^+$, $^{232}Th^{16}O_2^+$, and $^{238}U^{16}O_2^+$. Trace element measurements (Y, Zr, Nb, REE, Hf) are measured briefly (typically 1 to 4 sec/mass) immediately before the geochronology peaks, and in mass order. All peaks are measured on a single EPT® discrete-dynode electron multiplier operated in pulse counting mode with 5 scans (peak-hopping cycles from mass 89 through 270). The number of scans through the mass sequence and counting times on each peak are varied according to the sample age and the U and Th concentrations to improve counting statistics and age precision.

Measurements are made at mass resolutions of $M/\Delta M$ = 8,000-8,100 (10% peak height), which eliminates interfering molecular species, particularly for the REE and Zr.

The SHRIMP-RG was designed to provide higher mass resolution than the standard forward geometry of the SHRIMP I and II (Clement and Compston, 1994). This design, in addition to the high-abundance sensitivity, high mass resolution, HCl washing of the mount, and rastering the area before data is collected, assures that the background count-rates are low and any counts found at mass of $^{204}Pb^{+}$ are actually from Pb in the titanite and not surface contamination. The SHRIMP-RG geometry also allows trace elements to be measured without the need to energy filter the secondary beam, and thus, can be routinely measured without reducing the transmission of secondary ions to improve mass resolution.

For mount SAO3, titanite concentrations data for U, Th and all of the measured trace elements are standardized against well-characterized, homogeneous titanite standards BLR-1 titanite (Aleinikoff et al., 2007), which was co-mounted on the same mount as known samples. For chondrite normalized REE's, values from McDonough & Sun (1995) were used. Calculated model ages for titanite are standardized relative BLR-1 ($^{206}Pb/^{238}U$ age = 1047 Ma; Aleinikoff et al., 2007), which were analyzed every 5th analysis throughout the duration of the analytical session. Data reduction for geochronology follows the methods described by Williams (1997), and Ireland & Williams (2003), and uses the MS Excel add-in programs Squid2.51 and Isoplot3.76 of Ludwig (2003; 2012). The measured $^{206}Pb/^{238}U$ was corrected for common Pb using ^{207}Pb, whereas $^{207}Pb/^{206}Pb$ was corrected using ^{204}Pb. The common-Pb correction was based on a model Pb composition from Stacey and Kramers (1975). No addition error is propagated for the uncertainty in the common Pb composition. All reported $^{206}Pb/^{238}U$

and $^{207}Pb/^{206}Pb$ model ages and uncertainties (2σ) include error summed in quadrature from the external reproducibility (1σ SD) of the standard R33 or Temora during an individual analytical session (16-24 hours). The 1σ standard error of the mean for the reproducibility of the standards was 0.20%, 0.42% and 0.32% for BMC62, BMC63, and BMC64, respectively, which is also propagated into the final calculated $^{206}Pb/^{238}U$ weighted mean age.

Data reduction for the trace element concentrations are performed in MS Excel. Average count rates of each element of interest are ratioed to the appropriate high mass normalizing species (see above) to account for any primary current drift, and the derived ratios for the unknowns are compared to an average of those for the standards to determine concentrations. Spot to spot precisions (as measured on the standards) vary according to elemental ionization efficiency and concentration. For the MADDER titanite, precisions generally range from about ±3% for Hf, ±5-10% for the Y and HREE, ±10-15%, and up to ±40% for La which is present most often at the ppb level (all values at 2σ).

Ages were reached by quantifying ratios of $^{206}Pb/^{238}U$ and $^{207}Pb/^{235}U$, respectively and applying the basic decay equation:

(Equation 1) $$\left[\frac{^{206}Pb}{^{204}Pb}\right]_m = \left[\frac{^{206}Pb}{^{204}Pb}\right]_i + \frac{^{238}U}{^{204}Pb}(e^{\lambda_1 t} - 1)$$

$$^{238}U = \lambda_1 = 1.55125 \times 10^{-10}$$

(Equation 2) $$\left[\frac{^{207}Pb}{^{204}Pb}\right]_m = \left[\frac{^{207}Pb}{^{204}Pb}\right]_i + \frac{^{235}U}{^{204}Pb}(e^{\lambda_2 t} - 1)$$

$$^{235}U = \lambda_2 = 9.8485 \times 10^{-10}$$

An established decay constant unique to each system, the initial isotopic ratio of $^{207}Pb/^{204}Pb$ and $^{206}Pb/^{204}Pb$, as well as the measured ratio of $^{207}Pb/^{204}Pb$ and $^{206}Pb/^{204}Pb$ are used within the decay equation to calculate an age (Faure and Mensing, 2005). The initial lead compositions (Pb present at the time of crystallization) are quantified using counts of ^{204}Pb, which is naturally occurring and not produced by radiogenic decay. Measured ratios are present on Tera-Wasserburg concordia plots on which $^{238}U/^{206}Pb$ is on the x-axis and Pb isotopic composition ($^{207}Pb/^{206}Pb$) is on the y-axis. This iteration has several advantages for Phanerozoic-aged rocks: (1) measured values are directly plotted rather than having to calculate derivative values via the isotopic composition of U; (2) the errors in measuring $^{207}Pb/^{206}Pb$ and $^{238}U/^{206}Pb$ are much less correlated than in $^{238}U/^{206}Pb$ and $^{235}U/^{207}Pb$, thus regression analysis is easier; (3) visually more suited to younger rocks due to curvature of Concordia (Williams, 1998). Additionally, classical one-parameter, error-weighted average plots were made for each zircon and titanite population. These plots were created using IsoPlot v.3.764, a plotting and regression program used for radiogenic-isotope data in conjunction with Excel (Ludwig, 2012). The mean squared weighted deviate (MSWD) is reported with all graphs and is used to evaluate scatter within a dataset. A MSWD of ~1 means that scatter of the data is equal to that predicted from the analytical errors, greater than 1 results from excess scatter, while less than 1 results from less than predicted scatter.

2.4 Accessory Mineral Thermobarometry

Ti-in-zircon temperatures were calculated using the equation (Eq. 3) of Watson and Ferry (2007), Ti concentrations in zircon measured by SHRIMP-RG, and assuming the activity of $TiO_2 = 0.7$ and $SiO_2 = 1.0$. The values obtained are presented in Appendix A1. Due to the absence of rutile within these samples, the activity of TiO_2 is known to be less than 1, but the presence of titanite is interpreted to indicate an activity ~0.7 following the procedure of Fu et al. (2008). SiO_2 activity is equal to 1 at the time of zircon crystallization based on the presence of coexisting quartz.

(Equation 3) $$T = \frac{4800}{5.711 + \log a_{TiO_2} - \log a_{SiO_2} - \log \mathrm{Ti(ppm)}}$$

Zr-in-titanite thermobarometry was applied using the equation (eq. 4) from Hayden et al. (2008). Pressure was calculated by inserting the resulting temperature from the Ti-in-zircon thermometer for the same rock and using measured zirconium concentrations acquired simultaneously with Pb/U isotopes in titanite.

(Equation 4) $$P = \frac{T(10.52 - \frac{7708}{T} - \log a_{TiO_2} - \log a_{SiO_2} - \log \mathrm{Zr(ppm)}}{960}$$

Figure 2-1: Photo of the Danburg quarry located in NE Georgia. Currently, it is inactive, yet has been actively mined in the past. The Danburg pluton is host to mafic enclaves (1-2%) and is bordered by the Sandy Hill granite.

Table 2-1. Sample location and summary descriptions.

Sample	Latitude	Longitude	Location	Pluton	Major Mineralogy	SiO_2 (wt.%)	Zrn	Ttn	QAP Classification
14CG-SAO-6	33.84611	82.65215	Outcrop	Sandy Hill	Qtz, Pl, Afs, Ms, Bt	75.9	yes	—	Monzogranite
14CG-SAO-7	33.84575	82.65161	Outcrop	Sandy Hill	Qtz, Afs, Pl, Ms, Bt	74.5	yes	—	Monzogranite
14CG-SAO-8	33.84729	82.65249	Outcrop	Sandy Hill	Afs, Pl, Qtz, Ms, Bt	74.5	yes	—	Monzogranite
14CG-SAO10-2	33.88533	82.64576	Quarry	Danburg	Afs, Pl, Qtz, Bt, Ms	69.2	yes	yes	Monzogranite
14CG-SAO10-1	33.88533	82.64576	Quarry	Danburg (enclave)	Pl, Bt, Qtz, Hbl, Afs, Ttn	53.6	—	yes	Quartz Monzodiorite
14CG-SAO10-5A	33.88533	82.64576	Quarry	Danburg (enclave)	Afs, Pl, Qtz, Bt, Ms, Ttn	64.2	yes	yes	Monzogranite
14CG-SAO10-5B	33.88533	82.64576	Quarry	Danburg (enclave)	Pl, Afs, Bt, Qtz, Hbl, Ttn	55.3	—	yes	Quartz Monzodiorite
14CG-SAO10-5C	33.88533	82.64576	Quarry	Danburg (enclave)	Pl, Bt, Afs, Qtz, Hbl, Ttn	58	—	yes	Quartz Monzonite
14CG-SAO12	33.92622	82.680122	Quarry	Delhi	Afs, Pl, Hbl	63.6	yes	—	Syenite
14CG-SAO13	33.92622	82.680122	Quarry	Delhi	Afs, Pl, Hbl, Qtz	62.5	yes	—	Syenite

CHAPTER 3: RESULTS

3.1 Descriptive Petrography

Point counts were performed on eleven thin sections from the Danburg granite and contained enclaves, Sandy Hill granite, and Delhi syenite for the purpose of classification using the ternary QAP system (Streckeisen, 1975) (Figure 3-1). A summary of the modal mineralogy, and normalized proportions of quartz, alkali feldspar, and plagioclase is provided for each thin section in Table 3-1.

Samples 14CG-SAO6, 7, 7-2, 8 — Sandy Hill monzogranites

In hand sample, the Sandy Hill has a pinker hue in comparison with the Danburg granite. It is very coarse grained, with some alkali feldspar, plagioclase, and quartz grains reaching 6mm. The plagioclase composition was optically determined and ranges from An_0-An_{16}. In contrast to samples from the other plutons studies, muscovite is the prominent mica and exists as euhedral grains up to 5 mm in length. The only mafic mineral present is biotite, occurring in trace to low abundances (0.0-4.7%). Apatite is present in trace amounts (<0.5%). Alteration minerals chlorite and sericite are present. In some feldspars, clusters of muscovite inclusions exist.

Sample 14CG-SAO10-2 — Representative sample of Danburg monzogranite

This sample is coarsely crystalline. Feldspars commonly exhibit rapakivi texture, in which alkali feldspar crystals are rimmed with plagioclase (Sederholm, 1891). These rapakivi feldspar phenocrysts can be up to 3 cm in length; however,

most range from 3-5 mm (Figure 3-2). The plagioclase composition was optically determined to range from An_5-An_{35}. Plagioclase was typically found to be normally zoned, becoming more Na-rich towards the rim, and occasionally show oscillatory zoning. The rock has experienced some alteration, evident by the presence of chlorite and the sericitization of the feldspars. The only mafic mineral present is biotite, which comprise 14.2% of the sample and exist as large (~1.5mm) sub to euhedral crystals. Myrmekite texture, or the intergrowth of quartz in plagioclase, is also seen confirming alteration. Large (~1mm), sub to euhedral titanite crystals as well as magmatic epidote is notable. Muscovite is present but only in trace amounts. Apatite crystals exhibit a needle-like habit.

Sample 14CG-SAO10-1 — Danburg granite - mafic enclave

This sample is a quartz monzodiorite that is phaneritic, yet has a smaller average grain size (0.1-0.5mm) than its host (1-5 mm) although phenocrysts of alkali feldspar, plagioclase, and quartz exist up to 4.5mm. The quartz within the enclave is largely interstitial to the other grains. The feldspars are dominated by plagioclase, optically measured to range from An_{14-18}. Zonation of the feldspars is not as prominent as in the host granite. Titanite is present within this and other enclaves as optically continuous, anhedral or skeletal grains (Figure 3-3). Biotite (15.2%) and hornblende (8%) make up the mafic portion of this enclave. They generally are found in clusters, and thus the modal proportions vary. The mafic phases appear to define a concentric orientation along the periphery of the large titanite crystals (Figure 3-4).

Many grains are rich in acicular apatite inclusions. Alteration minerals chlorite and sericite are present.

Sample 14CG-SAO10-5A Mafic enclave, Danburg granite

This sample is a monzogranite. Macroscopically, it is the lightest in terms of color of the sampled enclaves. This is reflected in its mineralogy. The titanites and associated depletion haloes are still observed, yet are smaller and less distinct than the other enclaves. This sample is dominated by interlocking grains of plagioclase, alkali feldspar, and quartz with biotite grains randomly assorted. The plagioclase composition could not be confidently determined due to a lack of plagioclase grains suitable for the Michel-Levy method. The only mafic mineral present is biotite (13%). This enclave lacks hornblende, which is present in other enclaves examined in this study. Titanite grains are present, yet are as not as large nor do they exhibit the pronounced skeletal texture as in other enclaves. Alteration is evident as myrmekite texture, chlorite, and sericite.

Samples 14CG-SAO10-5B,C Enclaves, Danburg granite

These two enclaves are of the same textural variety and are thus described together. However, slight differences in modal mineralogy are observed, and they are classified differently; 14CG-SAO10-5B is quartz monzodiorite, while 14CG-SAO10-5C is quartz monzonite. Macroscopically these are darkly colored with titanite (1-3mm) distributed throughout the enclave. In hand sample, titanite is surrounded by

pronounced Fe-depletion haloes (Figure 3-4), in which mafic minerals are absent. Hornblende is present in these enclaves, is generally finer-grained than the biotite, and most commonly occur as elongate grains in clusters. These enclaves have a grain size comparable to 14CG-SAO10-1 (0.1-0.5mm) with large feldspar (6mm) and titanite (2.5mm) phenocrysts. Both chlorite and sericite are present.

Sample 14CG-SAO10-6 Mafic enclave, Danburg granite

This sample is an especially small (~5 cm) enclave showing three distinct textural domains (Figure 3-5). One zone consists of a large 1.5 cm, rapakivi feldspar among a few other mineral grains (biotite, titanite). The second separate area is strikingly similar to sample 14CG-SAO10-2 (Danburg). It is coarse grained, dominated by feldspar, biotite, and euhedral titanite. The third domain is texturally unique in comparison to the rest of the enclaves. It has an equigranular, almost granoblastic texture that is finer than the other two zones. The minerals that dominate are plagioclase, quartz, and biotite. Titanite exist in this zone as well; however, they exhibit the anhedral, skeletal habit. Phenocrysts of alkali feldspar interrupt this equigranular texture. Hornblende is noticeably absent in this thin section. Acicular apatite is present across all three domains. The fine and coarse grained zones are separated by a clear margin from one zone to the next. Alteration minerals chlorite and sericite are present.

Samples 14CG-SAO12,13 — Delhi syenite

The Delhi is phaneritic, yet has small zones of finer grain size. Two samples were used for thin section analysis. Due to their similarity this description will encompass both. Coarse (5 mm) alkali feldspar dominates the samples with lesser plagioclase and little to no quartz. Two plagioclase compositional populations exist with an average of An_{16} and An_{8}. Perthitic texture is very common throughout both thin sections. The mafic minerals are biotite and amphibole. The amphiboles are large, vibrant green to turquoise and thus are likely hornblende and riebeckite, the sodium end-member of the amphibole group (Figure 3-6). Accessory phases zircon and apatite are present. Alteration minerals sericite and chlorite exist.

3.2 Whole Rock Geochemistry

Geochemistry results are compiled in Table 3-2 along with CIPW normative mineralogy of the samples. The results are plotted on Harker-style variation plots and granitoid classification schemes defined by Frost et al., (2001) (Figure 3-7, 3-8).

Overall, the Danburg, included enclaves, and Sandy Hill samples define a compositional suite that increases in SiO_2 content from the enclaves (53.6 wt.%) to the Sandy Hill granite (75.9 wt.%) with the Danburg granite plotting in between (69.2 wt.%) (Figure 3-7). When plotted against SiO_2, the major elements of the Danburg granite, included enclaves, and the Sandy Hill granite, generally define broadly linear trends. Fe_2O_3, P_2O_5, TiO_2, CaO, Al_2O_3, MnO, and MgO versus SiO_2 define trend lines with a negative slope. K_2O and Na_2O are not as well correlated. The three Sandy Hill

samples exhibit similar compositions and cluster together at the high-SiO_2 end. The Danburg sample (14CG-SAO10-2) is the median value in all major elements except K_2O and Na_2O.

The classification schemes proposed by Frost et al. (2001) and later refined by Frost and Frost (2008) focus solely on the elemental chemistry within a rock by implementing four separate parameters:

(1) The Fe-number is defined as $Fe^* = [FeO^{tot} / (FeO^{tot} + MgO)]$ against wt. % SiO_2. It conveys information about the differentiation history of a granitic magma and subsequently categorizes the rock as either ferroan or magnesian.

(2) The modified alkali lime index is defined as $MALI = (Na_2O+K_2O+CaO)$ against wt. % SiO_2. It conveys information regarding the abundances and compositions of feldspars in a rock, and is used to categorizes the rock as either alkalic, calcic, calc-alkalic, or alkalic-calcic.

(3) The aluminum saturation index (ASI) is defined as the molecular ratio [Al/(Ca - 1.67P + Na + K)] against wt.% SiO_2. It conveys information regarding the micas and minor minerals in a rock and subsequently used to categorize the rock as peraluminous or metaluminous

(4) The alkalinity index is defined as AI = the molecular ratio [Al - (Na + K)] against wt.% SiO_2. It conveys information regarding the relative abundances of aluminum and alkalis and subsequently allows a rock to be categorized as peralkaline or metaluminous/peraluminous.

The combination of these four schemes assists in dividing the spectrum of granitoid compositions into 14 common groups. These groups correspond to one of four tectonic environments: Cordilleran, Ferroan, Caledonian, and Himalayan (Frost and Frost, 2008).

Results of the granite classification scheme of Frost et al. (2001) are presented in Figure 3-8 and Table 3-3. Overall, the geochemistry of the suite of rocks studied is most consistent with Caledonian granites. These granites are typical of post-collisional tectonics whereby late anatexis of crust is expressed as numerous granitic plutons. Caledonian rocks are typically K-rich, as these are. Frost and Frost (2008) shows the four granitoid classifications often follow a differentiation path on a QAP diagram. The spread of rocks seen in Figure 3-1 follow a trend of potassic evolution as reported for Caledonian granite suites. The ferroan and alkalic nature typical of the enclaves has implications regarding its possible source.

The element geochemistry for the two Delhi whole-rock samples are compiled in Table 3-2. These two samples do not follow the compositional trend defined by the Danburg-Sandy Hill suite (Figure 3-7, 3-8). The Delhi is enriched in the alkalis relative to its calcium content and iron relative to its magnesium content. Frost and Frost (2008) expanded their classification to further classify alkaline rocks. It utilizes both whole rock geochemistry and CIPW normative mineralogy (Table 3-2). The two Delhi syenite samples classify as metaluminous, silica-saturated quartz-bearing rocks though they are close to the peralkaline boundary (Table 3-3), and are most consistent

with the ferroan classification of granitoids. In a K_2O vs SiO_2 plot, the Delhi samples plot as highly shoshonitic (Figure 3-9).

3.3 U-Pb Geochronology

The zircons from the Danburg granite, associated mafic enclaves, and Sandy Hill granite are subhedral to euhedral, largely prismatic and tabular in habit, and range from ~200-500μm. Zoning is apparent in most populations but is not observed in the CL-black grains of 14CG-SAO7. Oscillatory zoning is seen in the majority of the Danburg, enclave, and Sandy Hill zircons, especially in the outer edges. This textural feature is indicative of a magmatic origin. Patchwork zoning is evident in both the Danburg and enclave zircons. Cores were identified based on zoning discontinuities; however, analyses on both the core and rim of the same zircon showed no pattern of discernible age difference. The Delhi zircons are morphologically different, being more rounded and equant, and largely unzoned (Figure 3-10).

The titanite populations consist primarily of broken pieces of crystals that occasionally exhibit sector-type zoning. The skeletal habit seen in thin section is again observed in SEM-BSE images of the enclaves where that is a common texture (Figure 3-11). It is not observed in the titanites separated from the Danburg, as expected.

U-Pb isotope concentrations were collected for 86 individual zircon grains from seven separate samples and 36 titanite grains from five samples. The results are

compiled in Tables 3-5 and 3-6 (zircon data and titanite data, respectively). Trace element data for both the zircon and titanite populations were collected on the same spots, and are presented in Appendix A.

Twenty spots were analyzed from sample 14CG-SAO6. Seven of the analyses were not included in the final age calculation (Figure 3-12). Four of the seven had high iron content (72.9 - 224ppm; Appendix A) which may reflect overlap of the beam onto an inclusion or crack that may also be sourced of common Pb. The analyses were examined visually using post-analysis imaging, where it was confirmed that an inclusion was hit in one grain, and cracks were overlapped in three other grains. One grain was exceptionally dark in CL, and one was a second analysis on the same grain. All these analyses were found to be discordant (Figure 3-12) and were excluded when determining the sample weighted mean age. The ^{207}Pb corrected ^{206}Pb/^{238}U crystallization age for 14CG-SAO6 is 305.1±4.3Ma.

All fifty zircons separated and mounted from 14CG-SAO7 were extremely dark in CL, which is usually an indication of high-U concentration. Eight exploratory analyses were conducted, 6 of which define a coherent population on Concordia (defining a weighted average age of 288.8±4.7Ma, MSWD = 1.6). The decay of U causes structural damage in the zircon, and at high concentrations leads to metamictization, which could facilitate open system behavior with respect to Pb. Evidence for this from these samples comes from the high-Fe content seen in the eight zircons analyzed (five have Fe concentrations ranging from 123.2ppm to 5610.7ppm). Since igneous zircon typically contain less than a few 10's ppm zircon

(Grimes et al., 2009), analyses with >100 ppm Fe are taken to have incorporated some non-zircon component or reflect altered or metamict domains that are unlikely to preserve primary igneous isotopic ratios. These grains are discordant in all cases on concordia as well, reducing the confidence in the measured ratios as solely indicative of age. All grains from this sample were therefore rejected from further age considerations. Due to the evidence for open system behavior and small sample size, 14CG-SAO7 is not included in the mean age for the Sandy Hill granite. Thirteen zircons were used to calculate the age of 14CG-SAO8 to give the sample a ^{207}Pb-corrected ^{206}Pb/^{238}U crystallization age of 304.0±5.0Ma (Figure 3-12). The ages of 14CG-SAO6 and 14CG-SAO8 are statistically indistinguishable, and they give a combined ^{207}Pb corrected ^{206}Pb/^{238}U crystallization age of 304.7±3.0Ma (MSWD = 3.2) for the Sandy Hill granite. The age is taken as the best estimate of the emplacement age for the Sandy Hill intrusion, and is slightly older than the previously reported Rb/Sr whole rock age, though the ages overlap within 2-sigma errors.

Seventeen spots from the Danburg granite (14CG-SAO10-2) were analyzed. One analysis was rejected due to high Fe content (146.2ppm). The remaining 16 analyses define a weighted average ^{207}Pb-corrected ^{206}Pb/^{238}U crystallization age of 307.0±4.7Ma (MSWD = 5.7). Additionally, eight spots were analyzed on zircon separated from the enclave 14CG-SAO10-5; these define a ^{207}Pb-corrected ^{206}Pb/^{238}U crystallization age of 292±14Ma. This age is the least well constrained, giving a wide range of nearly concordant ages from 272±4Ma — 335±6Ma (Figure 3-13). The older

ages may signify some inheritance, though it is difficult to confirm from the size of the dataset and there is no textural evidence to support this possibility.

Seventeen spots from the Delhi syenite sample 14CG-SAO12 were analyzed and resulted in a ^{207}Pb-corrected ^{206}Pb/^{238}U crystallization age of 468.9±6.7Ma. Seven zircons from the Delhi syenite sample 14CG-SAO13 were analyzed and gave a sample weighted mean ^{207}Pb-corrected ^{206}Pb/^{238}U crystallization age of 468.8±6.6Ma. Together, all 24 spots (all with <100 ppm Fe) define a weighted mean ^{207}Pb-corrected ^{206}Pb/^{238}U crystallization age of 468.9±4.8Ma (Figure 3-14). Based on this result, the Delhi syenite is demonstrably unrelated to the Alleghanian magmatic event that led to the emplacement of the Danburg-Sandy Hill suite.

Titanite populations from the Danburg granite and four enclaves gave ages broadly consistent with the zircon ages (Figure 3-15). Fifteen titanite were analyzed from the Danburg granite, giving a weighted mean ^{207}Pb-corrected ^{206}Pb/^{238}U crystallization age of 303.6±3.7Ma. Nine analyses for 14CG-SAO10-1 result in a ^{207}Pb-corrected ^{206}Pb/^{238}U crystallization age of 302.6±3.7Ma. The remaining enclaves (14CG-SAO10-5A, B, C) were grouped as a single population of 16 analyses that resulted in a ^{207}Pb-corrected ^{206}Pb/^{238}U crystallization age of 311.4±5.1Ma. If all the enclaves are considered together, they give a weighted mean ^{207}Pb corrected ^{206}Pb/^{238}U crystallization age of 307.3±3.7Ma. This age is within error of the Danburg granite age. Additionally, these ages are within error of the ages indicated using zircon analyses.

3.4 Accessory Mineral Thermobarometry

Crystallization temperatures calculated with Ti-in-zircon are compiled in Table 3-6. Temperatures were not calculated on zircon spot analyses with > 100ppm Fe because many possible rock forming minerals that contain iron (and could have been an inclusion inadvertently analyzed in zircon) also contain Ti. Ti-in zircon mean temperatures for the Sandy Hill granite samples are 805±46°C (14CG-SAO6), 767±14°C (14CG-SAO7), and 784±23°C (14CG-SAO8). The Danburg granite and enclave zircon populations resulted in equivalent average crystallization temperatures of 771±27°C and 765±50°C, respectively. The Delhi syenite samples resulted in distinctly lower Ti-in-zircon average temperatures of 676±22°C (14CG-SAO12) and 689±25°C (14CG-SAO13).

Pressures calculated using Zr-in-titanite thermobarometry are summarized alongside the temperature data in Table 3-6. Estimated crystallization temperatures were calculated using the average Ti-in-zircon crystallization temperatures from coexisting zircon in enclaves and the Danburg granite, and used along with measured Zr-concentrations in each titanite grain to result in crystallization pressures of 5.1±1.4 kb and 6.5±1.7 kb, respectively. Assuming the accessory minerals preserve conditions near depth of melt formation, and are reliably recorded in the accessory mineral thermobarometers, they can be used to estimate an average geothermal gradient under which melting occurred. From the available data, the average geothermal gradient was calculated to be ~37°C/km from the Danburg granite sample, while a gradient of

~46°C/km was calculated from the enclave. These gradients are elevated compared to the standard geothermal gradient of 25-30°C/km of continental crust.

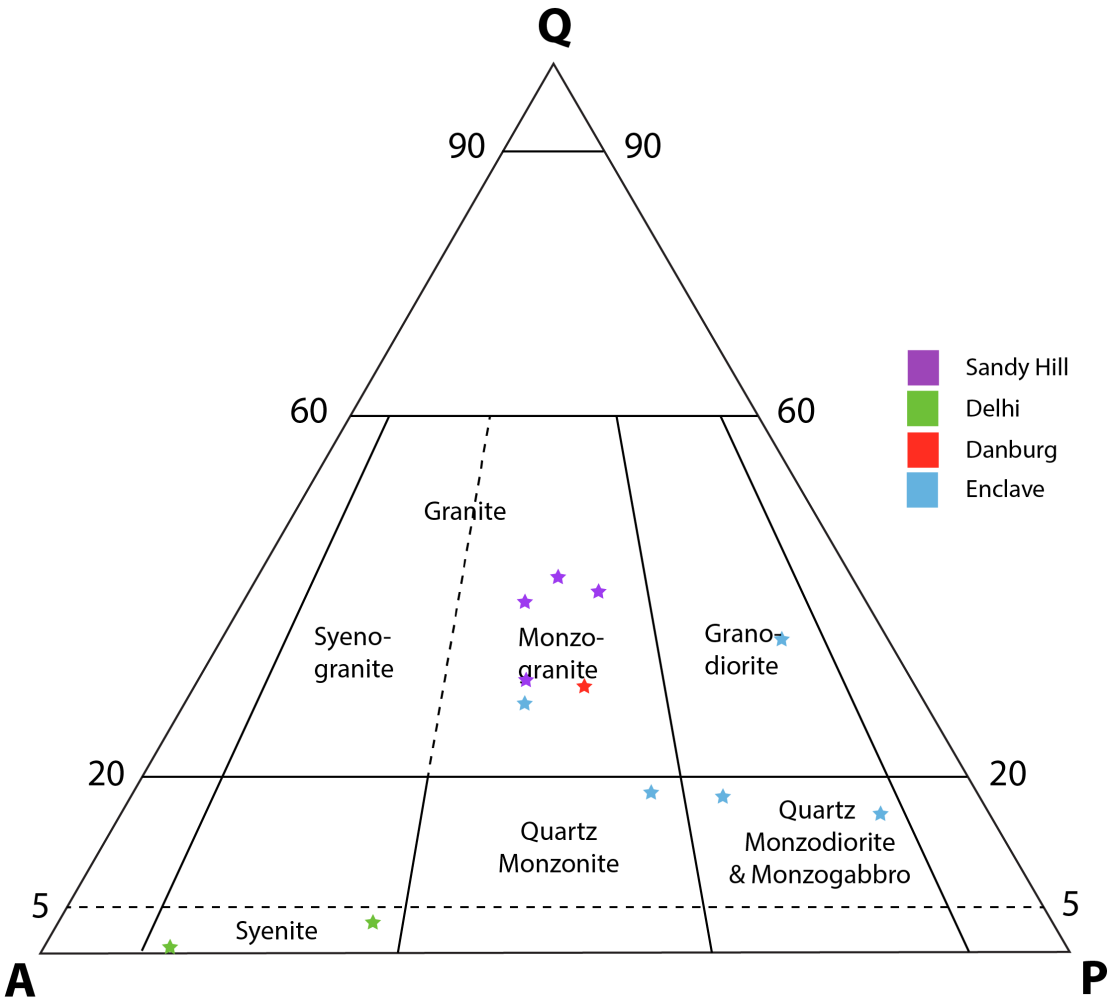

Figure 3-1: IUGS Q-A-P diagram (Streckeisen, 1975) showing modal mineralogy determined by point counting (400 counts per slide).

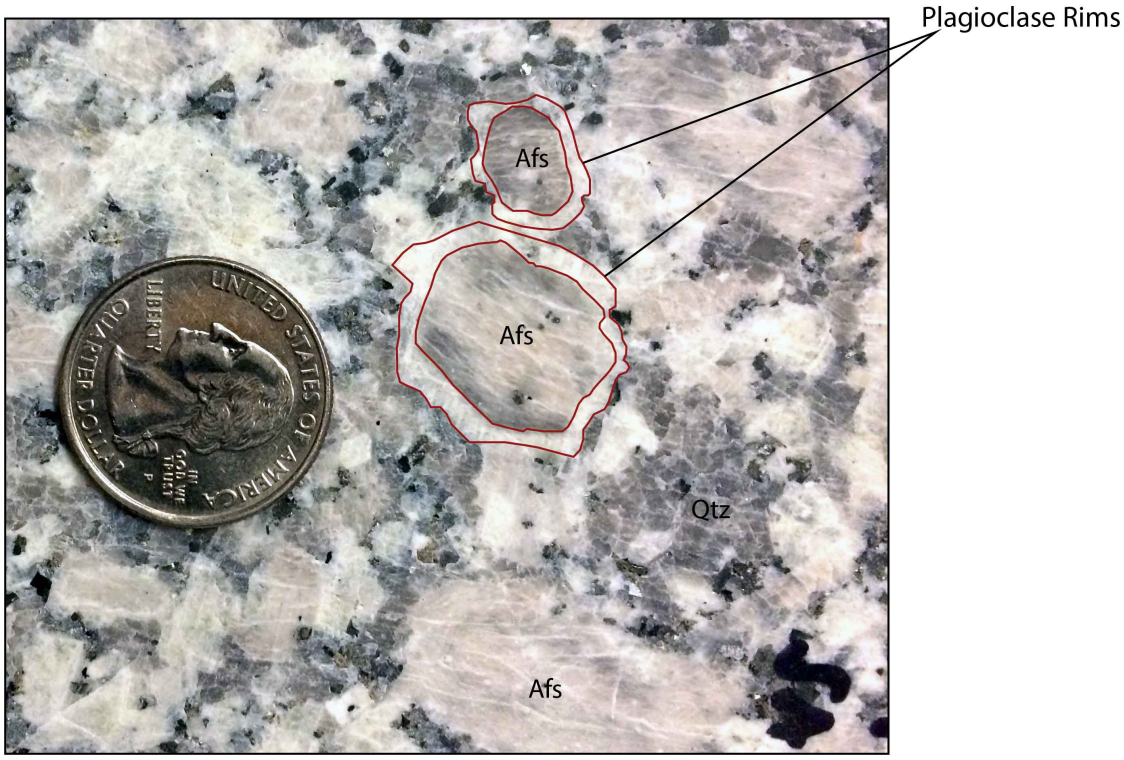

Figure 3-2: Representative photomicrograph of the Danburg granite, emphasizing feldspars with rapakivi texture. The texture is typified by ovoid alkali feldspar phenocrysts mantled by plagioclase.

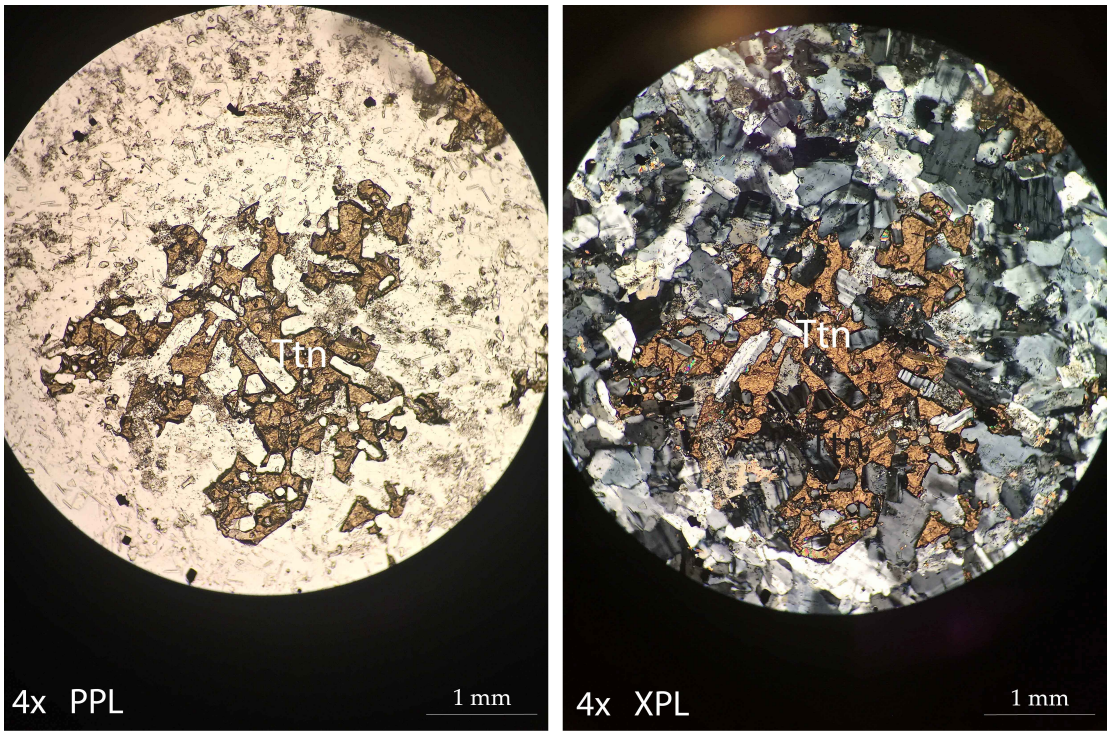

Figure 3-3: Photomicrographs depicting the anhedral, skeletal-habit of titanite within mafic enclaves identified from the Danburg pluton.

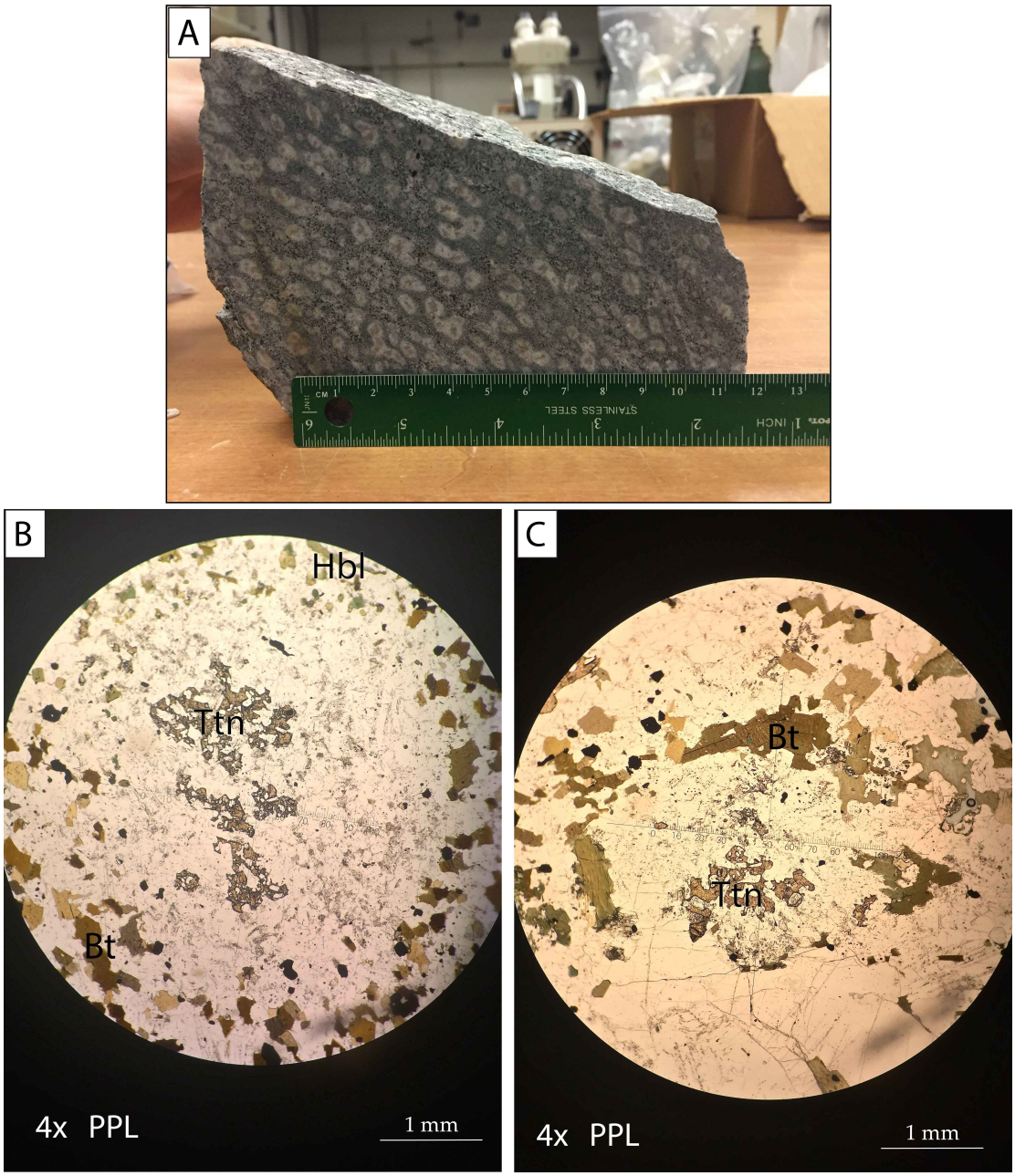

Figure 3-4: Mafic enclave sample 14CG-SAO10-5B identified in the Danburg pluton. In (A), the macroscale habit of the titanites with large depletion haloes is shown. (B) and (C) demonstrate the skeletal habit of the titanites with mafic phases appearing at the margin of the depletion halo, and in places appear to define a concentric orientation around the haloes.

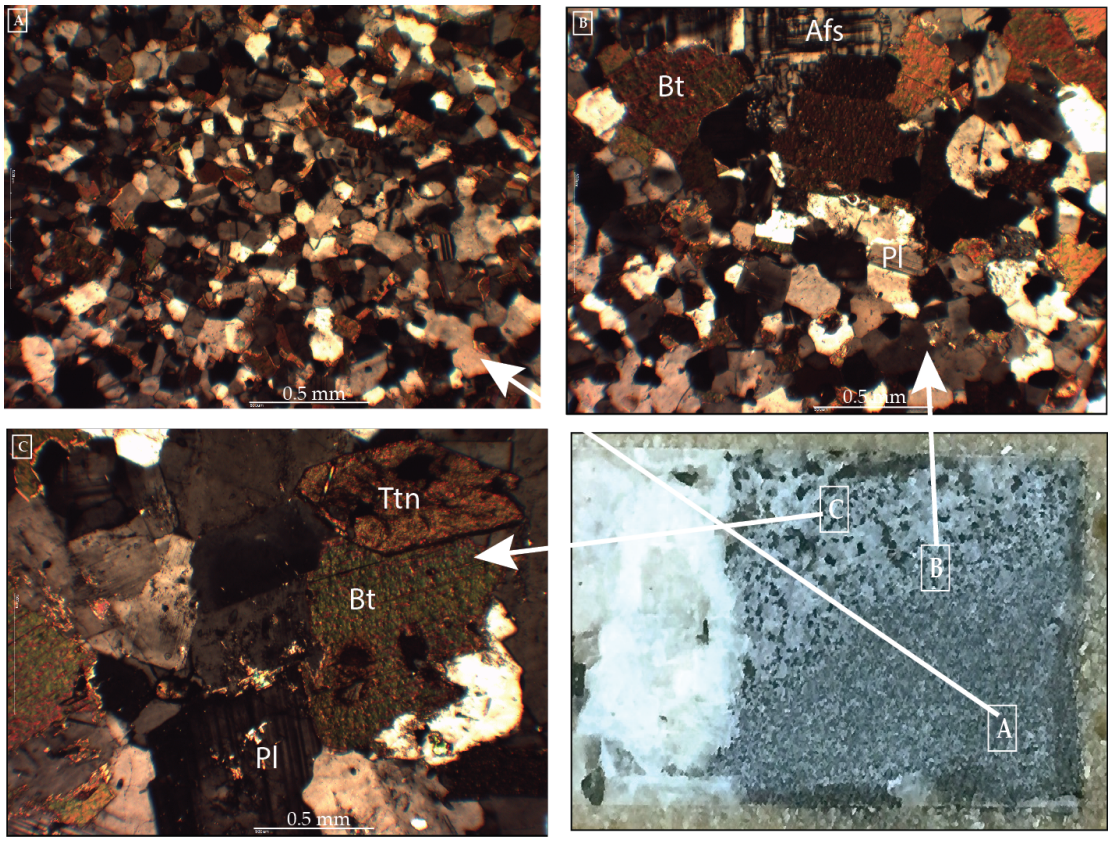

Figure 3-5: Photomicrographs of a mafic enclave identified within the Danburg pluton. Three separate domains can be distinguished by grain size. In (A), a well-developed granoblastic texture is observed in the finest-grained domain; (B) There is abrupt increase in grain size between two distinct zones, along with the appearance of alkali feldspar in the coarser domain. (C) Mineralogy is similar to host pluton.

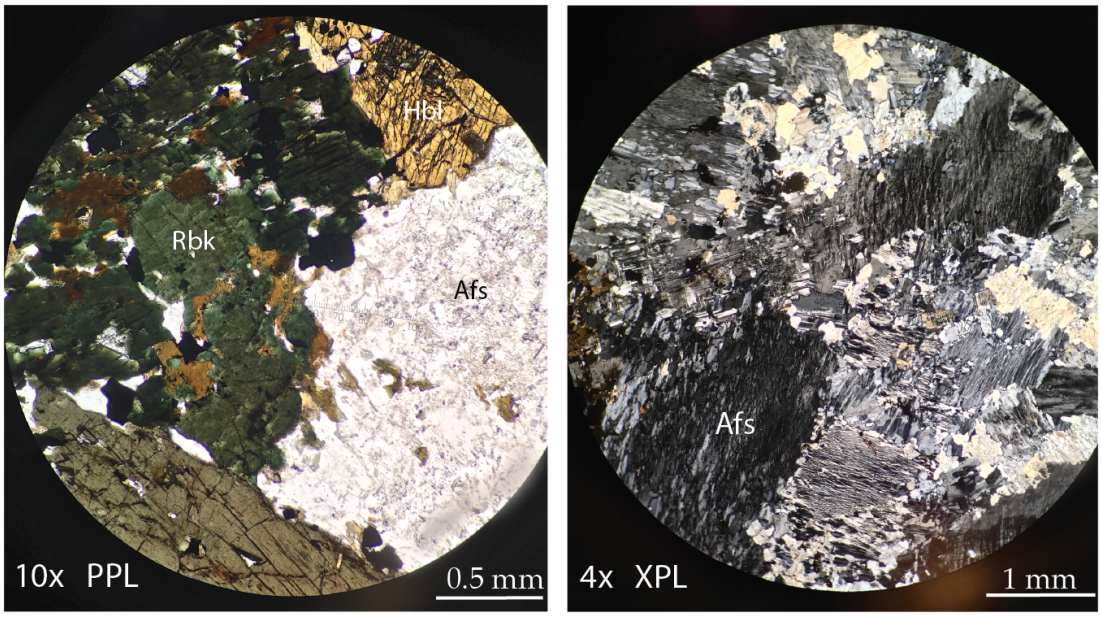

Figure 3-6: Photomicrographs showing representative texture and mineralogy in the Delhi syenite. It is dominated by alkali feldspar with lesser plagioclase. Both hornblende and riebeckite (sodium-rich amphibole) are present.

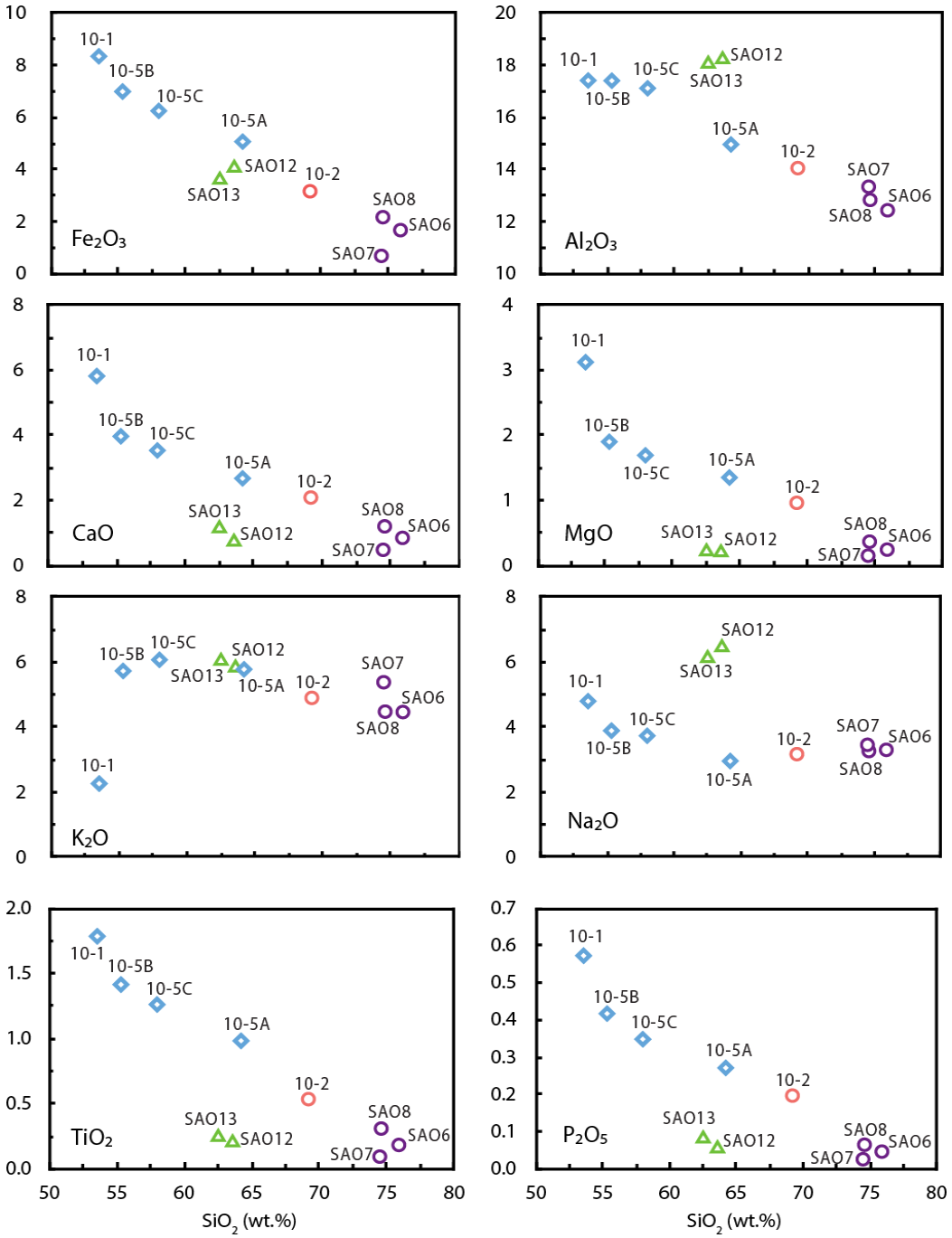

Figure 3-7: Harker diagrams plotting major element oxides of the Danburg granite, contained enclaves, the Sandy Hill granite, and the Delhi syenite against SiO_2 (wt.%). The plots show a cogenetic relationship between the Danburg granite, enclaves, and Sandy Hill granite. The Delhi syenite samples have no clear correlation with the other rocks within this study. Blue diamond – mafic enclaves, red circle – Danburg granite, purple circle – Sandy Hill granite, green triangle – Delhi syenite.

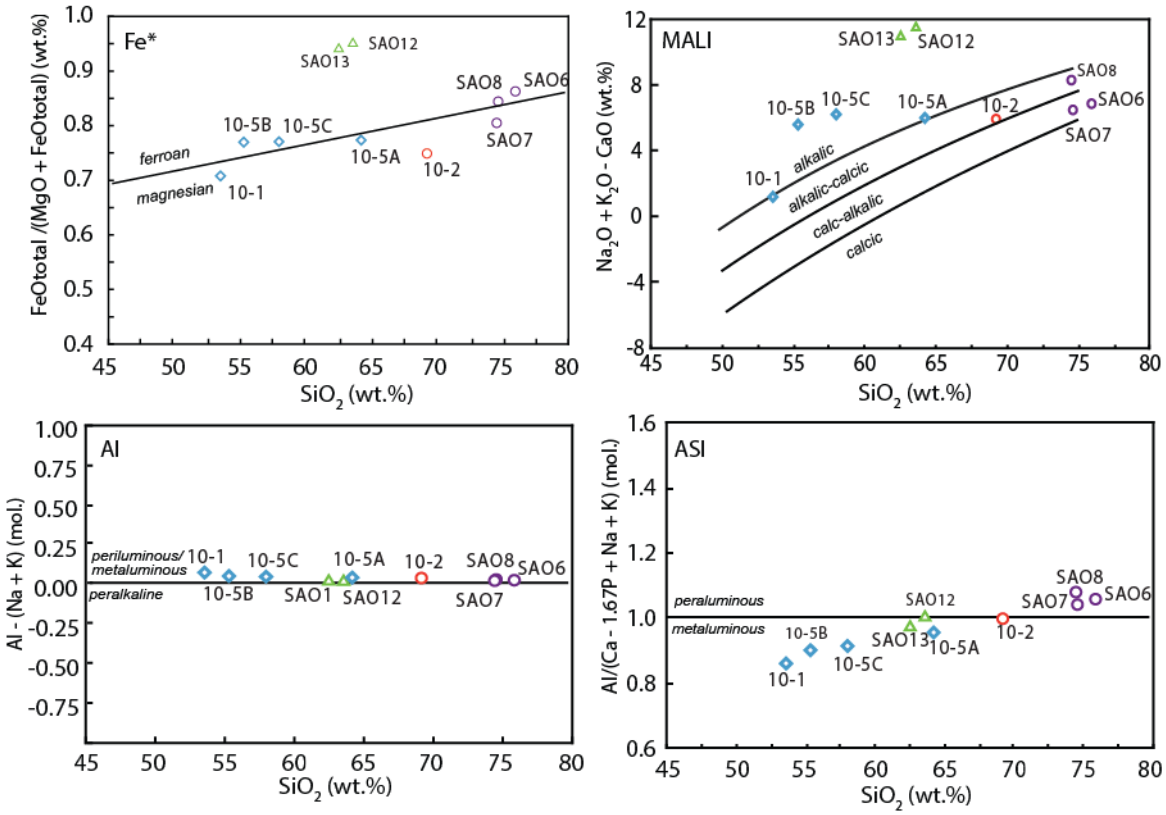

Figure 3-8: Classification diagrams for feldspathic igneous rocks (Frost and Frost, 2008) including the Fe*, MALI, AI, and ASI vs SiO_2 wt.%. Data points represent the Danburg granite, Sandy Hill granite, mafic enclaves, and Delhi syenite. Blue diamond – mafic enclaves, red circle – Danburg granite, purple circle – Sandy Hill granite, green triangle – Delhi syenite.

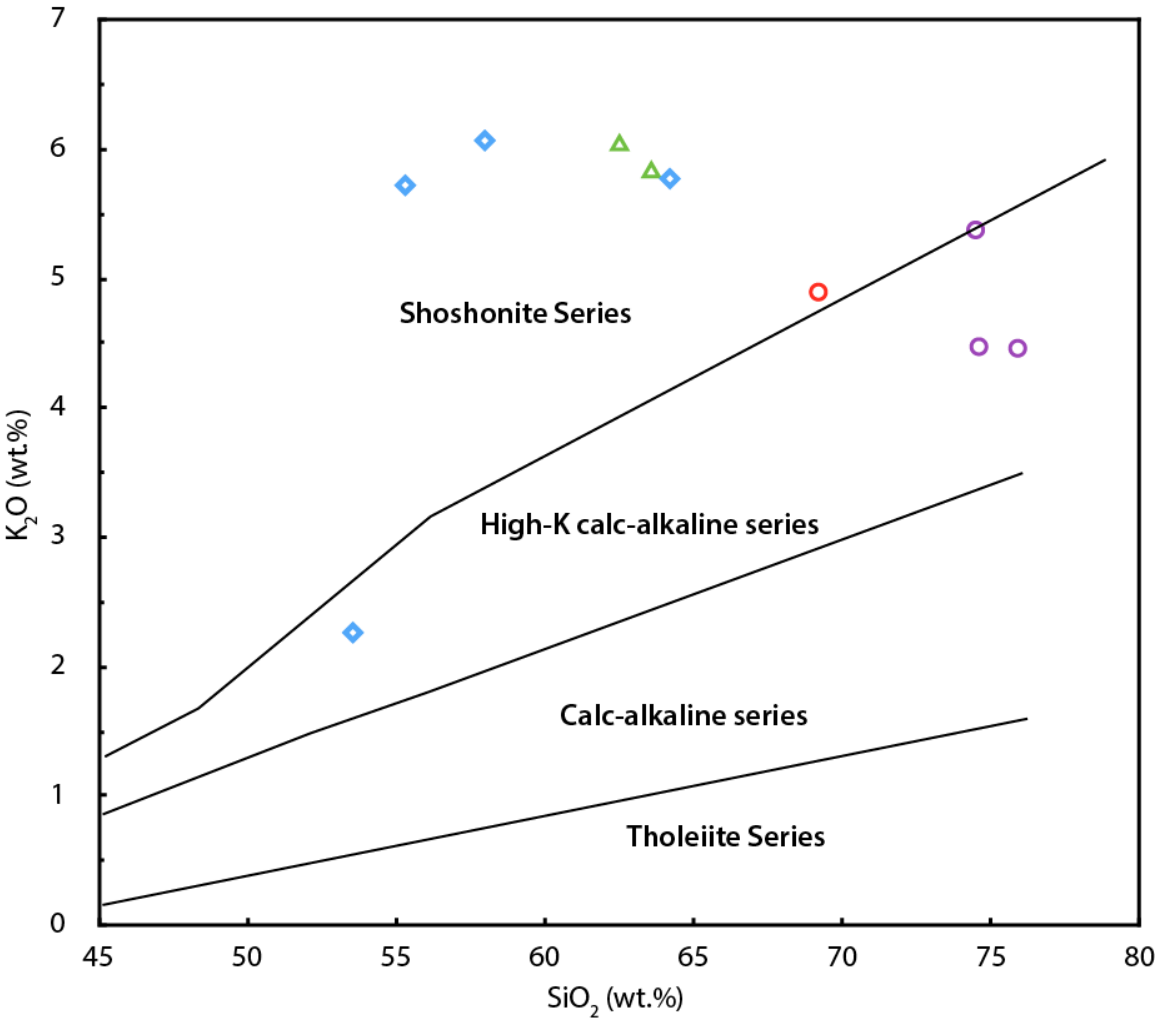

Figure 3-9: Plot of K_2O (wt.%) vs SiO_2 (wt.%)that is used to show potassium enrichment. The Delhi syenite as well as the Danburg enclaves are shoshonitic while the Danburg and Sandy Hill granites plot as high potassium calc-alkaline rocks. Blue diamond – mafic enclaves, red circle – Danburg granite, purple circle – Sandy Hill granite, green triangle – Delhi syenite.

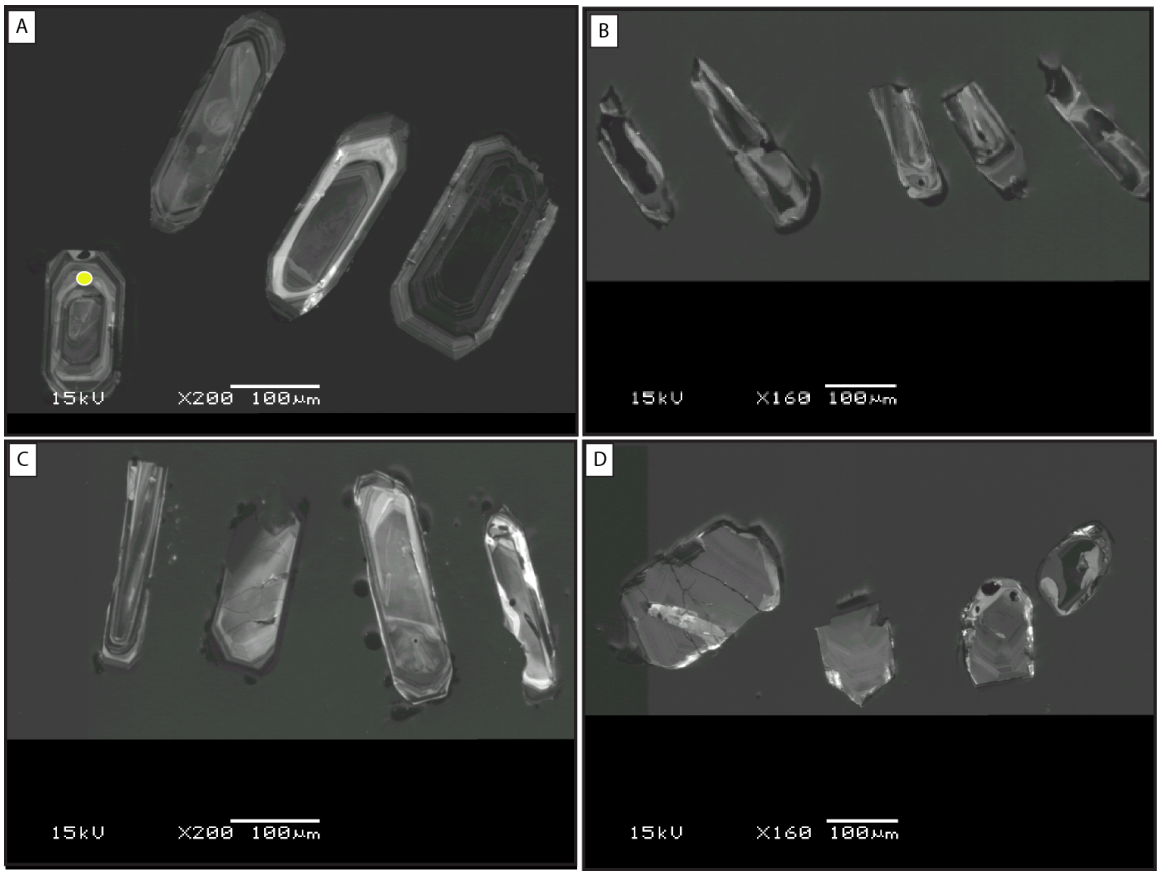

Figure 3-10: SEM-CL images of representative zircons from the Danburg granite (A), its enclaves (B), the Sandy Hill granite (C), and Delhi syenite (D). The morphological differences are apparent, with the Delhi zircons exhibiting a rounded, equant habit, while the Danburg, enclave, and Sandy Hill zircons are elongate with sharp crystal faces. Contrasting zoning patterns can be seen, with the Danburg and Sandy Hill zircons exhibiting oscillatory zonation (especially in the outer edges) while the enclave zircons have patchy zonation. The Delhi zircons show limited zoning. The yellow circle on the first zircon in A represents the size of an analysis spot in analysis by the SHRIMP-RG. zircon in A represents the size of an analysis spot in analysis by the SHRIMP-RG.

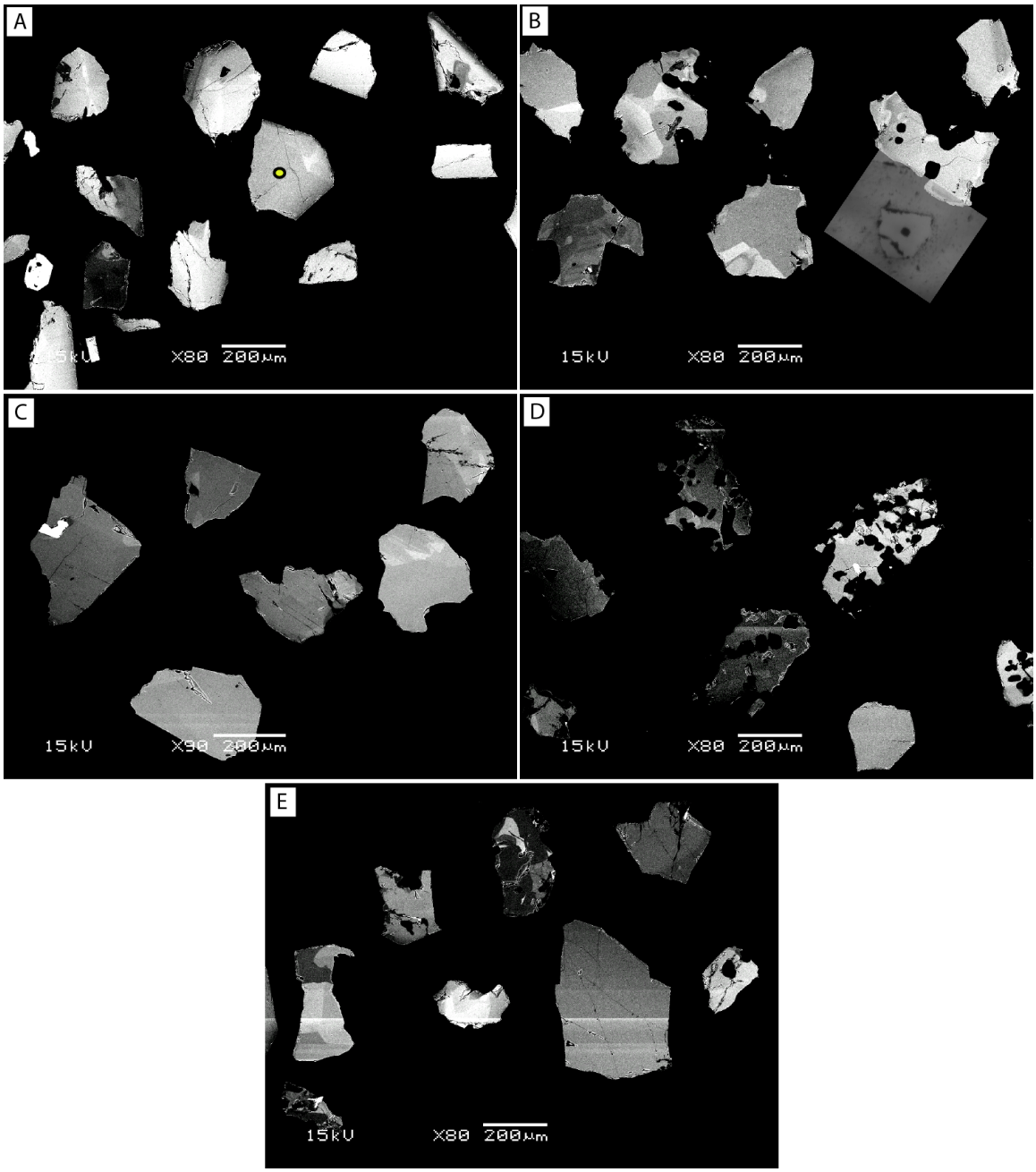

Figure 3-11: SEM-BSE images of representative titanite from the Danburg granite (A), and contained enclaves: 14CG-SAO10-1 (B), 14CG-SAO10-5A (C), 14CG-SAO10-5B (D), 14CG-SAO10-5C (E). Most of the grains picked and shown here are broken fragments. The poikiloblastic or 'skeletal' habit seen in thin section is preserved by the examples shown in (D).. The yellow circle on a central titanite in A represents the size of an analysis spot during analysis by the SHRIMP-RG.

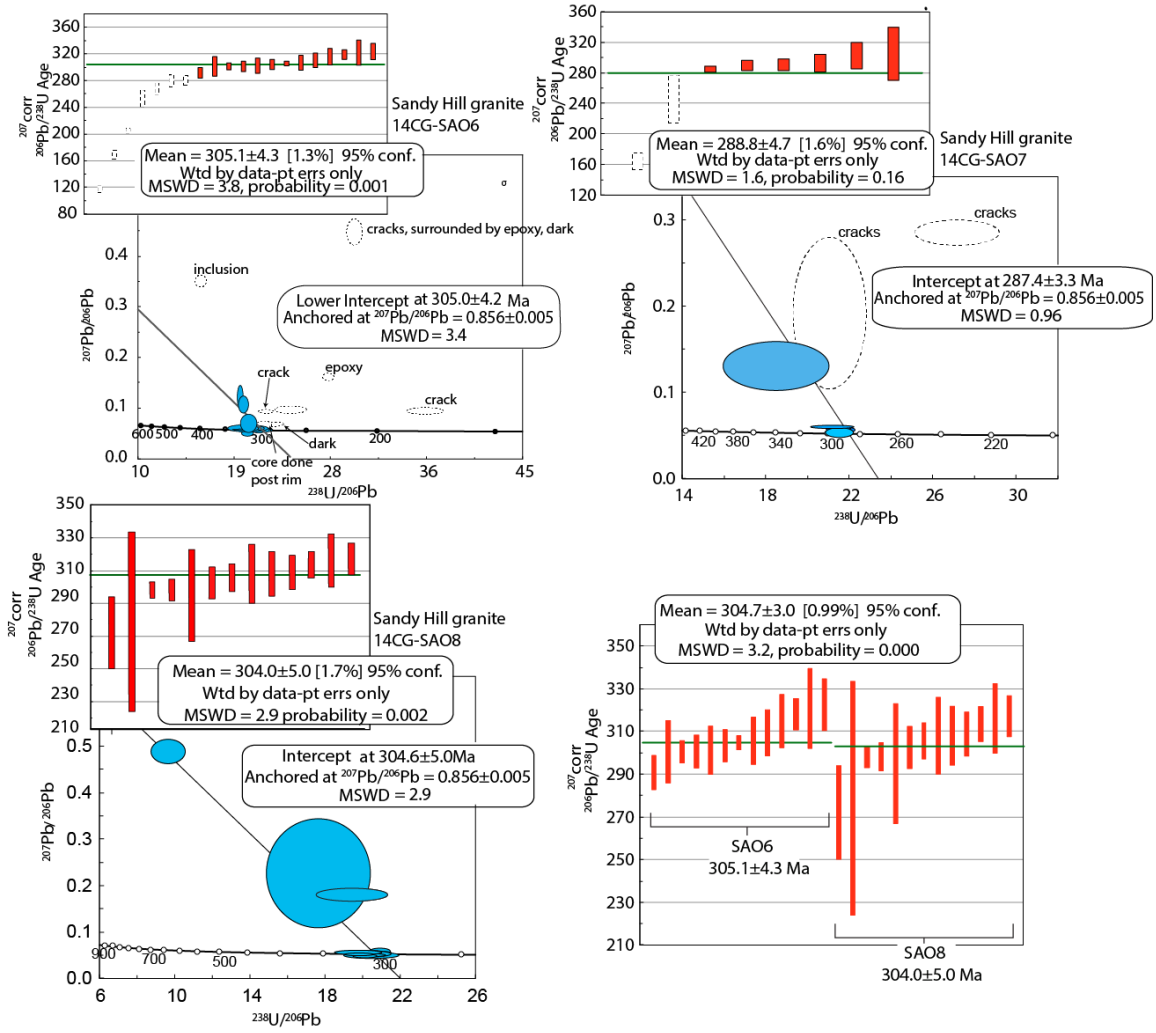

Figure 3-12: Weighted average and Concordia plots of zircon analyses for the Sandy Hill granite. Data-point error ellipses are 2σ for Concordia plots and box heights are 2σ for weighted average plots.

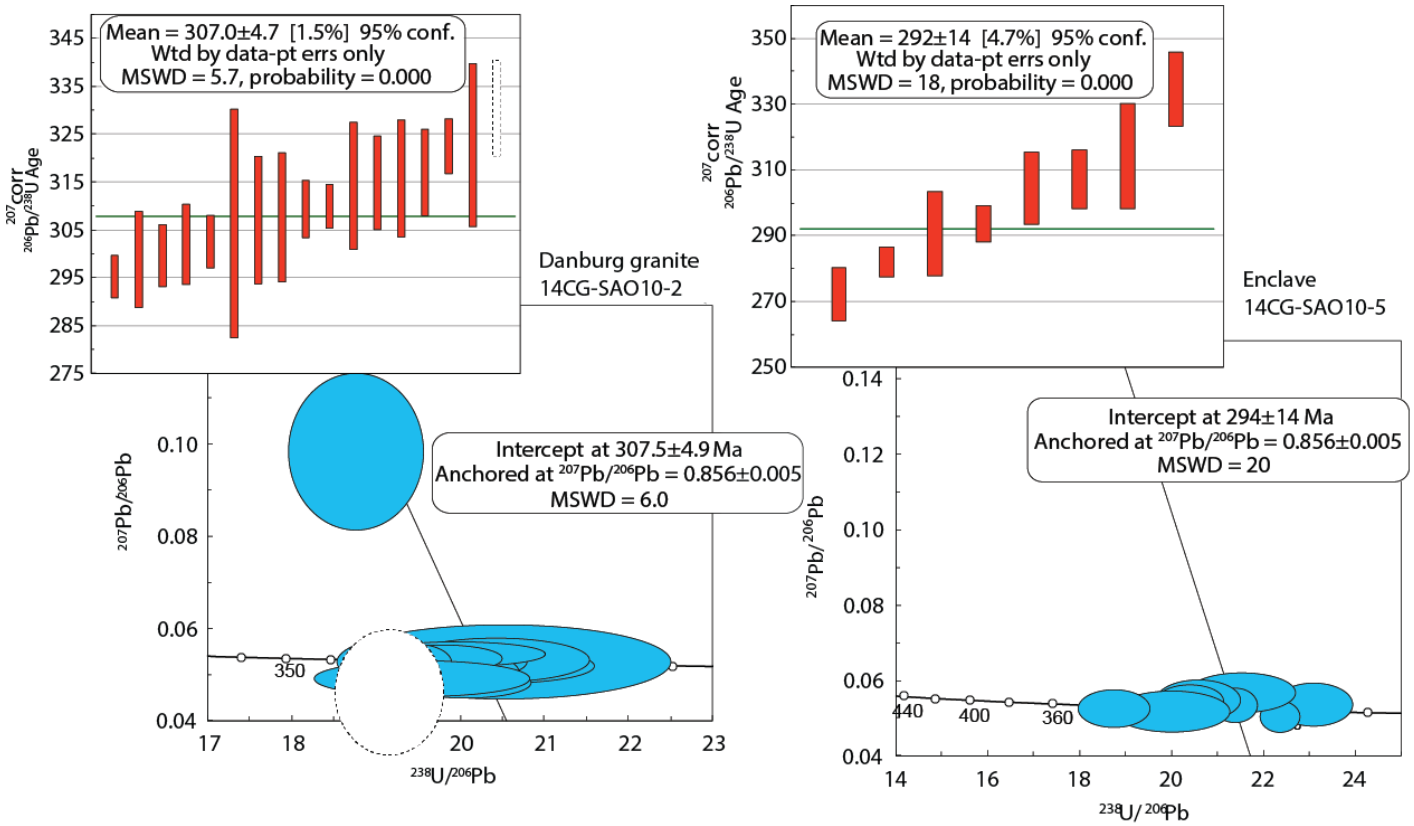

Figure 3-13: Weighted average and Concordia plots of zircon analyses for the Danburg granite and mafic enclaves. Data-point error ellipses are 2σ for Concordia plots and box heights are 2σ for weighted average plots.

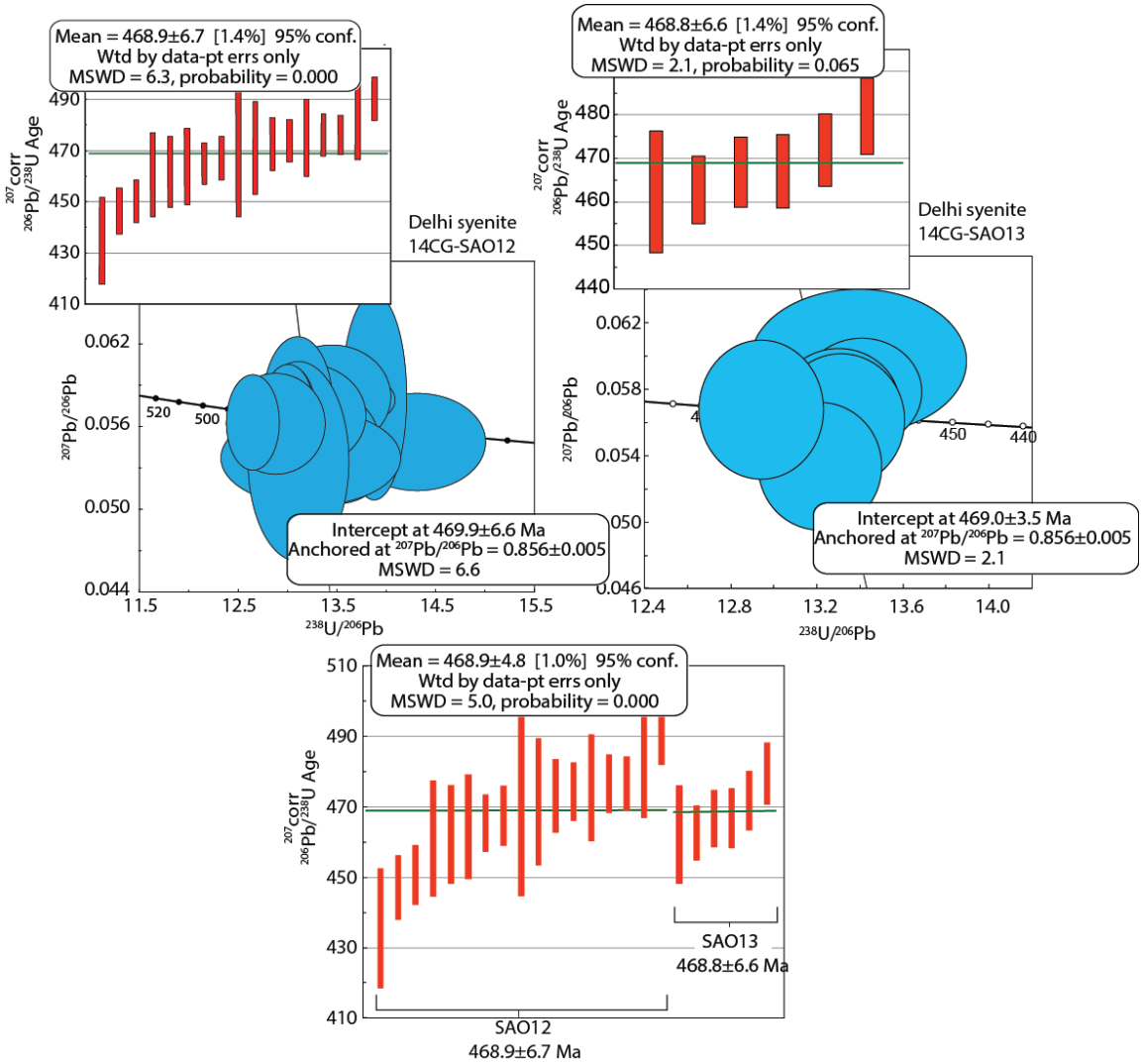

Figure 3-14: Weighted average and Concordia plots of zircon analyses for the Delhi syenite. Data-point error ellipses are 2σ for Concordia plots and box heights are 2σ for weighted average plots.

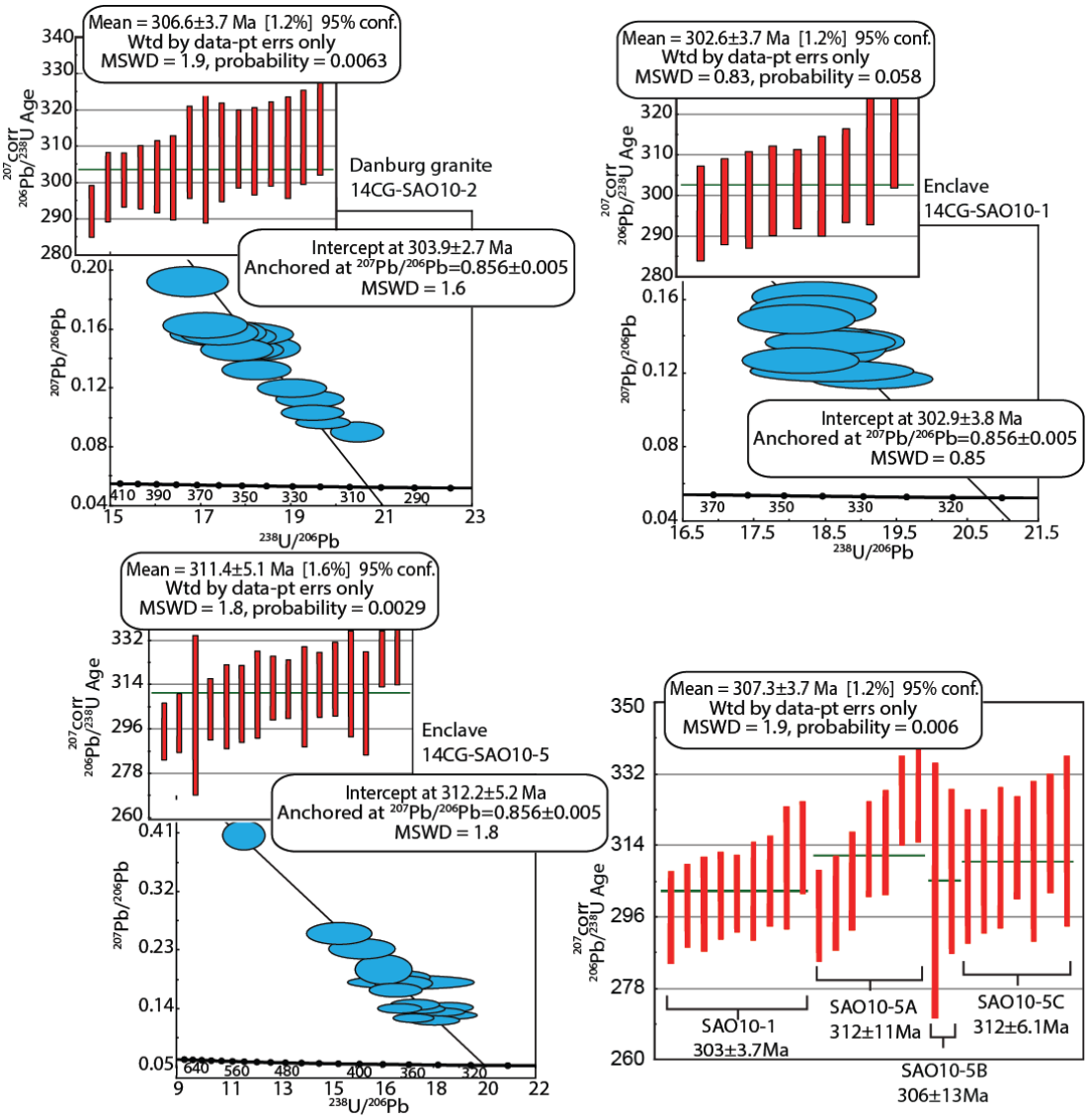

Figure 3-15: Weighted average and Concordia plots of titanite analyses for the Danburg granite and contained enclaves. Data-point error ellipses are 2σ for Concordia plots and box heights are 2σ for weighted average plots.

Table 3-1. Modal mineral assemblages (vol.%) determined from point counting (400 points per slide).

Sample	Qtz	Pl	Afs	Bt	Ms	Op	Ttn	Ep	Zrn	Ap	Hbl	Cal	% Q	% A	% P	Rock Type
14CG-SAO6	32.7	30.5	22.7	4.7	7.5	0.2	0.0	0.0	1.0	0.5	0.0	0.0	38.1	26.4	35.5	Monzogranite
14CG-SAO7	34.0	24.2	33.0	1.0	6.7	0.5	0.0	0.0	0.0	0.5	0.0	0.0	37.3	36.2	26.5	Monzogranite
14CG-SAO7-2	37.7	25.5	26.2	0.0	7.7	2.2	0.0	0.0	0.2	0.2	0.0	0.0	42.2	29.3	28.5	Monzogranite
14CG-SAO8	26.2	30.2	37.0	0.7	2.2	3.5	0.0	0.0	0.0	0.0	0.0	0.0	28.1	39.6	32.3	Monzogranite
14CG-SAO10-2	21.2	24.5	28.5	14.7	1.2	5.5	0.7	1.0	0.2	2.2	0.0	0.0	28.6	33.0	38.4	Monzogranite
14CG-SAO10-1	10.0	47.5	6.7	15.2	0.2	3.0	6.0	0.7	0.7	1.7	8.0	0.0	15.6	10.4	74.0	Quartz Monzodiorite
14CG-SAO10-5A	20.0	23.0	27.7	13.0	1.7	4.0	5.2	1.5	0.5	2.4	0.0	0.7	28.3	39.2	32.5	Monzogranite
14CG-SAO10-5B	11.5	31.7	20.0	12.2	1.5	3.5	5.7	2.0	0.7	2.7	5.5	2.7	17.8	24.7	57.5	Quartz Monzodiorite
14CG-SAO10-5C	10.2	33.0	14.2	22.5	0.2	4.2	2.5	2.0	1.2	1.5	7.2	1.0	18.2	31.6	50.2	Quartz Monzonite
14CG-SAO10-6	23.5	35.8	7.0	22.9	0.0	3.7	3.2	0.7	1.0	2.2	0.0	0.0	35.4	10.6	54.0	Granodiorite
14CG-SAO12	0.0	11.0	84.5	0.5	0.0	2.2	0.0	0.0	0.0	0.0	1.7	0.0	0.0	88.5	11.5	Syenite
14CG-SAO13	2.7	23.7	50.5	3.7	0.0	7.5	0.0	0.0	1.0	0.7	6.5	3.5	3.5	65.7	30.8	Syenite

Notes: Qtz - quartz, Pl - plagioclase, Afs - alkali feldspar, Bt - biotite, Ms - muscovite, Op - opaques, Ttn - titanite, Ep - epidote, Zrn - zircon, Ap - apatite, Am - amphibole, Cal - calcite. The Q, A, and P columns represent normalized percentages used in determining rock classification.

Table 3-2. Whole rock geochemistry of selected samples constrained by XRF.

Sample: 14CG-	SAO6	SAO7	SAO8	SAO10-2	SAO10-1	SAO10-5A	SAO10-5B	SAO10-5C	SAO12	SAO13
	Sandy Hill granite				Danburg				Delhi syenite	
Major Oxide (wt. %)				main body	enclave	enclave	enclave	enclave		
SiO_2	75.9	74.49	74.6	69.2	53.56	64.21	55.32	57.99	63.59	62.52
TiO_2	0.18	0.09	0.31	0.53	1.78	0.98	1.41	1.26	0.2	0.24
Al_2O_3	12.44	13.34	12.84	14.06	17.42	14.97	17.41	17.12	18.23	18.06
Fe_2O_3	1.67	0.69	2.17	3.17	8.35	5.07	6.99	6.25	4.07	3.61
MgO	0.24	0.15	0.37	0.96	3.12	1.35	1.9	1.69	0.2	0.22
MnO	0.04	0.02	0.06	0.05	0.16	0.09	0.1	0.09	0.12	0.1
CaO	0.85	0.48	1.2	2.09	5.82	2.68	3.97	3.53	0.73	1.14
Na_2O	3.3	3.46	3.26	3.17	4.79	2.96	3.89	3.73	6.45	6.11
K2O	4.46	5.38	4.47	4.9	2.26	5.77	5.72	6.07	5.82	6.03
P_2O_5	0.05	0.03	0.06	0.2	0.57	0.27	0.42	0.35	0.05	0.08
LOI	0.74	1.74	0.5	1.42	1.89	1.31	2.3	1.28	0.36	1.69
Total	99.87	99.85	99.83	99.74	99.72	99.65	99.43	99.36	99.83	99.81
Trace Elements (ppm)										
Ba	185	118	523	1184	426	1357.2	2597.3	2974.1	63	110
Rb	408	694	240	165	153	176.05	148.7	156.7	43	66
Sr	0	0	79	308	330	340.7	689	691.8	18	50
Y	36	30	28	36	39	40.65	59.4	62.3	27	28
Zr	154	112	186	328	576	692.7	1036.05	1058.9	946	1094
Nb	25	42	32	28	48	33	45.5	55	77	60
Ce	42	29	60	76	257	211.45	327.05	270.4	58	37
Normative Mineralogy										
Q	37.60	32.61	35.58	26.66	2.79	18.14	1.47	4.65	2.08	1.59
C	0.76	1.02	0.60	0.22					0.11	
Or	26.36	31.79	26.42	28.96	13.36	34.10	33.80	35.87	34.39	35.64
Ab	27.92	29.28	27.59	26.82	40.53	25.05	32.92	31.56	54.58	51.70
An	3.89	2.19	5.56	9.06	19.36	10.52	13.15	12.04	3.30	4.04
Di					0.18					0.51
Hy	0.60	0.37	0.92	2.39	7.69	3.36	4.73	4.21	0.50	0.31
Il	0.09	0.04	0.13	0.11	0.34	0.19	0.21	0.19	0.26	0.21
Ap	0.12	0.07	0.14	0.46	1.32	0.63	0.97	0.81	0.12	0.19
Hm	1.67	0.69	2.17	3.17	8.35	5.07	6.99	6.25	4.07	3.61
Tn					3.93	0.72	2.68	2.24		0.31
Ru	0.13	0.07	0.24	0.47		0.59	0.20	0.24	0.06	

*Q — quartz, C — corundum, Or — orthoclase, Ab — albite, An — anorthite, Di — diopside, Hy — hypersthene, Il — ilmenite, Ap —apatite, Hm — hematite, Tn — titanite, Ru — rutile.

Table 3-3. Frost et al. (2001) classifications of the Danburg, its enclaves, the Sandy Hill, and the Delhi.

Sample: 14CG-	SAO6	SAO7	SAO8	SAO10-2	SAO10-1	SAO10-5A	SAO10-5B	SAO10-5C	SAO12	SAO13
Fe*[1]	F	M	F	M	M	M	F	F	F	F
MALI[2]	C-A	C-A	A-C	A-C	A-C	A	A	A	A	A
ASI[3]	Pera	Pera	Pera	Pera/Meta	Meta	Meta	Meta	Meta	Pera	Meta

[1]M = magnesian; F = ferroan

[2]A = alkalic; A-C = alkalic calcic; C-A = calc-alkalic

[3]Pera = peraluminous; Meta = metaluminous

Table 3-4. SHRIMP-RG zircon Pb-U isotopic data for the Sandy Hill granite, Danburg granite, enclaves, and Delhi syenite.

	Concentration	Atomic Ratios				^{207}Pb corrected Ages (Ma)				
Sample	^{207}Pb corrected ^{206}Pb[ii] (ppm)	^{238}U/^{206}Pb[iii]	% err	^{207}Pb/^{206}Pb[iii]	% err	^{207}Pb corrected ^{206}Pb/^{238}U[iv]	% err	^{206}Pb/^{238}U[v]	1σ err	Weighted Average ± 2σ err
Sandy Hill granite										
SAO6-7.1core	10.2	29.7	1	0.4106	2.4	0.0183	0.78	~~117~~	~~3~~	305.1± 4.3 (1.3%)
SAO6-4.1	6.3	36.1	1.9	0.0862	2.9	0.0264	0.62	~~168~~	~~3~~	MSWD = 3.8
SAO6-1.1	5.6	27.28	0.8	0.1478	1.8	0.0322	0.28	~~204~~	~~2~~	
SAO6-13.1core	4.1	23.9	2.5	0.0883	3	0.04	0.81	~~253~~	~~6~~	
SAO6-18.1	4.6	15.7	1.4	0.3218	1.4	0.0423	0.51	~~267~~	~~4~~	
SAO6-5.1core	42	22.3	1.7	0.0623	2.7	0.0443	0.55	~~279~~	~~5~~	
SAO6-9.1core	28.2	21.6	1.3	0.0853	1.8	0.0444	0.43	~~280~~	~~4~~	
SAO6-11.2core	1.8	21.4	1.3	0.0605	5.2	0.0462	0.45	291	4	
SAO6-12.1rim	4.8	21	2.4	0.0516	3.7	0.0478	0.79	301	7	
SAO6-15.1	5.8	21	0.9	0.0504	3.1	0.0478	0.28	301	3	
SAO6-8.1rim	126.6	19.3	0.6	0.1161	7.5	0.0478	0.42	301	4	
SAO6-11.1rim	5.2	20.8	1.9	0.0543	3.5	0.0479	0.61	302	6	
SAO6-3.1core	14.6	19.56	0.9	0.0976	6.5	0.0482	0.4	304	4	
SAO6-16.1rim	60.5	20.6	0.5	0.0523	1	0.0485	0.18	305	2	
SAO6-14.1core	5	20.5	1.8	0.0546	3.3	0.0486	0.59	306	6	
SAO6-10.1	1.4	20	1.6	0.0635	10.6	0.0492	0.57	310	5	
SAO6-2.1	6.2	19.99	2	0.0516	3.4	0.0501	0.65	315	6	
SAO6-17.1	3.3	19.9	1.1	0.0455	4.6	0.0506	0.38	318	4	
SAO6-6.1	3.4	19.5	3	0.0547	4.3	0.0511	0.95	321	9	
SAO6-3.2rim	80.6	19.48	1.9	0.0522	0.9	0.0514	0.62	323	6	
Sandy Hill granite										
SAO7-1.1core	19.6	27.1	3	0.2861	2.1	0.0259	1.03	~~165~~	~~5~~	288.8 ± 4.7 (1.6%)
SAO7-5.1core	26.1	21.1	3.4	0.1927	18.7	0.039	2.07	~~247~~	~~16~~	MSWD = 1.6

Table 3-4: continued

SAO7-8.1core	11.9	21.9	0.7	0.057	2.1	0.0453	0.23	286	2	
SAO7-2.1core	19	21.5	1.1	0.0581	1.9	0.0461	0.36	291	3	
SAO7-7.1core	2.7	21.6	1.3	0.0539	4.4	0.0463	0.41	292	4	
SAO7-6.1core	134.4	21.2	2	0.0605	1.3	0.0466	0.64	294	6	
SAO7-4.1core	16.3	18.7	2.9	0.1318	1.2	0.0482	0.93	303	9	
SAO7-3.1	270.8	18.6	5.6	0.1312	8.8	0.0486	1.86	306	17	
Sandy Hill granite										
SAO8-2.2rim	57.9	19.46	4	0.1801	3.2	0.0432	1.31	272	11	304.0 ± 5.0 (1.7%)
SAO8-1.1	24.3	17.68	6.4	0.2268	21.2	0.0442	3.21	279	27	MSWD = 2.9
SAO8-12.1	8.7	21.13	0.8	0.0517	3	0.0474	0.27	298	2	
SAO8-10.1core	3.2	20.95	1.1	0.058	4.6	0.0474	0.36	298	3	
SAO8-3.1rim	8.1	9.7	3.8	0.4901	2.2	0.0469	1.55	295	14	
SAO8-5.1rim	11.2	20.72	1.6	0.0551	2.5	0.0481	0.53	303	5	
SAO8-11.1rim	8.5	20.51	1.4	0.0552	3.2	0.0486	0.45	306	4	
SAO8-4.1rim	2.8	20.48	2.9	0.0496	5.6	0.049	0.95	308	9	
SAO8-8.1rim	3.3	20.41	2.3	0.0524	4.8	0.049	0.73	308	7	
SAO8-9.1rim	8.8	20.42	1.7	0.0498	2.8	0.0491	0.55	309	5	
SAO8-7.1rim	6.5	20.16	1.3	0.0479	3.5	0.0499	0.42	314	4	
SAO8-4.2core	6	19.8	2.6	0.0557	3.4	0.0503	0.85	316	8	
SAO8-6.1rim	16.8	19.84	1.5	0.0512	2.2	0.0505	0.49	318	5	
Danburg granite										
SAO10-2-6.1	10.6	21.34	0.7	0.0519	2.5	0.0469	0.25	295	2	307 ± 4.7 (1.5%)
SAO10-2-13.1core	17.3	21.01	1.7	0.0547	2	0.0475	0.55	299	5	MSWD = 5.7
SAO10-2-3.2core	3	21.04	1.1	0.0514	4.8	0.0476	0.35	300	3	
SAO10-2-4.1	7.6	20.84	1.4	0.0526	2.9	0.048	0.45	302	4	
SAO10-2-12.1core	6.5	20.72	0.9	0.0557	3.1	0.0481	0.3	303	3	
SAO10-2-8.2rim	5.1	20.53	3.9	0.0527	6.3	0.0487	1.28	306	12	

Table 3-4: continued

SAO10-2-11.1	7.9	20.51	2.2	0.0518	3	0.0488	0.71	307	7	
SAO10-2-8.1core	5.1	20.44	2.2	0.0531	3.7	0.0489	0.72	308	7	
SAO10-2-9.1	12	20.33	1	0.0527	2.4	0.0492	0.32	310	3	
SAO10-2-14.1rim	10.5	20.36	0.7	0.0502	3	0.0493	0.24	310	2	
SAO10-2-7.1	17.7	19.97	2.1	0.0544	2	0.05	0.69	314	7	
SAO10-2-5.1	11.3	20.08	1.6	0.0482	2.8	0.0501	0.51	315	5	
SAO10-2-10.1rim	13.2	18.78	1.7	0.0985	7.1	0.0502	0.63	316	6	
SAO10-2-2.1	13.7	19.82	1.4	0.0534	2.2	0.0504	0.47	317	5	
SAO10-2-3.1rim	6.7	19.49	0.9	0.0524	3.2	0.0513	0.29	323	3	
SAO10-2-1.1	7.5	19.56	2.7	0.049	3.2	0.0514	0.86	323	9	
SAO10-2-15.1rim	1.9	19.17	1.4	0.0457	12.5	0.0526	0.5	~~331~~	~~5~~	
Danburg enclave										
SAO10-5-1.1core	15.7	175.92	11.4	0.0541	1.5	0.0056	3.63	~~36.2~~	~~4~~	292 ± 14 (4.7%)
SAO10-5-3.1	3.8	23.12	1.5	0.0535	4.4	0.0432	0.49	272	4	MSWD = 18
SAO10-5-6.1	6.3	22.39	0.8	0.0503	3.4	0.0448	0.26	282	2	
SAO10-5-4.1	4.8	21.54	2.2	0.0567	3.8	0.0462	0.72	291	6	
SAO10-5-8.1	5.2	21.41	0.9	0.0533	3.5	0.0466	0.31	294	3	
SAO10-5-7.1	3.8	20.61	1.8	0.0547	4	0.0484	0.59	305	5	
SAO10-5-1.2rim	19.8	20.43	1.5	0.0544	3.2	0.0488	0.48	307	4	
SAO10-5-2.1	4.1	20.03	2.6	0.0516	4.3	0.05	0.83	314	8	
SAO10-5-5.1	5.2	18.77	1.7	0.0524	3.9	0.0533	0.55	335	6	
Delhi syenite										
SAO12-11.1	8.1	14.3	2	0.0551	2.6	0.0699	0.64	436	8	468.9 ± 6.7 (1.0%)
SAO12-5.1	7.1	13.88	1	0.0583	5.2	0.0718	0.34	447	5	MSWD = 6.3
SAO12-14.1core	45.3	13.8	1	0.0581	1.1	0.0724	0.31	451	4	
SAO12-15.1	8.3	13.5	1.8	0.0583	2.6	0.0742	0.59	461	8	
SAO12-8.1	11	13.5	1.5	0.0536	2.3	0.0744	0.5	462	7	

Table 3-4: continued

SAO12-7.1	6.2	13.4	1.6	0.0547	3	0.0747	0.53	464	7	
SAO12-16.1	9.5	13.4	0.9	0.0535	2.6	0.0749	0.29	466	4	
SAO12-12.1	8.4	13.3	0.9	0.0545	2.7	0.0752	0.3	468	4	
SAO12-10.1	8.9	13.2	2.8	0.0539	2.6	0.0758	0.91	471	13	
SAO12-4.1	8.4	13.17	1.9	0.057	2.7	0.0759	0.63	472	9	
SAO12-9.1	4.8	13.1	1.1	0.0579	3.3	0.0762	0.36	473	5	
SAO12-2.2core	8.4	13.11	0.9	0.0552	2.7	0.0764	0.29	474	4	
SAO12-13.1	2.2	13.1	1.6	0.0536	5.5	0.0766	0.52	476	8	
SAO12-3.1	8.4	13.02	0.9	0.0568	2.7	0.0768	0.28	477	4	
SAO12-1.1rim	13.1	13.01	0.8	0.0576	2.1	0.0768	0.26	477	4	
SAO12-6.1	8.9	12.9	1.6	0.0564	2.7	0.0777	0.51	482	7	
SAO12-2.1rim	10.6	12.65	0.9	0.0565	2.5	0.0791	0.29	491	4	
Delhi syenite										
SAO13-5.1	9.3	22.32	1.5	0.0518	2.6	0.0448	0.48	~~283~~	~~4~~	468.8 ± 6.6 (1.4%)
SAO13-3.1	6.4	13.39	1.5	0.0597	3	0.0743	0.5	462	7	MSWD = 2.1
SAO13-7.1	11	13.41	0.8	0.0579	2.3	0.0744	0.28	463	4	
SAO13-2.1	9.8	13.3	0.9	0.0571	2.4	0.0751	0.28	467	4	
SAO13-1.1	7.1	13.31	0.9	0.0561	2.9	0.0751	0.3	467	4	
SAO13-4.1	7.7	13.22	0.9	0.0534	3	0.076	0.29	472	4	
SAO13-6.1	7.4	12.95	0.9	0.0568	3	0.0772	0.3	480	4	

i errors reported at 1σ

ii radiogenic ^{206}Pb

iii uncorrected, measured ratios

iv ^{207}Pb-corrected ratios using age appropriate model Pb isotopic composition of Stacey and Kramers (1975)

v ^{207}Pb-corrected age; spot analyses with strikethrough are not included in the weighted average after careful consideration using imaging, mineral chemistry, and concordia diagrams

Table 3-5. SHRIMP-RG titanite Pb-U data for the Danburg granite and enclaves.

	Concentration	Atomic Ratios						^{207}Pb corrected Ages (Ma)		
Sample	^{207}Pb-corrected ^{206}Pb[ii] (ppm)	^{238}U/^{206}Pb[iii]	% err	^{207}Pb/^{206}Pb[iii]	% err	^{207}Pb corrected ^{206}Pb/^{238}U[iv]	% err	^{206}Pb/^{238}U[v]	1σ err	Weighted Average ± 2σ err
Danburg granite										
10-2-12.2dk	15.7	20.47	1.2	0.092	2.9	0.0464	0.4	292	4	303.6 ± 3.7 (1.2%)
10-2-11.1	28.1	19.43	1.6	0.114	2	0.0475	0.52	299	5	MSWD = 1.6
10-2-6.1	27.2	19.72	1.2	0.098	1.7	0.0478	0.4	301	4	
10-2-9.2dk	26	19.5	1.4	0.105	2	0.0479	0.47	302	4	
10-2-8.1	22.2	19.05	1.6	0.122	2.1	0.048	0.53	302	5	
10-2-13.1	33.2	18.37	1.9	0.149	2.1	0.0479	0.62	302	6	
10-2-2.1	27	17.98	2	0.148	1.9	0.0491	0.67	309	6	
10-2-4.1	42.2	17.72	3.1	0.158	2.2	0.049	1.02	308	10	
10-2-1.1	32.6	17.76	2.2	0.156	1.9	0.049	0.71	309	7	
10-2-5.1	24.6	18.26	1.7	0.134	2	0.0492	0.56	310	5	
10-2-7.1	33.4	17.67	1.9	0.159	2.1	0.0491	0.63	309	6	
10-2-9.1lt	27.5	17.84	1.8	0.148	2.1	0.0494	0.6	311	6	
10-2-12.1lt	44.1	16.74	2.2	0.194	2.2	0.0492	0.73	310	7	
10-2-3.1	39	17.46	2	0.159	2.2	0.0497	0.67	313	6	
10-2-10.1	29.3	17.13	2.2	0.164	2.1	0.0503	0.73	316	7	
Danburg enclave										
10-1-5.1	1.81	18.36	1.9	0.163	2	0.047	0.64	296	6	302.6 ± 3.7 (1.2%)
10-1-4.1	2.26	18.83	1.7	0.138	2	0.0474	0.57	299	5	MSWD = 0.83
10-1-6.1	1.84	18.35	1.9	0.155	2.1	0.0475	0.65	299	6	
10-1-1.1	2.74	19.17	1.8	0.118	1.8	0.0479	0.59	301	5	
10-1-12.1lt	3.2	18.69	1.5	0.136	3	0.048	0.52	302	5	
10-1-2.1	2.11	18.59	2	0.138	1.9	0.0481	0.66	303	6	

Table 3-5: continued

10-1-7.1	2.23	18.12	1.8	0.15	2.1	0.0485	0.61	305	6	
10-1-3.1	3.57	18.62	2.5	0.123	1.9	0.049	0.81	309	8	
10-1-12.2dk	2.39	18.18	1.8	0.128	2.2	0.0498	0.6	314	6	
Danburg enclave										
10-5A-7.1	21.4	18.83	1.9	0.144	2.2	0.047	0.63	296	6	312 ± 11 (3.6%)
10-5A-1.1	34.1	18.93	2	0.132	1.8	0.0476	0.64	300	6	MSWD = 4.2
10-5A-2.1	37.5	18.46	2	0.137	1.9	0.0485	0.66	305	6	
10-5A-3.1	31.8	17.85	1.9	0.142	2.1	0.0498	0.62	313	6	
10-5A-5.1	31.2	17.6	2.1	0.149	2.3	0.05	0.68	315	7	
10-5A-4.1	25.2	17.52	1.7	0.128	2.1	0.0518	0.56	325	6	
10-5A-6.1	36	17.06	1.9	0.143	2.1	0.0521	0.62	327	6	
Danburg enclave										
10-5B-1.1	23.8	17.44	5.3	0.182	2.3	0.0481	1.73	303	16	306 ± 13 (5.7%)
10-5B-2.1	34.9	11.41	2.7	0.408	2.3	0.0489	1.1	308	10	MSWD = 0.07
Danburg enclave										
10-5C-1.1lt	40.6	17.02	2.7	0.191	2.2	0.0487	0.9	306	8	312 ± 6.1 (1.9%)
10-5C-6.1	34.3	17.19	2.5	0.181	2.5	0.0489	0.83	307	8	MSWD = 0.25
10-5C-3.1	25.3	16.47	2.5	0.202	4.5	0.0494	0.93	311	9	
10-5C-4.1	29.5	18.28	2	0.124	2.3	0.0498	0.67	314	6	
10-5C-5.1	50.6	15.71	3.1	0.234	2.7	0.0493	1.06	310	10	
10-5C-1.2dk	20.3	16.91	2.3	0.171	2.5	0.0504	0.77	317	7	
10-5C-2.1	36.3	14.87	3.3	0.257	2.7	0.0501	1.11	315	11	
							cumulative enclave age (10-5)			311.4± 5.1 (1.6%)
										MSWD = 1.8

i errors reported at 1σ

ii radiogenic ^{206}Pb

iii uncorrected, measured ratios

iv ^{207}Pb-corrected ratios using age appropriate model Pb isotopic composition of Stacey and Kramers (1975)
v ^{207}Pb-corrected age; spot analyses with strikethrough are not included in the weighted average after careful consideration using imaging, mineral chemistry, and concordia diagrams

Table 3-6. Zircon and titanite geothermobarometry for selected samples.

Sample: 14CG-	SAO6	SAO7	SAO8	SAO10-2	SAO10-1	SAO10-5	SAO12	SAO13
Calculated T (°C)	805±46	766±36	784±23	771±27	N/A	765±50	676±22	689±25
Calculated P (kilobar)	N/A	N/A	N/A	6.5±1.7	5.1±1.4	4.9±1.4	N/A	N/A
Estimated thermal gradient (°C/km)	N/A	N/A	N/A	37.1	N/A	45.7	N/A	N/A

*Temperatures and pressures are reported with one standard deviation.

CHAPTER 4: DISCUSSION

One of the principal findings from this work is that the age of the juxtaposed igneous bodies differ by ~150 Ma. The Alleghanian-age Danburg-Sandy Hill suite is thus discussed separately from the Taconic-age Delhi syenite in the following discussion. Using textural evidence, whole rock geochemistry, and accessory mineral geochemical evidence, the petrogenetic relations between the coeval Danburg, mafic enclaves, and Sandy Hill bodies are evaluated further in the next section.

4.1. Alleghanian Magmatism Associated with the Danburg Pluton – Origin of Enclaves

4.1.1. Mafic Enclaves: Definitions and Background

Magmatic enclaves are volumes of rock surrounded by a host rock of distinct composition. They are common in igneous rocks; however, they represent only about 1% of the volume of the host granitoid in most cases. In calc-alkaline plutons they can make up ~2% which is considered abundant. Although relatively minor in terms of volume, enclaves can be an indicator of the petrogenesis of its host. Multiple hypotheses exist regarding the origin of mafic enclaves. Enclaves may be:

(1) restitic material from the protoliths that were melted to form the granitoids.

(2) the product of magma-mixing, with enclaves representing a less evolved (juvenile) component.

(3) formed through differentiation from a single, parent magma (with the mafic component being the early, least differentiated component) (Pin et al., 1990).

(4) xenoliths of the surrounding country rock included during the pluton's ascent.

A fundamental goal of this study has been to determine whether the enclaves originated as a liquid or a solid. Enclaves arising through each process outlined above will have distinct textural and chemical characteristics. For example, enclaves formed through mixing of a mafic melt with a (cooler) felsic melt may exhibit textures indicative of quenching, while enclaves resulting from early differentiation would exhibit cumulate textures (Dvoracek, 2003, Didier and Barbarin, 1991). Xenoliths from the surrounding country rock are expected to preserve textural evidence of dynamic or thermal metamorphism.

A liquid origin for the enclave implies interaction between at least two, distinct melts. The thermodynamics and rheological properties on how melts interact is not the focus of this study, but understanding how they interface with one another holds importance. Three main processes dominate the interactions of magmas in granitoid systems: mixing, mingling, and chemical exchanges. These processes are regulated by the chemical and physical properties of the mafic and felsic magmas, such as initial temperatures, volume, composition, and viscosity. Often they are sequential, with mixing occurring in the early stages, followed by mingling, and ending with chemical exchange. However, chemical exchange will begin when two chemically separate melts come in contact and outlast the other processes (Didier and Barbarin, 1991). Chemical transfer becomes very limited to nonexistent once the mafic component reaches full crystallization. Additionally, mixing and mingling refer to specific processes; mixing requires complete homogenization of the two components while in mingling the components retain some of their original identity (Chappell, 1996). The timing of the

injection of the mafic magma to the felsic system also significantly affects the evolution of the system.

The thermal disparity will regulate the level to which two melts homogenize. Complete hybridization of a granite-enclave system can only occur if both components behave as liquids at the same temperature (Didier and Barbarin, 1991). Thermal diffusion rates are several orders of magnitude higher than chemical diffusion, thus the mafic melt will solidify before homogenization can be achieved (Sparks and Marshall, 1986). A sequence of viscosity changes is recognized by Sparks and Marshall (1986) where the mafic magma will begin as less viscous, become more viscous due to forced crystallization, and will eventually behave as a solid due to high crystallinity, preventing complete mixing. This is consistent with the progression of mixing, mingling, and chemical exchange explained by Didier and Barbarin (1991).

4.1.2. Mafic Enclaves of the Danburg Pluton

Based on field observations, approximately 2% of the Danburg granite is mafic enclaves. They range in size from tens of centimeters to 4-5 meters across. Multiple types of enclaves are distinguished by texture and mineralogy. On the basis of color and abundance of hornblende, four varieties are defined here (14CG-SAO10-1, 14CG-SAO10-5A, 14CG-SAO10-5B,C, 14CG-SAO10-6). The enclaves within the Danburg are darker, much less coarse than their host (Figure 4-1) and are homogeneously dispersed, with no indication of accumulation in a specific region of the pluton (Dvoracek, 2003).

Based on textural and chemical evidence discussed in the following sections, the contained enclaves are interpreted to be most consistent with a liquid origin.

4.1.3. Geochronological Evidence of Coeval Relationship

Gathering robust ages for the plutons and enclaves can make their connections clearer. SHRIMP-RG ^{207}Pb-corrected ^{206}Pb/^{238}U zircon ages of 307.0±4.7 Ma for the Danburg granite and ^{207}Pb-corrected ^{206}Pb/^{238}U titanite ages of 307.4±3.7 Ma for its enclaves provides evidence that the zircon and titanite crystallized during the same event, although this could occur if 1) two liquids mixed and crystallized or 2) if the titanite grew during metamorphism of the enclaves after they were entrained by the granite melt. The Sandy Hill's ^{207}Pb-corrected ^{206}Pb/^{238}U zircon age of 304.7±3.0 Ma is within error of the Danburg and enclaves. If the mafic enclaves were not representative of a liquid, rather were xenoliths included during the pluton's ascent, the zircon collected from the enclaves might yield age evidence of inheritance. Zircons analyzed from the contained enclaves gave similar Alleghanian ages (272-335 Ma), but due to a spread of ages may signify some inheritance. This suggests that the enclaves could be partial melts of a preexisting source. However, with the deformed country rock (mafic metavolcanics) being a likely source for the xenoliths, an Alleghanian age would not be expected. A more voluminous sample size would need to be analyzed to define a more robust age for the mafic enclaves. Restitic material would likely be of similar age, yet "old" zircons interpreted to represent solid material brought from the source has also been used as evidence for restites (Chappell and White, 1991).

4.1.4. Mineralogical and Textural Features of the Danburg Granite and Contained Enclaves

Mineralogical and textural features of the enclaves analyzed in this study can assist in the interpretation of their origin. These contained enclaves consist of a remarkably similar mineralogy to their hosts, although proportions slightly vary dependent upon the variety of enclave. The Danburg granite is dominated by plagioclase, alkali feldspar, quartz, and biotite with accessory phases muscovite, epidote, titanite, and zircon. Differences in mineralogy include a higher abundance of mafic phases in some cases and the addition of hornblende, which is seen in several varieties of enclaves (14CG-SAO10-5B,14CG-SAO10-5C, 14CG-SAO10-1). A similar mineralogy is expected in mafic microgranular enclaves, with proportions expected to change across varieties. The absence of hornblende in the Danburg granite, but occasional presence in its contained enclaves is another feature consistent with comingled mafic and felsic liquids (Didier and Barbarin, 1991). This correlation between mineral assemblages results from the chemical and crystal exchange that occurs between the two magmas.

Variations in the enclave population within the Danburg granite include differing modal abundances of the major minerals, the presence of new phases, and distinguishing textures. The combination of these three features could suggest a unique cooling history along with the variable bulk composition for each enclave. As the mafic magma was mixed and mingled into the felsic host, it became separated into globules, which then evolved along paths heavily dependent upon size. Plagioclase exhibits compositional

overlap among the varieties but also cluster around distinctive compositions dependent upon type of enclave (Dvoracek, 2003) providing more evidence of the diversity of the enclaves within the Danburg granite. Cooling rates of each enclave is governed by equations concerning heat transfer by conduction that state cooling is determined by the inverse square of the diameter of the mafic body (Jaeger, 1959). Thus, larger mafic bodies will reach thermal equilibrium at a later time than smaller mafic bodies of the same composition. In this study, the lowest-SiO_2, most ferromagnesian enclave of the sampled enclaves is also one of the smallest. The smaller blobs can quench quickly and become rigid enough to limit and inhibit chemical changes (Didier and Barbarin, 1991), possibly preserving a composition more similar to the original source. This variation assists in limiting an origin for the contained enclaves, for mineralogical and textural variation seen within the mafic enclaves is not consistent with magmatic differentiation (Didier and Barbarin, 1991).

Titanite is abundant in the enclaves (2.5-6%) relative to the Danburg granite (0.7%) and could represent recrystallization products of former pyroxenes or amphiboles. This highlights that significant recrystallization of these enclaves is likely, which would mask their former state despite their origin. A possibility is that the contained enclaves were xenoliths, which were transformed to exhibit igneous textures due to interaction with the relatively high temperature Danburg magma (~700+ °C). Xenoliths broken off from the country rock could exhibit similar variation present in the enclave population due to localized metamorphism of each separate xenolith. Vernon (1991) noted euhedral plagioclase typifies mafic enclaves originating as a liquid and can be a monitor of

determining between the two possibilities. Euhedral and zoned plagioclase is seen across all enclave samples; however, some enclaves exhibit a granoblastic texture consistent with static recrystallization in the solid state (i.e., 14CG-SAO10-6, Figure 3-5A).

If the enclaves originated as restites, they likely would exhibit a higher-temperature, relatively anhydrous, refractory mineral assemblage (Didier and Barbarin, 1991). Instead, the enclaves are dominated by hydrous minerals, such as biotite and amphibole. Additionally, restite reported in granites is typically carried from the sources as small aggregates or single crystals, not large meter-sized enclaves (Chappell and White, 1991).

Textural features and microstructures in contained enclaves offer more constraints on their origin. A texture favoring magma mixing that is seen in the Danburg granite is the rapakivi feldspars, observed as large alkali feldspars mantled with plagioclase (Figure 3-2). A variety of theories exist in regards to the genesis of rapakivi granites. Two dominant theories stress an origin dominated by magmatic processes or those involving subsolidus processes (Dempster et al., 1994). With the presence of contained enclaves within the Danburg granite, these rapakivi feldspars are interpreted to be a consequence of magmatic mixing/mingling between two separate melts (Vernon 1991, Hibbard, 1991). The mixing of these two magmas creates changing conditions, causing the feldspars to be in disequilibrium with their environment. As the feldspars reequilibrate to the melt conditions, plagioclase again becomes stable and precipitates on the alkali feldspar phenocrysts, which act as nuclei for the plagioclase (Hibbard, 1981). The crystal shape of the rapakivi feldspars are commonly ovoid, which is an indicator of resorption of the

feldspars in response to introduction of the hotter, mafic liquid (Bussy, 1990). Similar An_x compositions are common within enclave-host populations from other intrusions, and the same is seen in this study by optically determining composition, which yields plagioclase compositions of An_{14-25} for the enclaves and An_5-An_{35} for the host.

Perhaps the least ambiguous evidence of a liquid origin for the enclaves is the common occurrence of feldspar phenocryst inclusions (~3 cm or more in length). These occasionally exhibit the rapakivi texture that is widespread throughout the host. The crystals must be foreign to the enclaves for they are not sufficiently potassic for the crystallization of large alkali feldspar phenocrysts. Furthermore, some of the crystals can be seen straddling the boundary of the enclave and host (Figure 4-2). This implies the feldspars were transported across the contact. This could only occur if the enclave material was in a semi-fluid state where mechanical mixing could transport a feldspar phenocryst into the enclave. The presence of these alkali feldspar phenocryst inclusions is strong evidence for magma mixing processes (Bussy, 1990, Didier, 1984) and is seen in many enclave-host pairs from other intrusions as well (Didier and Barbarin, 1991, Feng et al., 2011).

Textures consistent with quenching are observed in some Danburg enclaves, and are indicative of mixing of two liquids with thermal and viscosity contrasts. Within the Danburg, these features include chilled margins, which are discerned by a slightly darker border than the interior of the enclave (Figure 4-1C,E). This reflects the localized chilling of the hot mafic globule where it is in contact with the relatively cold, host melt. This texture is not as pronounced as in some enclave-host pairs where the margin is quenched

enough to produce a glassy boundary. However, the absence of chilled margins does not preclude a liquid origin and instead can signify interaction between the mafic enclave and felsic host (Weibe, 1991). Alternatively, the chill margins observed on some of the enclaves could also be interpreted as a reaction rim between a xenolith and the granitic magma. The enclave population consistently has a finer grain size than the host granite (Figures 4-1, 4-2). A skeletal crystal habit is prevalent in titanites within the more mafic enclaves (14CG-SAO10-5B,C, 14CG-SAO10-1) (Figure 3-3, 3-4). This unique morphology results from very rapid growth in a volatile-rich medium, which is consistent with the expected crystallization history of these hornblende-biotite-rich enclaves and enclaves in general (Didier and Barbarin, 1991). The titanites are often intergrown with plagioclase, termed an "ophitic" texture by Hibbard (1991) (Figure 3-3). The plagioclase are interpreted to be the result of rapid nucleation in an undercooled, likely more mafic system (Hibbard, 1991). The Na-rich composition of these plagioclase grains, however, is difficult to explain. This skeletal texture could also be explained as poikilitic porphyroblasts with the plagioclase grains being the included minerals. This would be consistent with a xenolithic origin for the contained enclaves. Lastly, apatite forms acicular prisms (aspect ratio up to 10:1) and is present in relatively large amounts (>1.5%) within the enclaves, a morphology that may also form by quenching (Wyllie et al., 1962, Vernon, 1983, Hibbard, 1991).

Determining the origin of mafic enclaves is difficult due to the complex interaction that occurred between the enclaves and the felsic host that produced sometimes the ambiguous mineralogical and textural features noted earlier. The strongest

textural evidence for a liquid origin includes both the rapakivi texture, which occurs due to evolving melt conditions (i.e., introduction of a new magma) and the presence of these feldspar phenocrysts not only within the Danburg host and its enclaves, but also straddling the boundaries. Their positioning and presence is hard to explain by any other means. Combined with several other mineralogical and textural features outlined, an origin involving magma mixing between a more mafic parent and a granitic melt is considered the most plausible.

4.1.5. The Cogenetic Danburg, Mafic Enclaves, and Sandy Hill Intrusions

The Sandy Hill represents the most geochemically evolved melt composition (SiO_2 ~74-76 wt. %) within the analyzed suite of rocks, whereas the Danburg is intermediate in composition between the Sandy Hill and the enclaves (Figure 3-7). The enclaves are typically lower in Si, relative to the host, and enriched in Al, Fe, Mg, Mn, P, Ca, and Na. The elements K and Na are less systematic, as is frequently observed in other studies (Debon, 1991). Experimental evidence has shown that major element diffusion between two melts of differing compositions exhibits systematic exchange of all elements on both sides of the contact surface (Yoder, 1973, Johnston and Wyllie, 1988). Typically, K, Si, and Na migrate from the felsic component to the mafic one, while Ca, Fe, Mg, Ti, and Al show the reverse relationship (Figure 4-3) in an effort to achieve chemical equilibrium (Debon, 1991). Through this chemical exchange, the Danburg granite and enclaves become new, hybridized compositions that are not representative of their original sources. The extent of the chemical exchange observed is also supportive of a

model whereby two liquids mix; solid/liquid interdiffusion can occur but is typically of a lesser magnitude than that observed for the enclaves here (Maury and Didier, 1991).

Harker diagrams for the Danburg-Sandy Hill suite (Figure 3-7) are a means to visualize the compositional data and evaluate potential relationships between this coeval suite of rocks. The geochemical trends indicate that the Danburg formed from a hybridized magma created through the mixing of more mafic source (enclave parent material) and a more evolved, felsic source (Sandy Hill magma). Binary mixing of two sources on element-element variation diagrams will produce a linear trend (Wall et al., 1987, Chappell, 1996), such as those observed in Figure 4-4, whereas assimilation-fractional crystallization models tend to produce various inflections depending on the fractionating mineral assemblage. For most of the samples analyzed (the most mafic sample being the exception), a strong correlation exists between SiO_2 and TiO_2, Al_2O_3, Fe_2O_3, CaO, MgO, and P_2O_5 ($R^2 > 0.90$), a moderate correlation for MnO ($R^2 = 0.77$), and weak to no apparent correlation in Na_2O and K_2O ($R^2 = 0.5041$ and 0.0135, respectively). K_2O is often the most poorly defined correlation between enclaves and their host (Debon, 1991), which is likely due to post-crystallization alteration. The ASI-index also shows a clear positive trend ($R^2 = 0.9687$) (Figure 4-4). The association reflects the trend of increasing excess of aluminum from enclave to Danburg to Sandy Hill. This highlights the systematic change from metaluminous to peraluminous as the mafic melt hybridized with the peraluminous felsic melt.

The linear trends outlined above are indicative of binary mixing of two sources. In the study of mafic enclaves, determining the original source often remains unresolved

due to the degree to which the enclaves change through interaction with the host magma (Chappell, 1996, Didier and Barbarin, 1991). However, both end-members must fall on the mixing line defined by the suite of hybridized whole rocks, and some constraint on the end-member compositions and mixing proportions can still be determined with a few assumptions. Using a simple mixing model, the proportions of end-member sources mixed to create the Danburg granite is evaluated in Figure 4-4. Although original end-member compositions are not known, the mixing model was performed assuming the Sandy Hill granite (highest Sr/Sr, highest SiO_2, peraluminous) represents the felsic end-member melt composition. Through visual inspection of the enclave textural and geochemical data, the second-most mafic enclave (14CG-SAO10-5B) is used as a proxy for the mafic melt inferred to have hybridized to produce the Danburg pluton. The lowest-SiO_2, most ferromagnesian enclave (14CG-SAO10-1) does not fit the linear trend defined by the rest of the data, and so it is not an appropriate candidate to model with the data that define a mixing trend. Under these assumptions, the Danburg granite would have formed as a mixture with a proportion of 30/70 (30% enclave parent material, 70% felsic melt) (Figure 4-4). The proportion of enclave parent material would be less if the actual parent were lower in SiO_2. This proportion is at odds with the current volume of enclaves, and if accurate it indicates that a significant proportion of the original enclave-parent material was digested during hybridization. It is suggested that the abundance of preserved enclaves can only qualitatively measure the respective mantle and crustal contributions (Didier and Barbarin, 1991) just as the absence of enclaves does not conclusively indicate zero mantle involvement in producing a granitic melt.

Considering the lowest-SiO_2, most ferromagnesian enclave 14CG-SAO10-1, it is clear that other processes besides mixing are required to explain the compositional variability seen in the enclaves, since it does not fall on the linear mixing trend. If the enclaves were in fact sourced from a mafic melt, fractional crystallization prior to mixing may also contribute to some of the compositional variation. During open system fractional crystallization, minerals form and are effectively removed from the melt, and do not interact with it further. This is achieved by crystals either settling to the bottom of a magma chamber or being left behind as the melt continues to move (e.g., filter pressing). To investigate the possibility that samples 14CG-SAO10-1 to 14CG-SAO10-5B are related through fractional crystallization of a like-parent, a different set of modeling was performed. Based on the observed enclave mineralogy, and expectations of minerals saturating in a hydrous, mafic melt, amphibole and Ca-rich plagioclase with the addition of ilmenite (samples were ilmenite normative) were considered the most likely early forming minerals. The most successful model consists of a solid composed of 45% Ca-rich plagioclase, 45% amphibole, and 10% ilmenite as the fractionating assemblage, also shown in Figure 4-4. Average composition of amphibole cores, modal composition of ilmenite, and plagioclase with a composition of An_{47} were used based on the average composition of amphibole and most Ca-rich plagioclase present in other enclaves (determined by electron microprobe) reported by Dvoracek (2003). Using the geometric approach (lever-rule; e.g., Rollinson, 1993), the evolution from 14CG-SAO10-1 to 14CG-SAO10-5B in the major oxides Al_2O_3, Fe_2O_3, CaO, MnO, and MgO would require 11-35% crystallization of 45% amphibole:45% An_{47} plagioclase:10% ilmenite mixture.

The simplistic modeling indicates that the fractional crystallization of ~11-35% could explain the compositional change between the two most mafic enclaves.

Zirconium concentration in whole rocks can be used in a similar manner to major elements when applied to Harker diagrams. The Zr concentration is quite high in the enclaves (576-1059ppm), lowest in the Sandy Hill (112-186ppm), with the median being the Danburg (328ppm) (Figure 4-4). This implies the enclave parent-material was considerably enriched in Zr and other incompatible elements in general (other trace elements, including Nb, and Ce, are also elevated relative to Sandy Hill and Danburg intrusives; Table 3-2). Processes that affect the major oxides should also be observed in trace elements, such as Zr. In a typical differentiation trend, it would be expected to see a rise in Zr as the melt evolves by fractional crystallization due to incompatibility in most rock-forming minerals, followed by a decrease in Zr in the melt once zircon saturates. The difference between the lowest-SiO2, most ferromagnesian enclave (14CG-SAO10-1) and (14CG-SAO10-5B) again cannot be explained solely by mixing, although mixing in the proportions 30:70 can again reconcile the composition of the Danburg pluton. The amount of crystallization needed to evolve 14CG-SAO10-1 to 14CG-SAO10-5B was calculated using the Rayleigh Fractionation model. Rayleigh Fractionation is defined as as: $\frac{C_L}{C_O} = F^{D-1}$, where C_L is the concentration of Zr in the remaining material (i.e., 14CG-SAO10-5B), C_O is the concentration of Zr in the initial material (i.e., 14CG-SAO10-1), F is the fraction of melt remaining, and D is the bulk partition coefficient of the model fractionating assemblage (Rollinson, 1993). Mineral-melt partition coefficients (K) of $K^{Zr}_{amph\text{-}melt} = 0.50$, $K^{Zr}_{plag\text{-}melt} = 0.048$ (Rollinson, 1993), and $K^{Zr}_{ilm\text{-}melt} = 0.33$

(Nakamura et al., 1986) were used, giving D = 0.279. Under these assumptions, the change from 14CG-SAO10-1 to 14CG-SAO10-5B requires 55% crystallization prior to mixing (Figure 4-4). This is higher in comparison with the range seen in the major oxides.

Dvoracek (2003) reported Zr concentration for all sampled enclaves. They cluster at consistently lower values (400-650ppm) than seen in the mafic enclaves sampled for this study (576-1059ppm). It is possible the enclaves that are enriched in Zr (>1000 ppm) could attribute this enrichment to their concentration of titanite, which readily incorporates Zr. It is possibly more reasonable then, to model the change in Zr concentration from 14CG-SAO10-1 to an enclave from Dvoracek's (2003) suite of enclaves. In doing so, the percentage of the fractionating assemblage required lowers to 18%. This result is much more consistent with the oxides. More samples of the enclaves would need to be taken to see if this Zr enrichment is anomalous or widespread.

4.1.6. Controversy in Magmatic Enclave Research/Summary of Enclave Origins

The study of enclaves is a powerful petrologic tool for they may provide valuable information on granite petrogenesis that cannot be attained without them. As such, varying models and explanations exist for mafic enclave origins. Mapped in contact with the Danburg is a sizable body of mafic metavolcanic rock (Figure 1-1B), which is a possible source for igneous xenoliths. Meta-igneous xenoliths are common and can even be heavily reworked to resemble restites or mafic enclaves that was a liquid hybridized with a felsic source. Autolith enclaves, or differentiated cumulates, are fairly scarce in

granitoid magmas, yet would result in similar linear trends shown previously. The restite model for enclaves is in debate as well, with suggestions that mafic microgranular enclaves are simply a type of restite that exhibit igneous textures because they are melting meta-igenous rocks (Chappell and White, 1991). Often the cogenetic link between enclaves and their hosts is used to support restite and autolith models, yet the near identical mineral compositions and assemblages have been proposed as the result of physical and chemical transfer between two melts. Lastly, the source of a possible second melt is often debated, ranging from lamprophyres, alkaline or aluminous basalts, andesitic basalts, to gabbroic differentiates (Didier and Barbarin, 1991, Ayrton, 1991, Dvoracek and Roden, 2005). The original compositions are effectively disguised due to thorough interface between the two magmas. According to Didier and Barbarin (1991), despite voluminous study on mafic enclaves, the multitude of processes modifying their primary composition complicates defining their exact origin.

Based on the results of this study the enclaves within the Danburg granite are interpreted to have formed through mixing of two magma-compositions. Though some textural and geochemical features could be indicative of a different origin for the enclaves, phenocrysts of rapakivi feldspars, statistically contemporaneous titanite and zircon ages for both the enclaves and the host, and a successful model of fractional crystallization between 14CG-SAO10-1 and 14CGSAO10-5B are difficult to reconcile by alternate origins.

4.2. Geochemical Constraints on the Tectonic Setting of Danburg Emplacement

Geochemical classification schemes devised by Frost et. al (2001) provide a useful comparison for granites formed across a wide variety of settings, and can give insight into the origin and evolution of the Danburg-Sandy Hill-enclave system. Based on the comparison of the Fe*, MALI, ASI, and AI (Figure 3-8, Table 3-3), these are classified as Caledonian-type granites, which refers generally to post-collisional granites. Due to geochemical differences, the granite types described by Frost et al. (2001) follow distinct trends on QAP diagrams. Again, the Danburg-Sandy Hill-enclave system follows a Caledonian trend of potassic enrichment. The enclaves individually are more consistent with the ferroan granite type (high iron and alkalis). The corresponding tectonic environments of the Danburg granite and mafic enclaves should not be the same for they are not interpreted to be of the same source. A tectonic setting that can explain the presence of enclaves in a granitic system (two separate sources) includes collision of crust, initiating crustal thickening to result in crustal delamination to generate granitic magmatism. The convergence thickens the crust, causing the base of the lithosphere to experience greater pressure, becoming metamorphosed and more dense, eventually sinking into the underlying mantle (Bird, 1979). Hot asthenospheric mantle fills the void while undergoing decompression melting. This added heat can help partially melt the crust, creating the Caledonian-style plutons like the Danburg granite (Frost and Frost, 2008). This tectonic model is consistent with the presence of the less-evolved enclaves. While this model assumes that the mafic enclaves may have origins in the mantle, fractionation trends shown earlier are evidence that the melt likely underwent some

differentiation before interacting with the Danburg/Sandy Hill system. Several gabbroic intrusions with Alleghanian ages are known, and originate from mantle melting (Speer et al., 1994), so mantle involvement in Alleghanian magmatism is not unreasonable. These gabbroids are alkaline, yet do not reach the alkalinity of the enclaves within the Danburg granite (Speer and Hoff, 1997). Additionally, the Danburg pluton and granites nearby (Elberton, Siloam, Sparta, etc.) have $^{87}Sr/^{86}Sr$ ratios of <0.708, which is consistent with mixing of melted crust and an isotopically juvenile source (Fullagar and Butler, 1979).

Based on the tectonic discrimination diagram for granitoids utilizing Rb, Y, and Nb (Pearce et al., 1984; Figure 4-5), the Danburg and its enclaves plot as within-plate granites (WPG), although they are near the region of volcanic arc granite (VAG) and post-COLG (post-collisional granite). The Sandy Hill samples spread across the WPG and post-COLG. A weak trend is defined by the change from enclave to Danburg to Sandy Hill as the system evolves from WPG to post-COLG.

The presence of both titanite and zircon in the enclaves and host allow for the opportunity to calculate estimates of both crystallization temperature and pressure. Both the Danburg pluton and contained enclaves record values within error of one another, with calculated Zr-in-titanite pressures of 5.1-6.5 kilobars equivalent to emplacement depths of ~15-20 km depth. Ti-in-zircon thermometry indicates crystallization at 765-771°C. This is consistent with depths and temperatures expected for Alleghanian plutons determined through other means (Speer at el., 1994). The absence of titanite in the Sandy Hill samples prevents pressures to be calculated; however, crystallization temperatures are recorded within error of the Danburg granite and enclaves.

Assuming the calculated Ti-in-zircon temperatures approximate the ambient temperature at depth of melt formation, and that the highly viscous melt did not rise significantly before cooling, the combined temperature and pressure can be used to estimate a geothermal gradient. A temperature gradient of 37°C/km for the Danburg pluton and 46°C/km for included enclaves indicate an elevated gradient compared to the standard 25-30°C/km. This either requires some addition of heat at depth through the intrusion of deeper melts, or could be explained through advection by an ascending mafic melt. Though the constraints from accessory mineral thermobarometry involve many assumptions, the discussion above is consistent with models for formation of post-collisional granites, which commonly form in association with mantle-derived melts.

4.3. Summary/Geodynamic Setting

The textural, mineralogical, geochemical, and geochronological evidence gathered in this study is consistent with an interpretation whereby the enclaves represent an addition of a juvenile, more mafic magma to a felsic magma. This magma likely differentiated before it interacted with the Danburg/Sandy Hill source. Once in contact, this injection produced a thermal disequilibrium that created vigorous convection and stirring, favoring magma mixing/mingling (Sparks et al., 1977). A post-collisional petrogenesis is considered the most plausible geodynamic setting considering both observations from this study and regional studies. Post-collisional granites are typically younger than but still genetically related to the collisional event and are often associated with large oblique movement along major shear-zones. The Danburg-Sandy Hill-enclave

system is consistent with both qualifiers due to ~305Ma age which is on the younger side of the Alleghanian orogen in the SAO (330-290Ma) and is just north of one of multiple mega-shear zones associated with the Alleghanian (Foster et al., 2013). Additionally, crustal collision can result in delamination of the crust into the mantle, allowing for asthenospheric mantle to undergo decompression melting. This interaction between mantle and crustal sources creates an ideal environment to create the Danburg-Sandy Hill-enclave system (Figure 4-6). The interface involves the addition of heat and mass hypothesized to be involved.

4.4. Regional Significance

The Danburg-Sandy Hill-enclave system is part of a magmatic suite of plutons emplaced in the southern Appalachians during the Carboniferous-Permian. The ages reported for the rocks within this study match current Alleghanian ages for other SAO plutons. The Danburg and Sandy Hill pluton's geochemistry is consistent with emplacement within a post-collisional tectonic setting. The theory regarding the tectonics of the Alleghanian orogeny has evolved, from subduction to current models suggesting magmatism caused through a transpressional boundary with associated crustal anatexis (Wenner, 1981, Mueller et al., 2013). This debate, fueled by seemingly contradictory evidence, may reflect changing tectonic regimes over time. In addition to those age constraints discussed here, a large compilation of modern ages for SAO plutons suggests a continuum of granites from ~340 to 290 Ma, implying continuous magmatism from the Acadian to Alleghanian (Lin 2015, personal communication), with subduction leading to

collisional crustal thickening. Inheritance of geochemical signatures from source rocks could also play a role. The Charlotte belt is a volcanic arc, thus melting this material to create the Danburg/Sandy Hill granitoids might impart some subduction-related chemical signatures. Resolving such a debate is not in the scope of this study; however, the new data associated with the Danburg-enclave-Sandy Hill system can be added to the mounting compilation of SAO granitoids to better understand the Alleghanian Orogeny.

4.5. Emplacement Models for the Delhi Syenite: New Ideas About an Old Pluton

The Delhi granitoid is a syenitic pluton located in NE Georgia. It intrudes the Charlotte belt; a largely metaigneous terrane that is often included in the larger Carolinia. Initially the Delhi pluton was expected and proposed to be chronologically related to the nearby Danburg/Sandy Hill intrusion (Dvoracek, 2003). It had also been mapped as cross-cutting the Danburg, suggesting it is not only related, but a younger intrusive event (Allard and Whitney, 1994). Contrarily, McSween and Harvey (1997) included the Delhi syenite as part of a ~400Ma, post Acadian intrusive suite throughout the Charlotte belt comprised primarily of gabbros and syenites, known as the Concord plutonic suite (Figure 4-7). The crystallization age determined here of 468.9±6.7Ma refutes both models. Instead, it is shown that the Delhi significantly predates the Danburg-Sandy Hill suite, being emplaced as part of the Taconic arc, and field relations require revision (Figure 4-8).

4.5.1. The Charlotte Belt and Tectonic Setting of Delhi Emplacement

The Charlotte Belt is a major belt of rock in the central and southern Appalachians that extends from Virginia through Georgia. It is composed of numerous granitic to gabbroic plutons, metamorphosed mafic complexes, and metavolcanics (Wilson and Jones, 1986). Three age groups dominate the geology in the terrane: ~300, ~400, ~and 550 Ma (Wilson and Jones, 1986). Igneous activity is reported to be trimodal, involving gabbro, granite, and syenite (Sinha et al., 1989), and the entire terrane has been interpreted as a peri-Gondwanan volcanic island arc (Secor et al., 1983; Samson et al., 1995). Fossil evidence suggests they were not related to the Laurentian coast, rather positioned along the margin of west Gondwana (Secor et al., 1983). This distinction is generally accepted and has given the accreted terranes east of the Piedmont the notation as the Peri-Gondwanan realm. On its western border, the Charlotte belt is in contact with the King's Mountain Belt and the Inner Piedmont. Its eastern flank is in contact with the Carolina Slate belt. The literature is often unclear with respect to grouping the Charlotte belt with other terranes. It is rarely discussed as its own entity; rather, as a component of the larger Carolinia superterrane which includes the Carolina Slate Belt, Charlotte Belt, and other minor crustal blocks. The relative absence of research attempting to solely characterize the role of the Charlotte belt in the orogenesis of the Appalachians is a testament to the complexity that surrounds it. As such, these discussions concerning the Charlotte belt will be encompassed under Carolinia as is most common in the literature.

Carolinia has been defined as "including all exposed, proven peri-Gondwana rocks of the southern Appalachians that lie east of the central Piedmont shear zone and

extend to the Atlantic coastal plain" (Pollock et al., 2012). The oldest known magmatism is a low grade metamorphosed magmatic arc sequence intruded by a metagranodiorite dated at 670 Ma (Hibbard et al., 2007). The geologic evolution of Carolinia is complex, with conflicting lines of evidence placing the terrane at various paleogeographic locations since its formation off the coast of Gondwana, traversal across the Iapetus, and collision with the eastern margin of Laurentia. The history of Carolinia is further shrouded due to the buried contact zone between Carolinia and Laurentia beneath the central Piedmont shear zone. Multiple conflicting models exist concerning these events. The prevailing two models will be outlined while attempting to place the Delhi syenite within the framework of each model.

4.5.2. Late Ordovician - Early Silurian Model

Constraining the formation of Carolinia is the first priority in mapping its journey to the present location in Laurentia. The simple answer would place Carolinia as a magmatic arc off the coast of Laurentia, colliding at the conclusion of that process. However, evidence suggests that this is not likely the case. Fossils, specifically the presence of a species *Paradoxides* in a rock formation part of Carolinia is exotic to Laurentia (Secor et al., 1983). This faunal data suggests instead a relationship with the Gondwanan coast, as these species are only present in other peri-Gondwanan terranes (Pollock et al., 2012, Hibbard et al., 2002). Also, Carolinia's positioning on the coast of Laurentia is markedly similar to more northern known peri-Gondwanan terranes such as Avalonia (Hibbard et al., 2002).

Unfortunately, reliable paleomagnetic data is currently unavailable that can precisely track Carolinia's travel across the Iapetus. Two independent paleomagnetic studies, however, place Carolinia at a latitude of 22°S. This location is near Laurentia's paleogeographic position during the Late Ordovician (~455Ma) (Vick et al., 1987, Noel et al., 1988). The model adheres to multiple lines of evidence to suggest a collision between Carolinia and Laurentia during the Late Ordovician to Early Silurian (460Ma-430Ma):

(1) An Early Silurian unconformity that reflects loading of the Laurentian margin caused by accretion of terrane (Pollock et al., 2012)

(2) Voluminous magmatism during the Late Ordovician — Early Silurian in the Piedmont zone have geochemical signatures that suggest formation in a supra-subduction setting (Pollock et al., 2012)

(3) $^{40}Ar/^{39}Ar$ cooling ages from mica (455—444Ma) demonstrate Carolinia's response to Middle—Late Ordovician tectonism and metamorphism while $^{40}Ar/^{39}Ar$ cooling ages from amphibole (430-425Ma) indicate late Ordovician—Early Silurian uplift of Carolinia (Pollock et al., 2012)

This geological data is used to suggest that Carolinia and Laurentia's collision was marked by sinistral transpression with Carolinia being subducted beneath Laurentia. Hibbard et al. (2010) termed this event the Cherokee orogeny, named after the unconformity mentioned in (1) (Figure 1-4).

The Delhi syenite is a part of Carolinia and thus would have been involved in the aforementioned events. New SHRIMP-RG ^{207}Pb-corrected $^{206}Pb/^{238}U$ zircon ages from

the pluton have been dated at 468.9±4.8Ma. Its formation in this model would have occurred ~15Ma before collision with Laurentia. This would place it near the Laurentian margin, however not yet fully accreted. Constraining the actual initiation of subduction is not accounted for in this model. If ~450Ma represents the actual collision of the terrane to Laurentia then initiation of the subduction would likely have begun millions of years earlier. Thus, if the Delhi was an expression of the subduction it would have had to been part of the earliest magmas formed for it has been reported that arc magmatism lags behind subduction initiation by 5-15Ma (Tull et al., 2014). This is an unlikely scenario, for shoshonitic alkalic rocks are mainly seen as late stage differentiates in an arc setting rather than the first melts generated. However, it cannot be precluded as a possibility since shoshonites can be found in a variety of convergent and rift settings (Figure 3-9) (Müller et al., 1992).

Placing the Delhi in this framework is difficult relying solely on the data acquired. However, the presence of a syenitic pluton in the area may help discover the tectonic setting during this period since composition of plutonic rock suites is strongly correlated with tectonic province (Sinha et al, 1989).

4.5.3. Silurian - Devonian Model

A peri-Gondwanan origin for Carolinia is proposed, again based off faunal data present in clastic sedimentary rocks within the superterrane (Secor et al., 1983). Post origin the models diverge, with this interpretation again invoking fossil evidence (Secor et al., 1983) as well as paleomagnetic data (Van der Voo, 1988) to suggest Carolinia was

unlikely to be spatially related to Laurentia during Late Cambrian — Early Ordovician (Hatcher et al., 2007). This model rejects a Taconic-related accretion due to an absence of plutons of the appropriate age in Carolinia, specifically the Charlotte Belt. Instead it cites Silurian—Devonian (~360-420 Ma) magmatism in the Southern Appalachians, including a suite specific to the Charlotte belt, as an indicator of terrane suturing (Sinha et al., 1989). Metamorphic ages ranging from ~430-323 Ma are also cited as evidence of the event (Sinha et al., 1989). Tectonically, the model suggests a transtensional environment created through transpressional accretion of Carolinia to margin of Laurentia (Sinha et al., 1989, Sinha et al., 2012) (Figure 1-3). This would compensate for the trimodal plutonic suite seen in the Charlotte belt.

Situating the Delhi syenite within this framework is difficult. Its presence as a ~470Ma granitoid emplaced in the Charlotte belt contradicts the claim of no magmatic event during the Mid—Late Ordovician (Sinha et al., 1989). It is joined by the Barber gabbro complex (479Ma), Lowry's North granite (486Ma), and Southmont granite (479Ma) (McSween and Harvey, 1997, Sinha et al., 1989). Sinha et al. (1989) explains these as the last gasp of magmatism in a late-Cambrian magmatic episode. In this tectonic model the Delhi would be fully unrelated to the suturing of Carolinia to the North American margin. This timeframe would suggest the Delhi formed during its traversal towards the Laurentian margin. It is possible that the multitude of peri-Gondwanan terranes that were drifting across the Iapetus collided at some point. An arc-arc collision is an environment that could generate the Delhi's WPG signature (Figure 4-5).

4.5.4. Summary

The Delhi syenite is unique in its age and composition among the more voluminous plutonic suites in Carolinia. Placing it in the framework of one of the aforementioned tectonic models or general SAO magmatism leaves room for interpretation. The geochemistry of the Delhi syenite is most consistent with forming in an anorogenic setting. However, shoshonitic rocks can be found in continental arcs, post collisional arcs, initial oceanic arcs, late oceanic arcs, and within plate settings (Müller et al., 1992); all settings that likely existed throughout the history of the composite Carolinia terrane. The chronology of the models presented both agree that the Delhi would not yet be sutured onto North America's east coast at the time of crystallization (Figure 4-6). This is hardly limiting for Carolinia had a complex and shrouded evolution. Hibbard et al. (2002) describes an event in the Carolinia zone during the early Paleozoic responsible for plutonism and metamorphism in the Charlotte and Carolina belts as possibly representing back arc rifting or closure, arc-arc collision of the two belts, or subduction of an isotopically more evolved block. These tectonic settings are potential environments to create a magma like the Delhi. While this could be too early to generate a ~470Ma pluton, it is possible the Delhi was a last pulse of magmatism associated with this event. While plutonism, metamorphic ages, and fossil evidence can constrain parts of a ~250Ma journey, there are large gaps in the paleogeographic record that allow for potential events to cause magmatism. Paleomagnetic data is unreliable for these peri-Gondwanan terranes due to the metamorphic events that overprinted the signals, thus studying the geochemistry and geochronology of these plutons is key to unraveling the

mysteries of the Appalachian orogen and specifically Carolinia. Further isotopic and trace element data would serve to better characterize the Delhi syenite's petrogenesis.

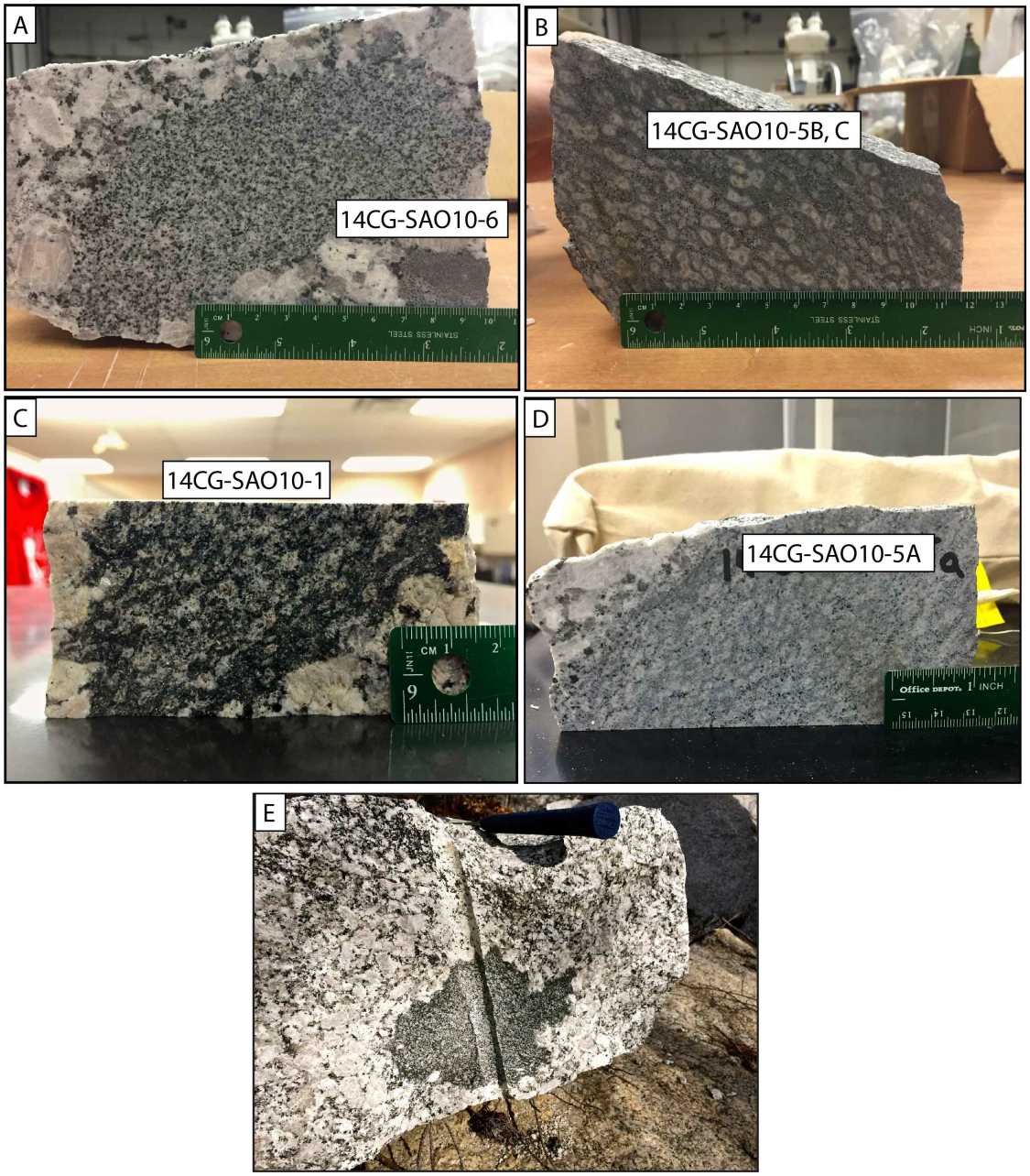

Figure 4-1: Representative enclaves from the Danburg quarry. The finer grain size and darker color immediately illustrate qualities consistent with mafic micro granular enclaves. Variation among the enclaves is also apparent. The enclaves shown in C has a weakly defined orientation of the depletion haloes around titanite parallel to the margin of the enclave. Both C and E have a boundary darker than its interior.

Figure 4-2: Feldspar phenocrysts entrained within and on the border of the enclaves. Texturally, these are most consistent with the enclaves forming through mixing of a mafic liquid with partially crystalline granitic melt.

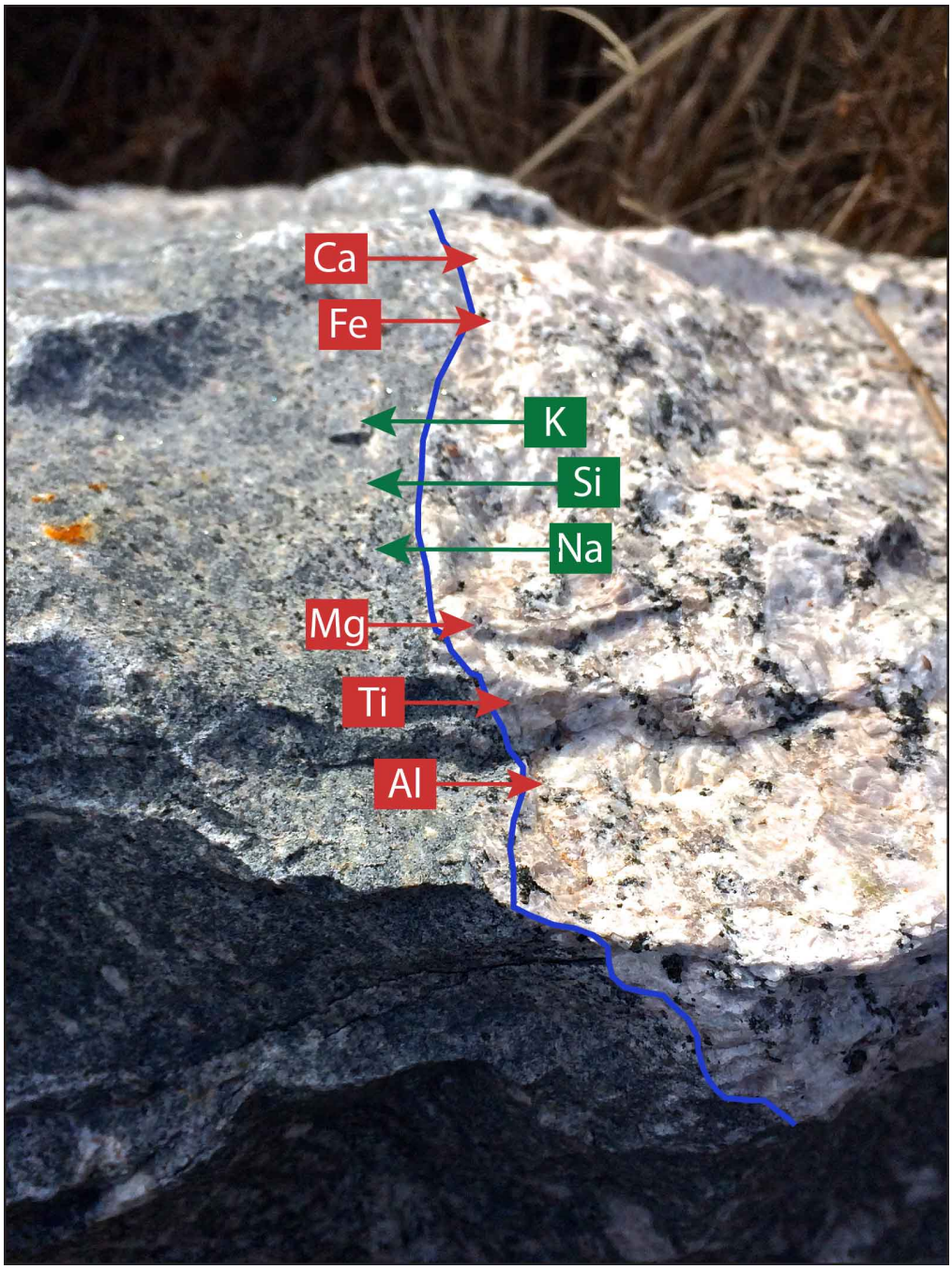

Figure 4-3: Field photo of the boundary between an enclave and the host granite. The exchange of major elements shown is interpreted to have occurred between the two separate magmas. While the magmas mix/mingle, they hybridize. The original thermal disparity between the melts prevents complete homogenization.

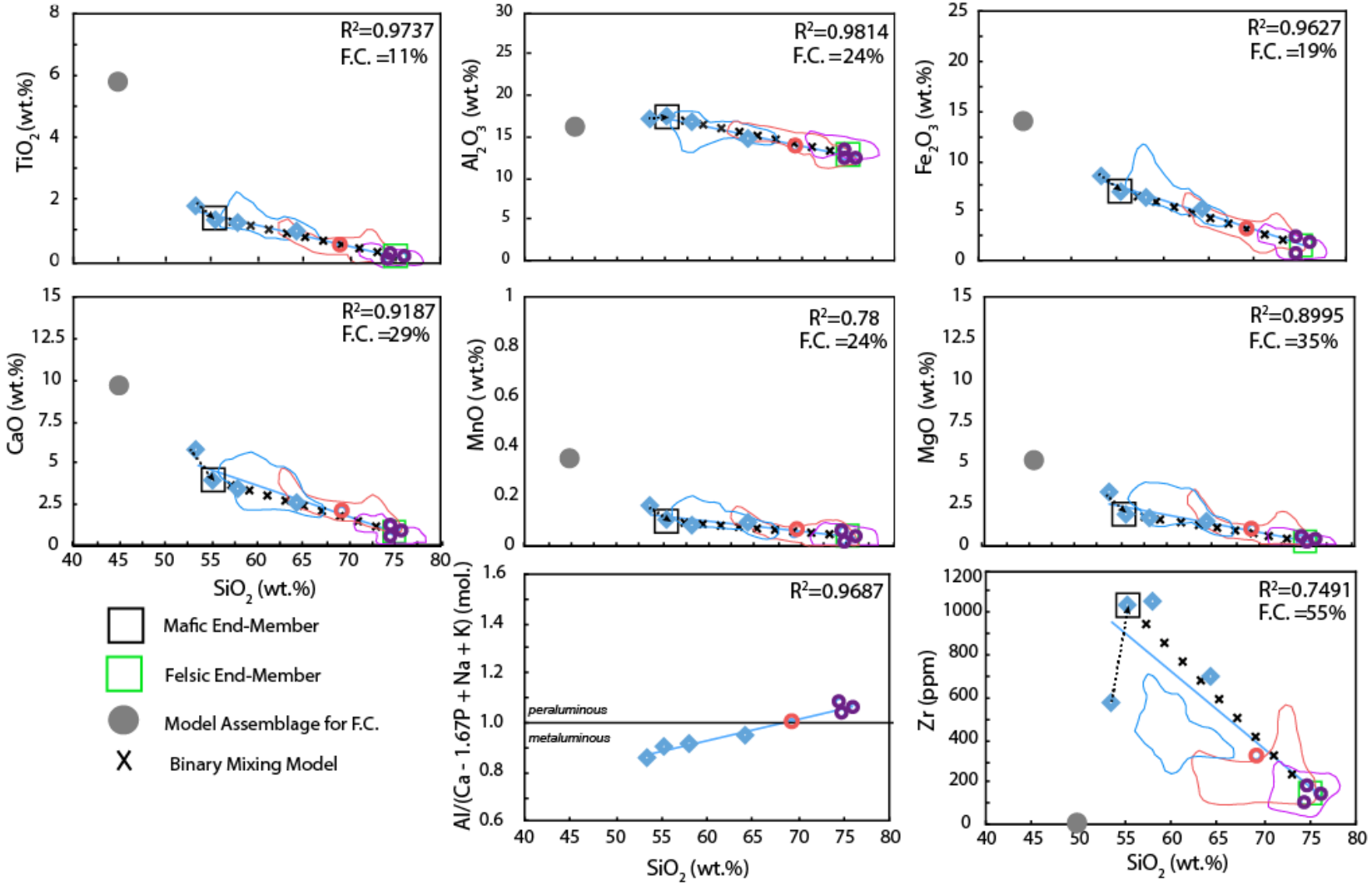
R²=0.9737
F.C. =11%
TiO2 (wt.%)
R²=0.9814
F.C. =24%
Al2O3 (wt.%)
R²=0.9627
F.C. =19%
Fe2O3 (wt.%)
R²=0.9187
F.C. =29%
CaO (wt.%)
R²=0.78
F.C. =24%
MnO (wt.%)
R²=0.8995
F.C. =35%
MgO (wt.%)
SiO2 (wt.%)
Mafic End-Member
Felsic End-Member
Model Assemblage for F.C.
Binary Mixing Model
R²=0.9687
peraluminous
metaluminous
Al/(Ca - 1.67P + Na + K) (mol.)
SiO2 (wt.%)
R²=0.7491
F.C. =55%
Zr (ppm)
SiO2 (wt.%)

Figure 4-4: Simple binary mixing and fractional crystallization model relating the Danburg granite, contained enclaves, and Sandy Hill granite. The model shown involves a change from fractional crystallization to binary mixing between the Sandy Hill and a parent material with the composition of the second most mafic enclave. The gray filled circle represents a bulk fractionating assemblage of 45% hornblende, 45% plagioclase (An47), and 10% ilmenite (see text for details). Percentage of fractionation required to go from the most mafic (SiO_2 = 53 wt. %) to the second most mafic enclave (SiO_2 = 55 wt. %) is shown in the upper right hand corner of each plot. The data with >55 wt. % SiO_2 define a linear array on each plot; the R-squared of a best fit line through these data is shown at upper right in each plot. Open boxes represent the modeled end-members for mixing, while the X's between them mark a 10% change in proportion. Fields with colored borders represent whole rock data reported by Dvoracek (2003): blue - mafic enclaves, red - Danburg granite, purple - Sandy Hill granite.

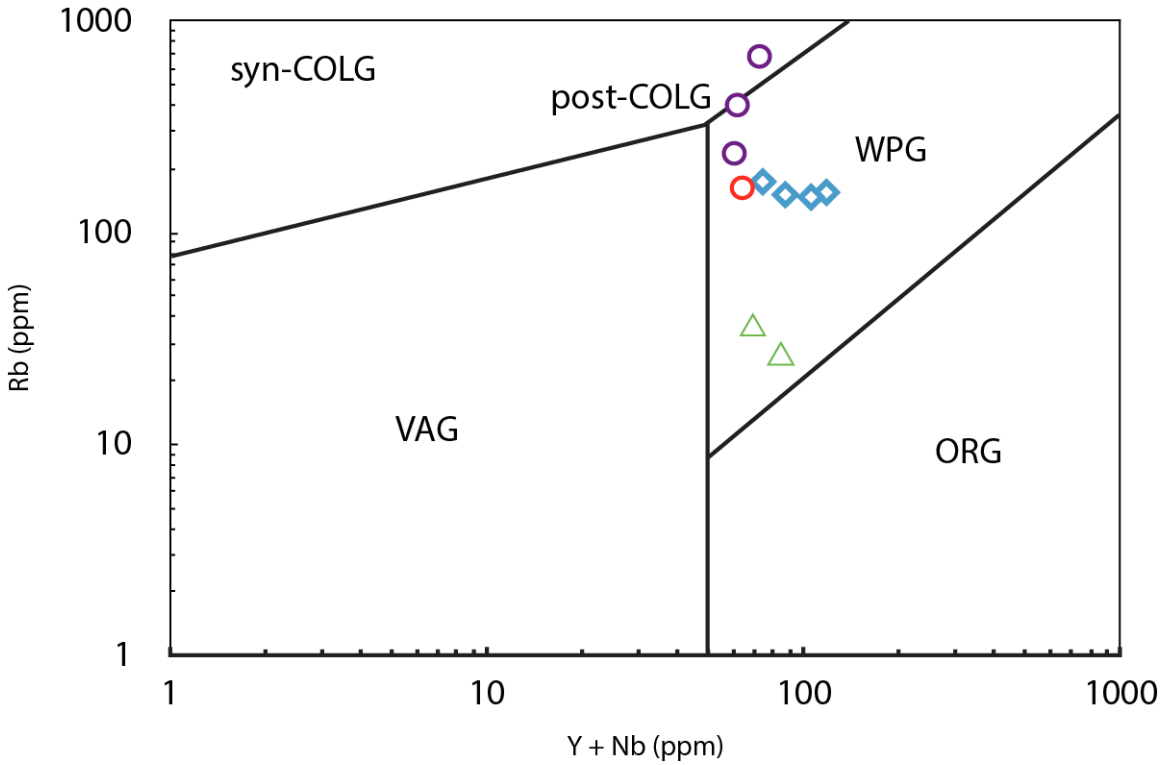

Figure 4-5: Granite trace element tectonic discrimination after Pearce et al. (1984). The enclaves, Danburg, and one of the Sandy Hill samples plot firmly as within plate granites (WPG). One Sandy Hill sample plots on the junction between WPG and post-collisional granite (post-COLG), while another plots as a true post-COLG. An arcuate trend from enclave to Danburg to Sandy Hill exists and may represent mixing. The Delhi syenite plots as a WPG. Blue diamond – mafic enclaves, red circle – Danburg granite, purple circle – Sandy Hill granite, green triangle – Delhi syenite.

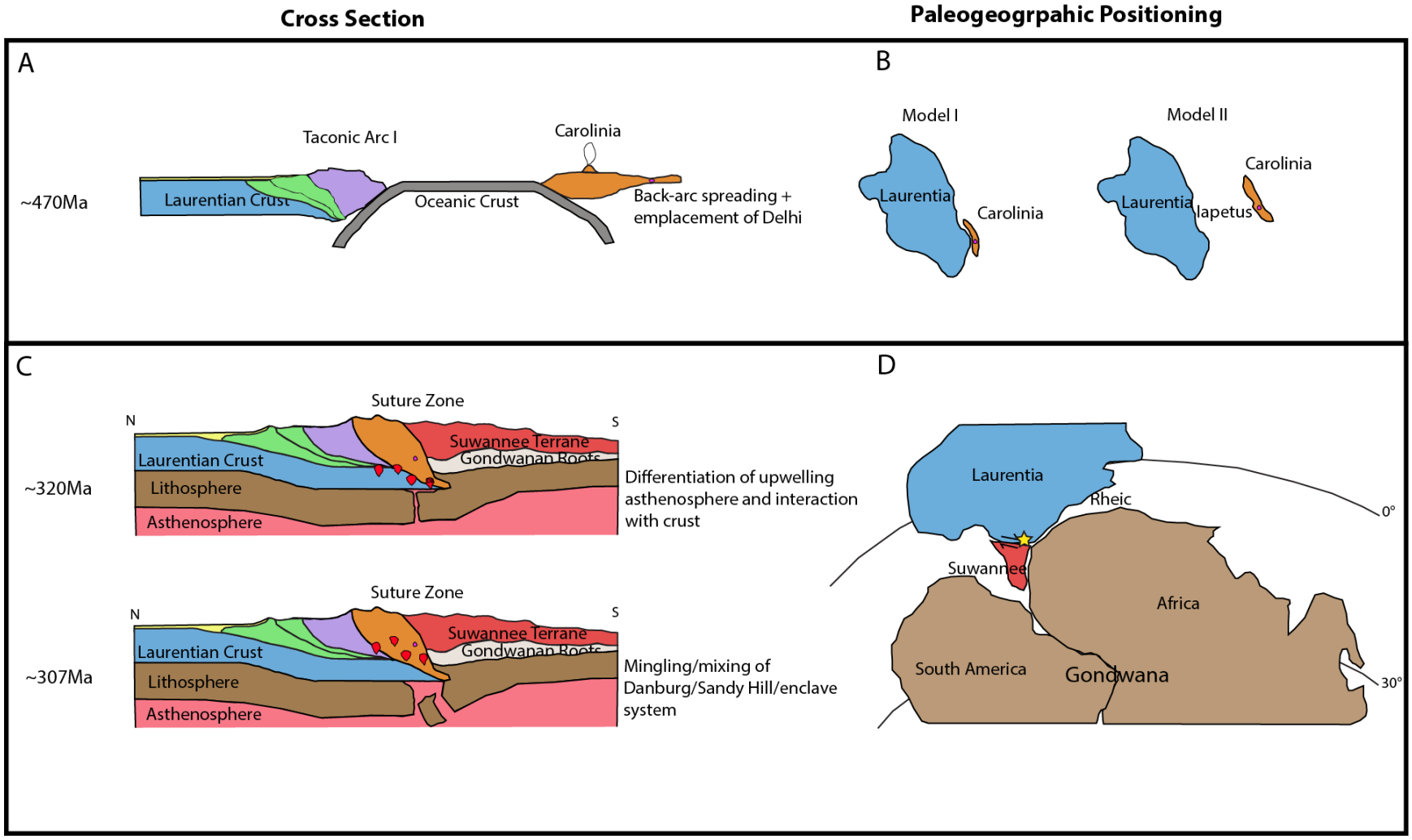
Cross Section
Paleogeogrpahic Positioning
A
~470Ma
Taconic Arc I
Carolinia
Laurentian Crust
Oceanic Crust
Back-arc spreading +
emplacement of Delhi
B
Model I
Laurentia
Carolinia
Model II
Laurentia
Carolinia
Iapetus
C
~320Ma
Suture Zone
N
S
Suwannee Terrane
Gondwanan Roots
Laurentian Crust
Lithosphere
Asthenosphere
Differentiation of upwelling
asthenosphere and interaction
with crust
~307Ma
Suture Zone
N
S
Suwannee Terrane
Gondwanan Roots
Laurentian Crust
Lithosphere
Asthenosphere
Mingling/mixing of
Danburg/Sandy Hill/enclave
system
D
Laurentia
Rheic
0°
Suwannee
Africa
South America
Gondwana
30°

Figure 4-6: Geodynamic model modified from Mueller et al., 2013 and Sinha et al., 2012. Both a cross sectional view and paleogeographic position of the major crustal blocks is presented during times relevant to this study. At 470Ma, the generation of the Delhi syenite occurs. It intrudes the Charlotte belt, whose position relative to the Laurentian margin at this time is not well constrained. Two scenarios are shown. From ~320-307Ma, the Alleghanian orogeny is in effect. Through crustal collision, the crust is thickened and metamorphosed. A portion of the basal lithosphere delaminates allowing interaction with the mantle. The generation of mafic magma from the upwelling mantle followed by partial melting in the mid-crust produces a setting possible for the genesis of the Danburg-enclave-Sandy Hill system.

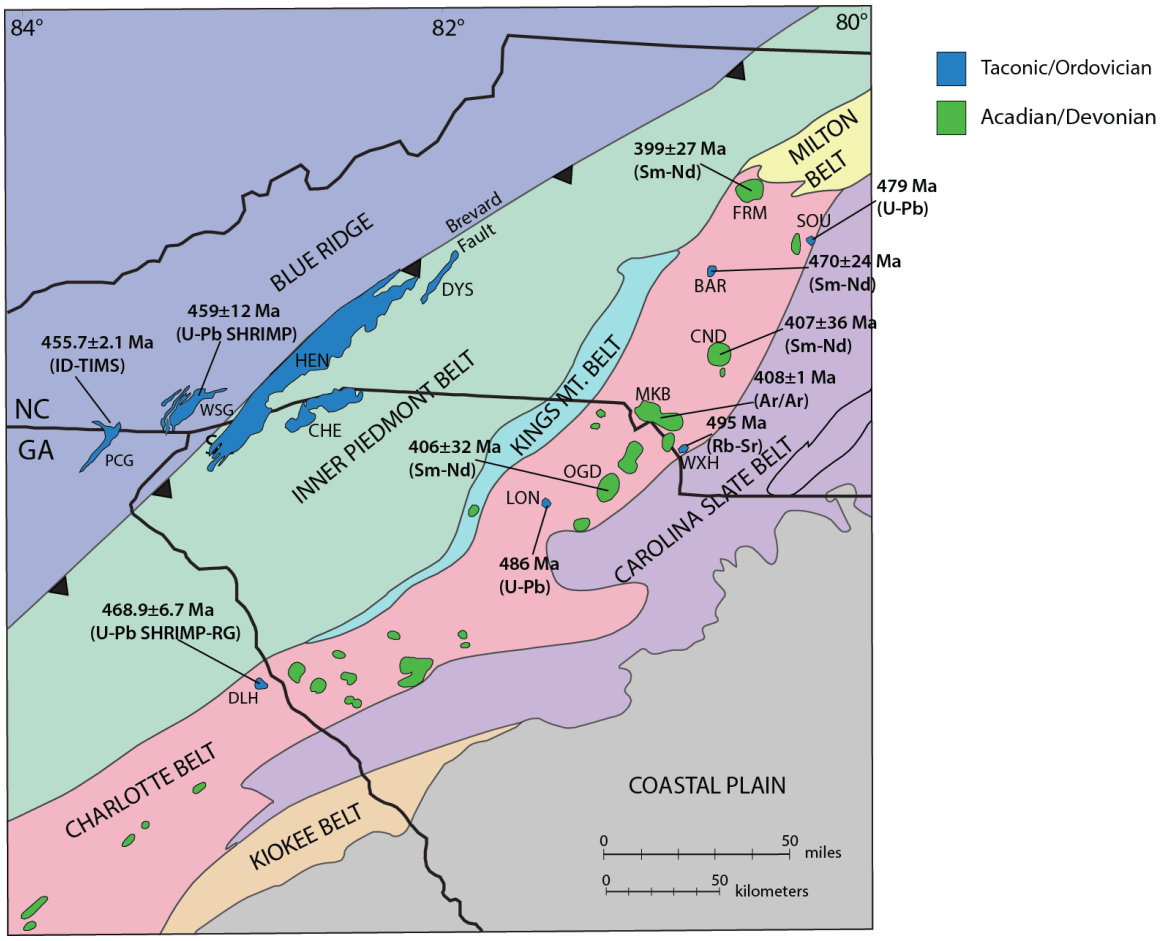

Figure 4-7: Geologic map of southeastern Laurentia highlighting the Charlotte Belt. The Delhi is shown to be part of the Taconic magmatic suite, in contrast to prior suggestions that it was either Alleghanian or Acadian. A U-Pb zircon age of 468.9±6.7Ma shows the Delhi is not related to either event, and instead interpreted to have been emplaced as part of the original arc prior to collision.

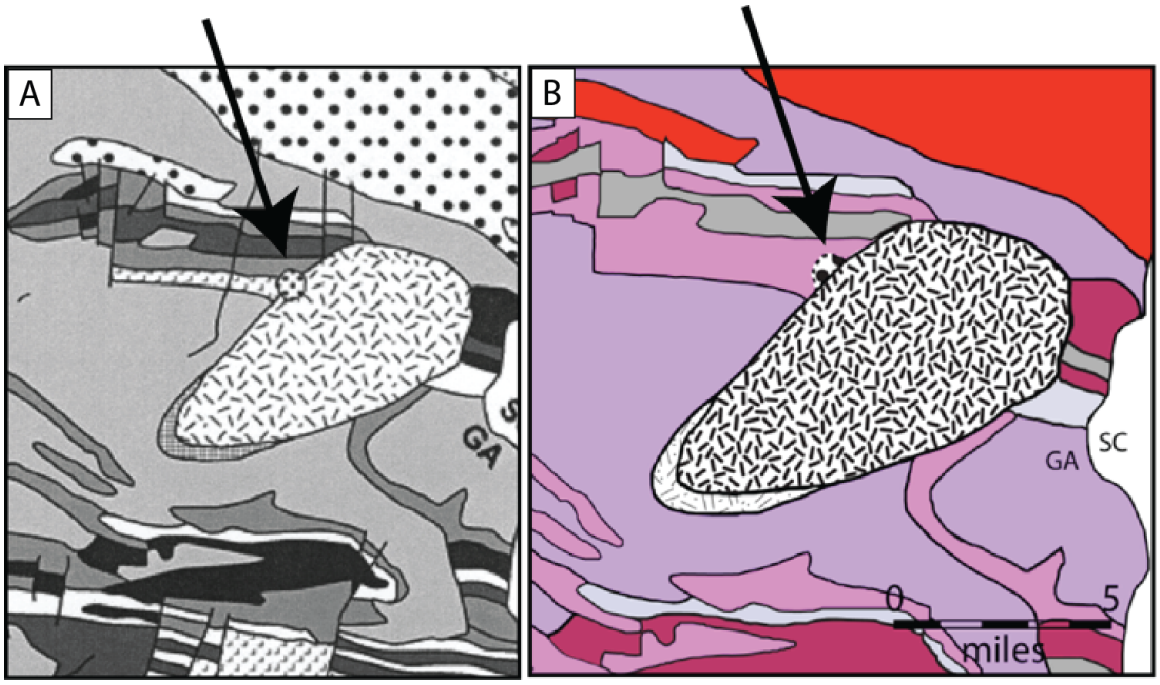

Figure 4-8: Geologic map of the study area, from Allard and Whitney (1994) (A) and Figure 1-1B (B). The arrow indicates the Delhi syenite and shows that new data from this study has resulted in a U-Pb zircon age of 468.9±6.7Ma, effectively changing the field map associated with this area.

CHAPTER 5: CONCLUSIONS

New SHRIMP-RG ^{207}Pb-corrected $^{206}Pb/^{238}U$ zircon and titanites yield statistically contemporaneous ages of 307±4.7Ma for the Danburg granite, 307.3±3.7Ma for the mafic enclaves, and 304.7±3.0Ma for the Sandy Hill granite confirming their connection to Alleghanian magmatism. Tectonic discrimination diagrams for whole rock data classify the Danburg-enclave-Sandy Hill suite as Caledonian granitoids forming through post-collisional magmatism; a geodynamic setting consistent with current theory on Alleghanian tectonics.

The presence of mafic enclaves within the Danburg granite presents a possible insight into its origin. A liquid origin for the enclaves is preferred due to several lines of evidence. Textural observations including chilled margins, skeletal titanites, rapakivi feldspars, and acicular apatite are consistent with mixing between mafic melts into a cooler, felsic magma chamber. Geochemistry shows well-defined linear trends between most enclaves, Danburg granite, and Sandy Hill granite, also consistent with hybridization. The composition of the most mafic enclaves suggest some degree of fractional crystallization (at least ~11-35%) occurred prior to significant hybridization. Both major element oxides and zirconium suggest the more juvenile melt experienced differentiation before interaction with the felsic source. Temperatures and pressures calculated through accessory mineral thermobarometry of 771±27°C and 6.5±1.7 kilobar for the Danburg granite and 765±50°C and 5.1±1.4 kilobar for the contained enclaves support crystallization under similar conditions. If correct, influx of a mafic melt

indicates mantle involvement (in the form of heat and mass) in the generation of the Danburg and Sandy Hill granites, a scenario consistent with its inferred tectonic setting.

Before this study, field relations and previous interpretations suggested the Delhi syenite was either younger than the Danburg granite, related to the Alleghanian orogeny, acted as a source for the mafic enclaves within the Danburg granite, or is part of an Acadian suite of gabbros and syenites outcropping in the Charlotte belt. A new SHRIMP-RG ^{207}Pb-corrected ^{206}Pb/^{238}U zircon age for the Delhi syenite place it firmly at 468.9±4.8Ma, contradicting these previous interpretations. Geochemically, the Delhi most resembles granites formed in an anorogenic setting. The timing of the Charlotte belt's accretion to Laurentia is not well established in the Southern Appalachians, with multiple models placing the terrane at various locations throughout its evolution, thus the Delhi syenite's role remains enigmatic.

REFERENCES

Aleinikoff, J.N., Wintsch, R., Tollo, R.P., Unruh, D.M., Fanning, C.M., and Schmitz, M.D., 2007. Ages and origins of rocks of the Killingworth dome, south-central Connecticut: Implications for the tectonic evolution of southern New England. American Journal of Science, v. 307, p. 63–118.

Allard, G.A., and Whitney, J.A., 1994. Geology of the Inner Piedmont, Carolina Terrane, and Modoc Zone in Northeast Georgia. Georgia Geologic Survey, Atlanta. 35 p.

Ayrton, S.N., 1991. Appinites, lamprophyres and mafic magmatic enclaves: Three related products of interaction between acid and mafic magmas: in Didier, J. and Barbarin, B. eds., Enclaves and Granite Petrology, Elsevier Amsterdam, p.465-475.

Barth, A. P. and Wooden, J. L., 2010. Coupled elemental and isotopic analyses of polygenetic zircons from granitic rocks by ion microprobe, with implications for melt evolution and the sources of granitic magmas; Chemical Geology, v. 277, no. 1, p. 149-159.

Bird, P., 1979. Continental delamintation and the Colorado Plateau. Journal of Geophysical Research, v.84, p.7561-7567.

Black, L.P., Kamo, S.L., Allen, C.M., Davis, D.W., Aleinikoff, J.N., Valley, J.W., Mundil, R., Campbell, I.H., Korsch, R.J., and Williams, I.S., Foudoulis, C., 2004. Improved $^{206}Pb/^{238}U$ microprobe geochronology by the monitoring of a trace-element-re- lated matrix effect: SHRIMP, ID-TIMS, ELA-ICP-MS and oxygen isotope documentation for a series of zircon standards. Chemical Geololgy, v. 205, p. 115–140.

Bussy, F., 1990. The rapakivi texture of feldspars in a plutonic mixing environment; a dissolution-recrystallization process? Geological Journal, v.25, p.319-324.

Chappell, B.W., 1996. Magma Mixing and the production of compositional variation within granite suites: evidence from the granites of Southeastern Australia. Journal of Petrology, v.37, p.449-470.

Chappell, B.W., and White, A.J.R., 1991. Restite enclaves and the restite model: in Didier, J. and Barbarin, B. {eds.}, Enclaves and Granite Petrology, Elsevier Amsterdam, p.375-381.

Clement, S.W.J. and Compston, W., 1994. Ion probe parameters for very high resolution without loss of sensitivity. U.S.: Geological Survery Circular, v.1107, p.62.

Debon, F., 1991. Comparative major element chemistry in various "microgranular enclave-pluton host" pairs: in Didier, J. and Barbarin, B. eds., Enclaves and Granite Petrology, Elsevier Amsterdam, p.293-312.

Dempster, T.J., Jenkin, G.R.T., and Rogers, G., 1994. The origin of rapakivi texture. Journal of Petrology, v.35, p.963-981.

Didier, J., 1984. The problem of enclaves in granitic rocks, a review of recent ideas on their origin: in Xu, K.W., and Tu, G.C. eds. Geology of Granites and Their Metallogenetic Relations, Beijing, p.137-144.

Didier, J., and Barbarin, B, 1991. Enclaves and Granite Petrology. Elsevier Science Publishers, Amsterdam, 625p.

Dvoracek, D.K., Geochemical and geochronological study of the Danburg and Sandy Hill granitoids and associated mafic enclaves, Northeast Georgia [dissertation]. [Georgia]: University of Georgia; 2003, 260 p.

Dvoracek, D. and Roden, M. 2005. The Danburg (GA) granite, Carolina terrane: An Alleghanian pluton showing evidence for mixing with relatively alkaline magma. Georgia Geological Society Guidebook, v. 25, p. 81-94.

Faure, G., Mensing, T.M., Isotopes: Principles and Applications. John Wiley and Sons, Inc. 2005.

Feng, C., Lin, S., Zou, G., Li, Z., Xie, T., Peng, Z., and Liang, T., 2011. Magma mixing of granites at Lianghe: In-siut zircon analysis for trace elements, U-Pb ages, and Hf isotopes. Science China Earth Sciences, v.54, p. 1346-1359.

Foster, D.A., Mueller, P.A., Chong, MA., Lin, Q., Grimes, C.B., Heatherington, A.L., and Wooden, J.L., 2013. Alleghanian magmatism and metamorphism in the Southern Appalachian Orogen: record of transpressional assembly of Pangea in southern Laurentia. Geological Society of American Abstracts with Programs, v.45, p.61.

Frost, R.B., and Frost, C.D., 2008. A geochemical classification for feldspathic igneous rocks. Journal of Petrology, v.49, n.11, p.1955-1969.

Frost, B.R., Barnes C.G., Collins, W.J., Arculus, R.J., Ellis, D.J., and Frost, C.D., 2001. A geochemical classification for granitic rocks. Journal of Petrology, v.42, n.11, p. 2033-2048.

Fu, Bin, Page, F. Zeb, Cavosie, A.J., Fournelle, J., Noriko, K.T., Lackey, J.S., Wilde, S.A., and Valley, J.W., 2008. Ti-in-zircon thermometry: applications and limitations. Contributions to Mineralogy and Petrology, v.156, pp.197-215.

Fullagar, P.D., and Butler, J.R., 1979. 325 to 265 m.y.-old granitic plutons in the Piedmont of the southeastern Appalachians, American Journal of Science, v.279, p.161-185.

Grimes, C.B., John, B.E., Cheadle, M.J., Schwartz, J., Mazdab, F.K., Swapp, S., and Wooden, J., 2009. On the occurrence, trace element geochemistry, and crystallization history of zircon from in situ ocean lithosphere. Contributions to Mineralogy and Petrology, v.158, p. 757-783.

Hatcher, R.D., 2005. Southern and Central Appalachians, in Selley, R.C., Cocks, L.R.M., and Plimer, I.R. eds., Encyclopedia of geology, Elsevier Academic Press, Amsterdam, pp.72-81.

Hatcher, R. D., Jr., Bream, B. R., and Merschat, A. J., 2007. Tectonic map of the southern and central Appalachians: A tale of three orogens and a complete Wilson cycle, in Hatcher, R. D., Jr., Carlson, M. P., McBride, J. H., and Martinez Catalan, J. R., editors, The 4D Framework of Continental Crust: Geological Society of America Memoirs, v. 200, p. 595– 632.

Hayden, L.A., E.B. Watson, and D.A. Wark, 2008. A thermobarometer for sphene (titanite). Contributions to Mineralogy and Petrology, v.155, pp.529-540.

Hibbard, J.P., Stoddard, E.F., Secor, D.T., and Dennis, A.J. 2002. The Carolina Zone: overview of Neoproterozoic to early Paleozoic peri-Gondwanan terranes along the eastern flank of the southern Appalachians. Earth-Science Reviews, v. 57, p. 299–339.

Hibbard, J. P., van Staal, C. R., and Rankin, D. W., 2007. A comparative analysis of pre-Silurian crustal building blocks of the northern and southern Appalachian orogen. American Journal of Science, v. 307 n. 1, p. 23– 45.

Hibbard, J.P, van Staal, C.R., and Rankin, D.W., 2010. Comparative analysis of the geological evolution of the northern and southern Appalachian orogen: Late Ordovician-Permian. Geological Society of America Memoir v.206, p.51-69.

Hibbard, M.J., 1981. The magma mixing origin of mantled feldspars. Contributions to Mineralogy and Petrology, v.76, p.158-170.

Hibbard, M.J., 1991. Textural anatomy of twelve magma-mixed granitoid systems: in Didier, J. and Barbarin, B. {eds.}, Enclaves and Granite Petrology, Elsevier Amsterdam, p.431-443.

Ireland, T.R., and Williams, I.S., 2003. Considerations in zircon geochronology by SIMS, in Hanchar, J.M., and Hoskin, P.W.O., eds., Zircon: Reviews in Mineralogy and Geochemistry, v. 53, p. 215–241.

Jaeger, J.C., 1959. Temperatures outside a cooling intrusive sheet. American Journal of Science, v.257, p.44-54.

Johnston, A.D., and Wyllie, P.J., 1988. Interaction of granitic and basic magma: experimental observations on contamination processes at 10kbar with H_2O. Contributions to Mineralogy and Petrology, v.98, p.352-362.

Lin, Q., 2013. Complex Sources of Alleghanian Granites in the Southern Appalachians. GSA's 125th Anniversary Annual Meeting and Exposition, 2013 Oct 27-30, Denver CO. Geological Society of America Abstracts with Programs. v. 45, n.7, p.294.

Ludwig, K.R., 2003. Isoplot version 3.0: A geochronology toolkit for Microsoft Excel Berkeley Geochronology Center. Special Publication 4, v.71, p.2.

Ludwig, K. R., 2009. User's manual for SQUID 2. Berkeley Geochronology Center Special Publication, Berkeley.

Ludwig, K.R., 2012. Isoplot 3.75, A geochronological toolkit for Microsoft Excel; Berkeley Geochronology Center Special Publication n.5.

Maury, R.C, and Didier, J., 1991.Xenoliths and the role of assimilation: in Didier, J. and Barbarin, B. {eds.}, Enclaves and Granite Petrology, Elsevier Amsterdam, p.529-542.

McBride, J. and Nelson, K., 1988. Integration of COCORP deep reflection and magnetic anomaly analysis in the southeastern United States: Implication for origin of the Brunswick and East Coast magnetic anomalies. Geological Society of America Bulletin v. 100, p. 436-435.

McDonough W. F. and Sun S., 1995. The composition of the Earth. Chemical Geology v. 120, p. 223-253.

McSween, H.Y. Jr., and Harvey, R.P., 1997. Concord plutonic suite: Pre-Acadian gabbro-syenite intrusions in the southern Appalachians, *in* Sinha, A.K., Whalen,

J.B., and Hogan, J.P., eds., The Nature of Magmatism in the Appalachian Orogen: Boulder, Colorado, Geological Society of America Memoir 191, p.221-234.

Mueller, P.A., Heatherington, A.L., Foster, D.A., Thomas, W.A., and Wooden, J.L., 2013. The Suwannee Suture: significance for Gondwana-Laurentia terrane transfer and formation of Pangaea. Gondwana Research, v. 26, p. 365-373.

Müller, D., Rock, N.M.S., and Groves, D.I., 1992. Geochemical discrimination between shoshonitic and potassic volcanic rocks in different tectonic settings: a pilot study. Mineralogy and Petrology v.46, p.259-289.

Nakamura, Y., H. Fujimaki, N. Nakamura, M. Tatsumoto, G. A. McKay, and J. Wagstaff (1986), Hf, Zr, and REE partition coefficients between ilmenite and liquid: Implications for lunar petrogenesis, J. Geophys. Res., 91(B4), 239–250.

Nelson, K.D., 1992. Are crustal thickness variations in old mountain belts like the Appalachians a consequence of lithospheric delamination? Geology, v.20, p. 488-502.

Noel, J., Spariosu, D., and Dallmeyer, D., 1988. Palemagnetism and $^{40}Ar/^{39}Ar$ ages from the Carolina slate belt, Albemarle, North Carolina: implications for terrane amalgamation with North American. Geology, v.16, p.64-68.

Pearce, J.A., Harris, N.B.W., and Tindle, A.G., 1984. Trace element discrimination of diagrams for the tectonic interpretation of granitic rocks. Journal of Petrology v.25, p.956-983.

Pin, C., Binon, M., Belin, J.M., Barbarin, B., and Clemens, J.D., 1990. Origin of micro granular enclaves in granitoids: equivocal Sr\Nd evidence from Hercynian rocks on the Massif Central (France). Journal of Geophysical Research v.95, p.17821–17828.

Pollock, J.C., Hibbard, J.P., and van Staal, C.R., 2012. A paleogeographical review of the peri-Gondwanan realm of the Appalachian orogen. Canada Journal of Earth Science, v.49, p.259-288.

Rollinson, H., 1993. Using geochemical data: evaluation, presentation, interpretation. Pearson Education Limited, New York, 352 p.

Sacks, P. E., and Secor, D. T., 1990, Delamination in collisional orogens: Geology, v. 18, p. 999-1002.

Samson, D.D., Coler, D.G., and Speer, J.A., 1995. Geochemical and Nd-Sr-Pb isotopic composition of Alleghanian granites of the southern Appalachians: Origin,

tectonic setting, and source characterization: Earth and Planetary Science Letters, v. 134, p. 359-376.

Secor, D.T., Samson, S.L., Snoke, A.W., and Palmer. A.R., 1983. Confirmation of the Carolina Slate belt as an exotic terrane. Science, v.2221, p.649-651.

Sederholm, J. J., 1891. Über die finnländischen Rapakiwigesteine, Tschermaks Mineral. Petrogr. Mitt. v.12, p.1–31.

Sinha, A.K, Hund, E.A., and Hogan, J.P., 1989. Paleozoic accretionary history of the North American plate margin (Central and Southern Appalachians): constrains from the age, origin, and distribution of granitic rocks. Geophysical Monograph Series, v.50, p.219-238.

Sinha, A.K., Thomas, W.A., Hatcher, R.D. Jr., and Harrison, M.T., 2012. Geodynamic evolution of the Central Appalachian Orogen: geochronology and compositional diversity of magmatism from Ordovician through Devonian. American Journal of Science, v.312, p.907-966.

Sparks, R.S.J. and Marshall, L.A., 1986. Thermal and mechanical constraints on mixing between mafic and silica magmas. Journal of Volcanology and Geothermal Research, v.29, p.99-124.

Sparks, R.S.J., Sigurdsson, H., and Wilson, L., 1977. Magma mixing: a mechanism for triggering acid explosive eruptions. Nature, v.267, p.315-318.

Speer, J.A., and Hoff, K., 1997. Elemental composition of the Alleghanian granitoid plutons of the southern Appalachians, in Sinha A.K., Whalen, J.B., and Hogan, J.P., eds., The Nature of Magmatism in the Appalachian Orogen: Boulder, CO, Geological Society of America Memoir 191.

Speer, J. A., McSween, H. Y., and Gates, A. E., 1994. Generation, segregation, ascent, and emplacement of Alleghanian plutons in the southern Appalachians: Journal of Geology, v.102, p.249-267.

Stacey, J.S. and Kramers, J.D., 1975. Approximation of terrestrial lead isotope evolution by a 2-stage model. Earth and Planetary Science Letters v.26, p.207-221.

Streckeisen, A., 1975. To each plutonic rock its proper name. Earth-Science Reviews, v.12, p.1-33.

Tull, J., Holm-Denoma, C.S., and Barineau, C.I., 2014. Early to Middle Ordovician back-arc basin in the southern Appalachian Blue Ridge: characteristics, extent, and tectonic significance. Geological Society of America Bulletin, doi: 10.1130/B30967.1.

Van der Voo, R., 1988. Paleozoic paleogeography of North American, Gondwana, and intervening displaced terranes: comparisons of paleomagnetism and paleoclimatology and biogeographical patterns. Geological Society of America Bulletins, v.100, p.311-324.

Vernon, R.H., 1983. Restite, xenoliths, and microgranitoid enclaves in granites. Journal and Proceedings of the Royal Society of New South Wales, v.116, p.77-103.

Vernon, R.H., 1991. Interpretation of microstructures of microgranitoid enclaves: in Didier, J. and Barbarin, B. {eds.}, Enclaves and Granite Petrology, Elsevier Amsterdam, p.277-291.

Vick, H., Channell, J., and Opdyke, N., 1987. Ordovician docking of the Carolina slate belt: Paleomagnetic data. Tectonics, v.5, p.573-583.

Wall, V.J., Clemens, J.D., and Clarke, D.B., 1987. Models for granitoid evolution and souce compositions. Journal of Geology, v.95, p.731-749.

Watson, E.B., and J.M. Ferry, 2007. New thermodynamic models and revised calibrations for the Ti-in-zircon and Zr-in-rutile thermometers. Contributions to Mineralogy and Petrology, v.154, pp.429-437.

Weibe, R.A., 1991. Commingling of contrasted magmas and generation of mafic enclaves in granitic rocks: in Didier, J. and Barbarin, B. eds., Enclaves and Granite Petrology, Elsevier Amsterdam, p.393-401.

Wenner, D. B., 1981. Oxygen isotopic compositions of the late orogenic granites in the southern Piedmont of the Appalachian Mountains, USA, and their relationship to subcrustal structures and lithologies. Earth, Planetary, and Science Letters, v. 54, p. 186-199.

Williams, I. S., 1997. U-Th-Pb geochronology by ion microprobe: not just ages but histories. Reviews in Economic Geology v.7, p.1–35.

Williams, I.S., 1998. U-Th-Pb Geochronology by ion microprobe, in McKibben, M.A., Shanks III, W.C., and Ridley, W.I., eds., Applications of microanalytical techniques to understanding mineralizing processes. Reviews in Economic Geology, v.7, p.1–35.

Wilson, F.A., and Jones, W.J., 1986. The Northern Charlotte belt, North Carolina and South Carolina: a deformed composite batholith. Geological Journal, v.21, p.319-335.

Wyllie, P.J., Cox, K.G., and Biggar, G.M., 1962, The habit of apatite in synthetic system and igneous rocks: Journal of Petrology, v.3, p.238-243.

Yoder, H.S., Jr., 1973. Contemporaneous basaltic and rhyolitic magmas. American Mineralogist, v.58, p.153-171.

APPENDIX: TRACE ELEMENT DATA AND GRAPHS

Table A-1. SHRIMP-RG zircon trace element data for the Danburg granite, Sandy Hill granite, enclaves, and Delhi syenite.

	Concentrations								
Sample	U (ppm)	Th (ppm)	Ti (ppm)	Fe (ppm)	Gd (ppm)	Y (ppm)	Yb (ppm)	Hf (ppm)	Calculated T (°C)[i]
Sandy Hill granite									
SAO6-7.1core	645	1155	64.1	224	91	2157	445	9880	1007
SAO6-4.1	279	350	17.1	23	13	403	94	10465	838
SAO6-1.1	203	335	29.5	151	26	772	199	10085	902
SAO6-13.1core	118	286	20.5	9	53	1245	219	8243	858
SAO6-18.1	126	167	11.6	121	14	493	124	9194	796
SAO6-5.1core	1104	1233	9.4	9	19	1006	387	10628	774
SAO6-9.1core	740	744	12.6	73	17	896	271	9813	804
SAO6-11.2core	46	52	15.9	0	13	402	98	8807	829
SAO6-12.1rim	117	111	8.2	5	9	378	106	9761	761
SAO6-15.1	141	226	13.8	1	45	1163	238	8904	814
SAO6-8.1rim	3084	1503	49.6	472	86	2095	732	12037	970
SAO6-11.1rim	126	136	11.2	0	16	574	144	9264	793
SAO6-3.1core	352	372	17.6	44	25	806	312	10176	841
SAO6-16.1rim	1454	1567	7.3	3	12	1139	493	10514	750
SAO6-14.1core	119	177	13.0	1	32	918	197	7974	808
SAO6-10.1	32	36	23.1	3	14	413	91	8368	872
SAO6-2.1	144	150	6.4	1	8	350	135	10568	737
SAO6-17.1	76	112	20.3	2	28	712	148	8286	857
SAO6-6.1	78	111	12.7	1	21	604	130	8981	805
SAO6-3.2rim	1827	1796	6.3	3	15	1046	569	11207	736
Sandy Hill granite									
SAO7-1.1core	879	935	34.3	534	101	2370	608	10386	921
SAO7-5.1core	780	617	20.9	471	27	987	344	11489	860
SAO7-8.1core	307	348	7.8	2	32	1054	259	9905	756
SAO7-2.1core	479	404	6.3	10	15	723	230	10565	737
SAO7-7.1core	67	59	12.9	0	8	319	79	9122	807
SAO7-6.1core	3356	1105	4.0	517	17	1792	676	14083	696
SAO7-4.1core	393	310	9.2	123	59	1953	544	9029	773
SAO7-3.1	6485	3252	74.6	5611	107	5735	2020	14328	1030
Sandy Hill granite									
SAO8-2.2rim	1561	1521	52.4	929	24	921	565	11400	978
SAO8-1.1	641	597	18.6	212	13	596	322	10641	847
SAO8-12.1	213	315	7.8	1	35	1111	256	8173	756

Table A-1: continued

SAO8-10.1core	78	64	7.6	0	5	268	73	8087	754
SAO8-3.1rim	200	199	21.0	565	25	756	265	9605	861
SAO8-5.1rim	272	326	9.5	1	19	789	197	8263	775
SAO8-11.1rim	205	244	11.0	1	16	564	141	7937	790
SAO8-4.1rim	66	94	15.8	0	22	647	165	6599	829
SAO8-8.1rim	78	110	12.3	0	15	478	121	6886	802
SAO8-9.1rim	208	217	10.0	1	15	635	190	7741	781
SAO8-7.1rim	151	186	12.1	1	15	521	140	7577	800
SAO8-4.2core	140	203	9.3	1	26	805	213	7801	773
SAO8-6.1rim	388	541	9.8	1	22	835	210	8006	778
Danburg granite									
SAO10-2-6.1	264	318	5.3	1	5	258	134	10960	720
SAO10-2-13.1core	425	651							
SAO10-2-3.2core	73	102	13.7	0	20	535	157	9454	813
SAO10-2-4.1	184	287	11.0	2	39	1231	321	10167	790
SAO10-2-12.1core	157	230							
SAO10-2-8.2rim	122	130	11.0	1	13	519	150	9827	790
SAO10-2-11.1	190	207							
SAO10-2-8.1core	121	196							
SAO10-2-9.1	283	298	7.2	2	6	300	132	10633	748
SAO10-2-14.1rim	248	277	176.6	146	17	565	192	10039	1178
SAO10-2-7.1	412	543	10.3	1	7	112	124	12868	784
SAO10-2-5.1	262	263	9.4	2	13	578	219	9912	774
SAO10-2-10.1rim	306	349							
SAO10-2-2.1	316	495	7.1	1	15	586	233	10235	748
SAO10-2-3.1rim	152	166	9.6	3	14	548	178	10072	777
SAO10-2-1.1	170	146	8.5	1	11	481	174	9888	765
SAO10-2-15.1rim	41	63	176.6	146	14	349	110	8510	1178
Danburg enclave									
SAO10-5-1.1core	3253	925	155.3	46	49	1063	448	11042	1153
SAO10-5-3.1	103	126	10.7	1	17	534	144	9241	788
SAO10-5-6.1	165	105	4.3	1	3	130	38	9646	702
SAO10-5-4.1	121	168	12.1	1	21	681	173	9299	800
SAO10-5-8.1	131	91	4.8	0	3	196	67	10982	712
SAO10-5-7.1	91	132	18.6	0	20	704	163	8517	847
SAO10-5-1.2rim	471	602	6.9	1	7	360	154	10372	745
SAO10-5-2.1	96	143	11.0	1	16	452	137	9293	790
SAO10-5-5.1	114	90	6.3	4	4	222	72	10916	736
Delhi syenite									
SAO12-11.1	135	54	2.7	10	26	941	209	5004	664

Table A-1: continued

SAO12-5.1	115	46	3.9	7	32	894	255	5852	693
SAO12-14.1core	728	600	9.7	303	280	6768	1271	4395	778
SAO12-15.1	130	51	3.6	6	32	1015	259	5563	688
SAO12-8.1	171	66	2.0	4	32	1216	285	5462	639
SAO12-7.1	97	36	4.7	5	29	868	193	5315	710
SAO12-16.1	147	60	3.3	5	30	1002	268	5038	681
SAO12-12.1	129	34	4.8	5	14	614	181	5348	711
SAO12-10.1	137	48	2.7	8	24	866	216	5730	665
SAO12-4.1	128	28	3.0	8	13	605	231	5614	673
SAO12-9.1	73	17	2.7	2	8	430	128	5171	664
SAO12-2.2core	128	46	2.6	2	25	844	265	5922	661
SAO12-13.1	33	7	3.8	1	4	163	49	5676	693
SAO12-3.1	128	50	3.7	2	33	1011	289	5506	689
SAO12-1.1rim	199	74	3.5	8	12	471	167	5694	684
SAO12-6.1	133	33	2.8	5	15	679	185	5545	666
SAO12-2.1rim	155	54	1.8	8	28	993	320	5235	633
Delhi syenite									
SAO13-5.1	243	24	3.3	4	5	283	115	8287	681
SAO13-3.1	101	22	4.5	2	13	572	203	5736	707
SAO13-7.1	172	30	2.0	3	12	680	279	5573	642
SAO13-2.1	152	38	5.2	3	17	838	258	5473	718
SAO13-1.1	110	25	3.8	4	11	551	206	5680	691
SAO13-4.1	118	47	4.2	2	34	1001	280	5631	700
SAO13-6.1	111	41	3.4	5	27	793	241	5703	683

i temperature calculated using formula from Ferry and Watson (2007) and an assumed TiO_2 activity = 0.7 and SiO_2 activity = 1.0

Table A-2. SHRIMP-RG titanite trace element data for the Danburg granite and enclaves.

	Concentrations															
Sample	Zr (ppm)	U (ppm)	Th (ppm)	Y (ppm)	Nb (ppm)	La (ppm)	Ce (ppm)	Pr (ppm)	Nd (ppm)	Sm (ppm)	Eu (ppm)	Gd (ppm)	Dy (ppm)	Yb (ppm)	Hf (ppm)	Calculated Pressure (kilobar)[i]
Danburg granite																
10-2-12.2dk	193	183	242	1444	193	1240	835	3431	515	2441	563	80	479	341	128	1.1
10-2-11.1	408	87	684	800	408	1212	1938	4999	505	1867	323	59	270	177	76	0.7
10-2-6.1	350	175	397	1392	350	1670	1413	4131	529	2336	517	79	445	326	121	0.8
10-2-9.2dk	379	116	628	746	379	1105	1630	4160	426	1585	284	53	238	163	70	0.8
10-2-8.1	371	84	845	787	371	1480	2520	5923	573	2022	325	61	256	173	73	0.8
10-2-13.1	541	58	1111	912	541	1787	4318	10351	978	3314	457	66	336	196	87	0.6
10-2-2.1	555	60	943	947	555	1539	3930	9798	973	3355	460	61	340	203	96	0.6
10-2-4.1	712	53	722	4204	712	1596	3019	11639	1701	7499	1537	135	1221	889	341	0.5
10-2-1.1	680	51	651	3139	680	1635	3304	11351	1536	6311	1078	99	852	606	287	0.5
10-2-5.1	452	70	883	795	452	1672	3549	7871	720	2404	360	60	280	179	74	0.7
10-2-7.1	641	54	873	1462	641	2004	3871	11324	1268	4599	666	72	470	280	150	0.5
10-2-9.1lt	471	60	1030	811	471	1473	4185	10145	907	2910	385	58	271	172	81	0.7
10-2-12.1lt	668	41	838	5189	668	2247	3187	12755	2001	9508	2270	181	1788	1299	353	0.5
10-2-3.1	680	49	736	4138	680	1663	2965	11333	1671	7330	1543	139	1240	913	341	0.5
10-2-10.1	571	49	957	1262	571	1920	4285	12003	1287	4503	628	67	438	254	127	0.6
enclave																
10-1-5.1	650	54	1031	1305	1955	4109	11186	1218	4429	655	80	459	269	125	35	0.5
10-1-4.1	531	67	757	568	955	2917	6473	572	1892	267	47	194	116	58	26	0.6
10-1-6.1	580	54	773	1409	1618	3336	9837	1120	4256	671	80	492	292	140	32	0.5
10-1-1.1	559	80	809	302	808	2191	3516	265	849	124	26	103	61	35	38	0.5
10-1-12.1lt	1413	93	1497	1024	3638	5418	12601	1251	4077	528	80	375	210	113	67	0.1
10-1-2.1	599	61	882	806	1416	3504	8390	808	2714	375	64	267	157	85	35	0.5

Table A-2: continued

10-1-7.1	628	64	873	1031	1302	3923	10509	1091	3766	513	76	358	202	113	34	0.5
10-1-3.1	720	102	1311	373	1543	3079	5223	403	1263	181	34	133	81	35	41	0.4
10-1-12.2dk	594	67	898	961	1149	3839	9756	972	3291	466	68	344	197	102	31	0.5
enclave																
10-5A-7.1	479	61	560	498	488	799	3303	7091	683	2402	326	54	239	121	41	0.6
10-5A-1.1	572	61	801	1542	583	1342	3405	9257	1057	4071	679	126	574	344	138	0.5
10-5A-2.1	620	61	776	3343	620	1634	3254	10415	1383	6209	1377	181	1219	790	262	0.5
10-5A-3.1	628	60	836	3401	628	1769	3234	10465	1382	6252	1419	192	1245	806	256	0.5
10-5A-5.1	610	58	827	2454	610	1919	2990	9423	1188	5020	1034	157	881	568	199	0.5
10-5A-4.1	517	76	910	734	517	769	4096	9088	891	3140	434	68	314	170	67	0.6
10-5A-6.1	616	62	856	4023	616	1758	3023	10364	1457	6625	1623	208	1388	975	291	0.5
enclave																
10-5B-1.1	712	32	565	693	503	829	3429	8480	892	3185	409	95	292	148	66	0.4
10-5B-2.1	1311	36	514	2636	638	1525	3199	10701	1452	6387	1210	225	968	611	197	0.1
enclave																
10-5C-1.1lt	669	34	460	2981	669	1546	2884	11237	1583	6890	1347	234	1072	691	219	0.5
10-5C-6.1	654	33	548	1282	654	1718	3636	10402	1175	4293	595	168	427	257	119	0.5
10-5C-3.1	581	33	495	1235	581	1475	3225	9855	1075	4024	571	158	402	243	114	0.5
10-5C-4.1	366	65	641	2074	366	1683	2327	6594	959	4881	1128	91	908	571	134	0.7
10-5C-5.1	979	20	416	3045	979	1827	3560	13181	1947	8872	1758	264	1339	814	200	0.3
10-5C-1.2dk	405	35	580	818	405	996	3001	6949	708	2621	427	76	245	140	69	0.7
10-5C-2.1	737	19	405	2470	737	2044	4163	14239	1974	8482	1540	245	1067	626	160	0.4

i pressure calculated using formula from Haden et al (2008), an assumed TiO_2 activity = 0.7 and SiO_2 activity = 1.0, a temperature of 765°C for all enclave samples and a temperature of 771°C for the Danburg granite (temperatures are averages of Ti-in-zrn calculated temperatures in Appendix A

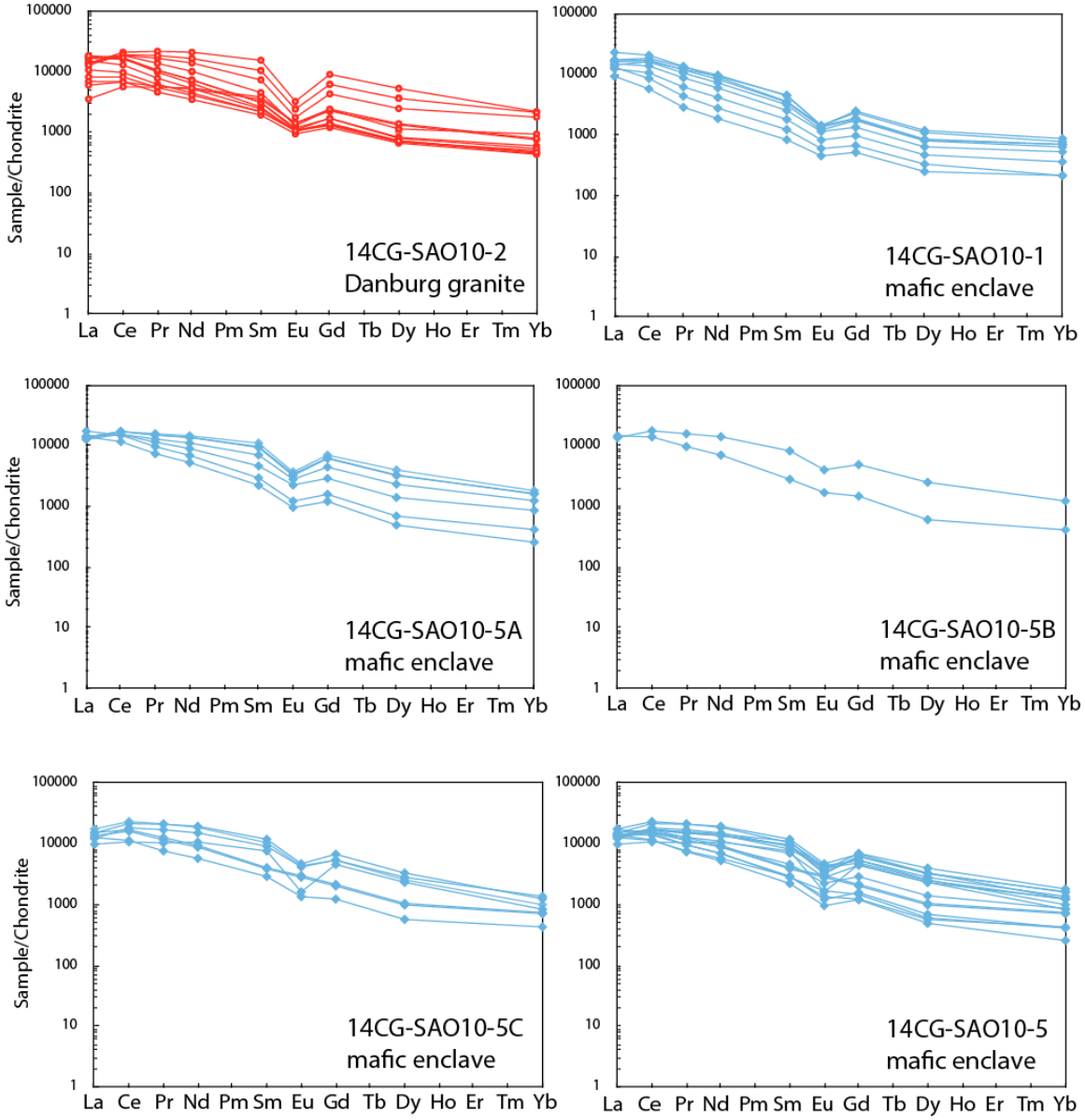

Figure A-1: REE Spider diagrams for titanites from the Danburg granite and its contained enclaves analyzed by SHRIMP-RG.

Thesis and Dissertation Services